Molecular Dynamics Simulations of Solid Sulphur Hexafluoride

Thesis submitted by

Lu Hua

For the Degree of

Doctor of Philosophy

Department of Physics
The University of Edinburgh

January 1992

Acknowledgements

I am indebted to my supervisor Prof. Stuart Pawley who has helped me throughout the completion of this thesis.

I am grateful to my wife for her exellent understanding and tolerance.

I owe many thanks to David Wallace, who first introduced me to this university, Arthur Trew whose knowledge of the DAP helped me getting over my computer-shy when I first came here, Jeremy Craven whose work on the ECS allowed me to have an easy access to the machine, Nigel Wilding, Martin Simmen, Duncan Potter and Jin Shangjie for many things, the department's secretaries, especially Mrs. McKirdy who is always willing to sort out my problems of living and studying in this alien country.

I would also like to thank the Sino-British Friendship Scholarship Scheme(SBFSS) for giving me the financial support, the Edinburgh Parallel Computing Centre(EPCC) for supplying the Edinburgh Concurrent Supercomputer and the DAPs and staff of the Edinburgh University Computing Service for their work of keeping the plotters, printers and other facilities in working order.

Finally I would like to express my gratitude to the late Sir Yue-Kong Pao, a major sponsor of the SBFSS, without whom I would not have been able to come to Edinburgh to study.

Abstract

This thesis is a study of a molecular crystal SF_6 through the molecular dynamics(MD) method. Solid SF_6 has a plastic phase below its melting point and in this phase the interactions between the molecules are highly anharmonic and the orientations of the molecules are highly disordered. At even lower temperatures, the substance has a truly crystalline phase which exhibits, according to our MD simulation, some highly anharmonic properties such as molecular reorientation especially when the temperature is near the plastic-crystal transition point.

In the simulation, a simple Lennard-Jones potential function is used to represent the interactions between the molecules. So far, it has been found that this model can give results which are well in agreement with experiments in both the plastic and the crystalline phase. The agreement between the lattice parameters from the simulation and from neutron experiments is very good. The plastic-crystal phase transition and melting are observed in the simulation. The melting point for a bulk sample is found to be 23% higher than the experimental values but the melting point estimated from the surface-initiated melting is found to be closer to the experimental value. In the study of the low-temperature phase we have found that the thermal motions of the molecules are very diferent for the molecules occupying the two different symmetry sites of the monoclinic structure. Highly anisotropic patterns of the molecular movements have also been revealed.

In order to study the plastic-crystal phase transition, a constant-pressure MD method is used to ensure the smooth transitions between single-crystals. Through the use of this method, we have found that in the search for new crystalline structures the phase transitions are not necessarily between single crystals – crystallites with certain orientation may prevail resulting in a large crystal with domain structures.

SF_6 is a substance which has not been fully studied through experiments. This offers us an opportunity to use the MD method to predict some of its properties to guide experiments. In this thesis, we present the work on the use the fluctuations of the simulated system to calculate the heat capacity and the elastic constants.

Contents

Units

Length	1 Å = 10^{-10} m
Timescale	1 ps = 10^{-12} s
Mass	1 a.m.u = 1.661×10^{-27}kg
Pressure	1 kbar = 10^{8} Pa
Frequency	1 THz = 10^{12} Hz

Chapter 1

Introduction

1.1 Molecular Dynamics

1.1.1 General Description

Molecular Dynamics(MD) is a widely used method to solve the classic many-body problem

$$m_i\ddot{\mathbf{r}}_i = -\frac{\partial u}{\partial \mathbf{r}_i} \tag{1.1}$$

where $\mathbf{r}_i$ is the coordinate of molecule i and u is the potential function governing the interactions between the molecules in a large system of interacting molecules. Given sufficient initial conditions, equation 1.1 can be solved numerically with the aid of computers and the solutions are the trajectories of the molecules in space or a path in the phase space provided we have a knowledge of u. Thereafter any thermodynamic property A can be obtained from the average along the path in the phase space[1]

$$A = \frac{1}{T}\int_0^T A(t)dt.$$

Because equation 1.1 has to be discretized and solved numerically, the solutions are in fact a finite number of points on the path. The above formula should therefore be replaced by

$$A = \frac{1}{N_T}\sum_{i=1}^{N_T} A(i). \tag{1.2}$$

where N_T is the total number of the known points of the path in phase space. This equation is the basic link between the microscopic MD method and the macroscopic physical properties of the simulated systems. When T or N_T is large compared to the typical time scale of the physical process in the system, the properties calculated by using the above equation are good approximations of the ensemble averages[1].

The theory of MD is simple, but the amount of the calculation work is very large and is determined by the size of the system and the complexity of the potential energy function. Hence a simulated system has to be limited in size and idealized in the interactions. In early MD simulations, as the computer power and availability were very limited, the molecules were simplified as hard spheres, interaction happening only when two molecules collide[4, 5]. The first of the early examples of applying the MD method to more realistic physical systems was the study of argon liquid by Rahman in 1964[3]. In his work the sample consisted of 864 molecules and the interaction between any pair of the molecules was described by a Lennard-Jones(L-J) type potential function, one of the potential functions which is still frequently used today. Since then, especially in the last decade, there has been a tremendous increase of interest in the MD method because of the rapid development of the computer technology. Nowadays, a simulated system often consists of several hundred to several thousand monatomic or multi-atomic molecules, and the method is applied in so many areas that it has become an arduous task to compose any comprehensive review. Some concise remarks of the method can be found in, for example, [1], [6], [7] and [8].

Apart from MD, another simulation method which is also widely used to study the microscopic many-body physical systems is the Monte Carlo(MC) method[1, 2]. In this method, the phase space is sampled *stochastically* and the direct solutions are many points in the phase space. The physical properties are then calculated through the means over these discrete points. Even though these points are produced in sequence in the simulation they are not related to the time evolution of the system. Therefore the time-dependent dynamic properties of the system are not available in this method. This is the major difference between the two methods and also one of the advantages of the MD method over the MC method.

One of the disadvantages of the MD method over the MC method is perhaps that the MD method cannot deal with systems which are not governed by any obvious equations of motion like equation 1.1, one well known example of such a system being the Ising model in statistical mechanics[1].

1.1.2 PR Method and Other Forms of MD

Despite the ever-increasing power of modern computers, the samples which can be dealt with by MD simulations are still small compared to any macroscopic systems. Consequently if the sample has a surface the surface-to-body ratio of this sample must be very large. Therefore if the bulk properties are to be studied, periodic boundary conditions are often imposed on the sample to remove possible artefacts caused by the surface. In doing so, space will be filled by the simulated system, the MD-cell, and its infinite number of images. When the intermolecular forces are calculated those images have to be taken into account. Under the periodic boundary conditions, the number of molecules in a fixed volume is kept a constant. If the system does not have any energy exchange with the outside world the energy of the system is also conserved and such an MD simulation carried out under these conditions is associated with a thermodynamic ensemble in which the volume, the total energy and the number of particles are conserved ((EVN) ensemble). We will call this type of MD an (EVN) MD.

The (EVN) MD method is the most commonly used in MD simulations, but MD methods which are related to other ensembles have also been developed and found to be useful. The main reason for developing these methods which generate ensembles other than (EVN) ensemble is that in experiments physical properties are often measured under constant presure, or constant temperature or under other conditions, rather than constant volume. Volume is simply too difficult to control for solids and liquids. In this work we are mostly interested in the ensemble in which the pressure, the enthalpy H and the number of molecules are fixed while the volume and the shape are allowed to fluctuate. This type of MD generates an (HPN) ensemble. As it will be demonstrated in the following chapters, the use of this MD method is important because it allows the structural transitions to

happen without being complicated by the stress in the system.

The first (HPN) MD was put forward by Andersen[9] who introduced the *scaled coordinate* s_i which is defined from cartesian coordinate r_i as

$$s_i = r_i/V^{1/3}, \tag{1.3}$$

and treated the volume V of the MD-cell as another dynamic variable. Because only the volume has become an extra variable the system can expand and contract while the shape of the system remains fixed. The Lagrangian of the system takes the form

$$\mathcal{L} = \frac{1}{2}V^{2/3}\sum_i m_i \dot{s}_i^2 - \sum_{i<j} u(V^{1/3} \mid s_{ij} \mid) + \frac{1}{2}M\dot{V}^2 - pV \tag{1.4}$$

where p is the external pressure, $s_{ij} = s_i - s_j$ is the inter-molecular vector between molecule i and j, V is the volume of the MD-cell and M is a non-zero positive parameter. This mass-like parameter determines how fast is the response of the volume change to the variation of the stress in the system. In writing out the Lagrangian in equation 1.4, it has been assumed that the potential energy is the function of the distance between two particles (pairwise interaction). In Andersen's method, the simulated system is no longer isolated as in the (EVN) MD but connected with an external system which allows the volume to change. This resembles the system with gas or liquid sealed in a cylinder, and the gas or the liquid makes contact with the outside world through a piston. Because of this, the parameter M can be called the *piston mass*[9]. This resemblance, however, is very limited because the piston only allows the gas or the liquid to expand or contract along one direction so some people may prefer to compare M with the mass of an elastic membrane which wraps the system.

As a natural extension of the Andersen's method, Parrinello and Rahman[10] developed another MD method which also generates the (HPN) ensemble but allows the shape as well as the volume of the MD-cell to change dynamically. In this method, instead of the volume as in the Andersen's method, a 3×3 MD-cell matrix h becomes the extra variable. The h matrix is formed from the three MD-cell vectors $\mathbf{a}$, $\mathbf{b}$ and $\mathbf{c}$ and the volume of the MD-cell satifies

$$V = \mathbf{a} \cdot (\mathbf{b} \times \mathbf{c}) = det(h). \tag{1.5}$$

So, altogether nine scalar variables are added to the system. The scaled coordinate s_i, where the index i points to the ith molecule, is defined as

$$\mathbf{r}_i = hs_i \tag{1.6a}$$

and the molecular velocity is defined as

$$\mathbf{v}_i = h\dot{s}_i. \tag{1.6b}$$

The Lagrangian of the system is

$$\mathcal{L} = \frac{1}{2}\sum_i m_i \dot{s}_i^t G \dot{s}_i - \sum_{i<j} u(r_{ij}) + \frac{1}{2}WTr(\dot{h}^t\dot{h}) - pV. \tag{1.7}$$

where $G = h^t h$, Tr represents the evaluation of the trace of a matrix, the superscript t represents the transpose operation of a matrix and W is a parameter similar to the M in equation 1.4 which we will still call the piston mass. From the Lagrangian, the differential equations for the scaled coordinates and the h matrix can be derived as

$$m_i\ddot{s}_i = h^{-1}\mathbf{f}_i - m_i G^{-1}\dot{G}\dot{s}_i, \tag{1.8a}$$

where $\mathbf{f}_i$ is the force that acts on the ith molecule, and

$$W\ddot{h}_{\alpha\beta} = \sum_\gamma (\Pi_{\alpha\gamma} - p\delta_{\alpha\gamma})\sigma_{\gamma\beta} \tag{1.8b}$$

where

$$\sigma_{\alpha\beta} = V(h^{-1})_{\beta\alpha} \tag{1.9}$$

and

$$\Pi_{\alpha\beta} = \frac{1}{V}\left(\sum_i m_i (h\dot{s}_i)^t_\alpha (h\dot{s}_i)_\beta + \sum_i \sum_{j>i} (\mathbf{f}_{ij})_\alpha (h(s_i - s_j))_\beta\right). \tag{1.10}$$

If there is more than one atom in each molecule and the molecules are treated as rigid bodies, the kinetic energy term in equation 1.7 can be split into a translational part and an angular part. When this is the case, the force $\mathbf{f}_i$ should be interpreted as the total force acted on the molecule i, m_i as the mass of the whole molecule and $\dot{s}_i$ as the scaled velocity of the centre of mass of molecule i. Another group of equations concerning the angular motions of the molecules will be needed. The equations are

$$I_i\dot{\omega}_i = L_i \tag{1.8c}$$

where I_i is the tensor of the momentum of inertia of molecule i, ω_i is the angular velocity and L_i is the torque acting on the molecule.

If the shape of the MD-cell is close to cubic so that $V \doteq L^3$, the fluctuation of the volume is close to harmonic and the period of it can be estimated from the following formula[11].

$$\tau = 2\pi \left(\frac{W}{3LB}\right)^{1/2}. \tag{1.11}$$

where B is the bulk modulus which is defined as

$$B = V\frac{\delta p}{\delta V}. \tag{1.12}$$

Thus the larger the ratio W/L is, the slower is the response of the volume fluctuation to the internal stress in the system. So far, there has not been any theoretical guide on choosing W. A general understanding about it is that while it certainly affects the speed at which the system approaches equilibrium, it does not change the equilibrium properties. At the end of this chapter, we will give a lower bound of the parameter based on the concern for the stability of the integration algorithm.

In the PR method, because of the introduction of the h matrix as a variable, the MD-cell may rotate as a whole, a macroscopic movement which is not our concern. To avoid the complication to the analysis caused by this unwanted movement, some restrictions can be imposed on the h matrix. One restriction is to make h symmetric[11] and the other is to fix the direction of one MD-cell vector while one of the other vectors is confined to a plane[36]. When the system is in equilibrium state, none of these restrictions has been found to have significant effect on the thermodynamic properties of the simulated system.

The (HPN) MD can be easily switched to obtain another constant volume MD by fixing the h matrix. The result is a slightly generalized constant pressure MD which can be called (EhN) MD. An application of this MD is to study the system under strain. The constant pressure MD can also be generalized to include not only the hydrostatic pressure but also the shear stress and the ensemble becomes (HtN) where t is the stress tensor.

Apart from the (HPN) MD and the (EVN) MD, a handful of other MD methods

are also in use. An important one is the canonical ensemble MD (the (TVN) MD) which was developed by Nosé and co-workers[12]. The MD methods that have just been mentioned are all for the closed systems in which no particles are able to leave or enter the system. More recently, there have been reports of MD methods dealing with open systems[13, 14]. The corresponding ensembles are the grand canonical ensemble (μVT) and adiabatic open ensemble(μVL), where μ is the chemical potential and L=E−Nμ.

1.2 Molecular Crystals and SF_6

1.2.1 Molecular Crystals

In molecular crystals, the interactions between the atoms in the same molecule (bonded interactions) are much stronger than the interactions between atoms in different molecules(non-bonded interactions)[15]. As a result, the molecules in these crystals move as if they are rigid units. This is certainly in deep contrast to the situations in ionic crystals, in which the basic units are ions, or a metal, in which ions are submerged in electron clouds. Another feature of the interactions in the molecular crystals is that thay are short-ranged, the effective distance of the interactions hardly extending beyond several lattice spacings.

Because the molecules keep their shapes in the crystal the packing of the atoms and the crystal structures are affected by these shapes. So it is certainly not realistic to treat a molecule as a volumeless point in MD simulations even when the molecules are nearly spherical. In order to study the structure and dynamics of a molecular crystal, a common method is to develop empirical atom-atom potential functions, and the total potential energy between two molecules is then the sum of all the atomic pair interactions between the atoms in different molecules. The following L-J potential is often used to model the interactions between atoms

$$u(r_{ij}) = -4\epsilon\left[\left(\frac{\sigma}{r_{ij}}\right)^6 - \left(\frac{\sigma}{r_{ij}}\right)^{12}\right] \tag{1.13}$$

where r_{ij} is an interatomic distance, the parameter ϵ is the depth of the potential

well and σ is the distance at which the potential function equals zero, and the point where the force is zero is at $r = 2^{1/6}\sigma$. At zero temperature, the lattice structure is determined by the potential energy. For a stable structure it should have the minimum potential energy, so it is σ that determines the structure. The first term in the L-J potential function represents the attractive part of the interaction and thus it produces the van der Waals force. The second term is responsible for the repulsive force which is caused by the repulsion between the nuclei of the atoms in the molecules and the overlapping of the electron clouds when the molecules approach each other. An alternative potential function to the L-J type, can be obtained by replacing the repulsion term in equation 1.13 with an exponential term

$$Aexp(-Br_{ij})$$

where A and B are parameters which are usually chosen to fit the experimental data for the specific substance being studied.

For large molecules which have many constituent atoms the above atom-atom approach becomes unrealistic. This is mainly due to the large amount of work which is needed to calculate all the atom-atom interactions. If there are N_a atoms in a molecule, the computer time spent on the calculation is proportional to $N_a \times N_a$. Because of this difficulty, the point-point method can be used. In this method, the interactions centres in a molecule are not necessarily the positions of the atoms. These points are chosen so that the main characteristics of the molecules are preserved and the structure and other properties derived from the model are the best fit to the experimental data. To reduce the computation effort, the interaction centres should be as few as possible.

The difference in the strength of the interaction can be further demonstrated by comparing the periods of the internal vibration and the lattice vibration. These periods are the typical time scales of the corresponding processes. For SF_6, the typical Raman frequency of the internal modes, which are the vibrations dominated by the intramolecular forces, is about $700cm^{-1}$[16] which is equivalent to a period of 0.04ps. The time scale of the external vibration of the SF_6 molecules can be estimated through the L-J potential function (equation 1.13). By expanding

the potential function around $r=2^{1/6}\sigma$, the period of an oscillator with mass m is found to be approximately

$$2\sigma\sqrt{\frac{m}{\epsilon}}. \tag{1.14}$$

If m is substituted by the mass of a fluorine atom and ϵ and σ are chosen to be what will be used for the F-F interaction in the present simulation of SF_6, the period of the oscillator is calculated to be 2ps. This value is larger than the internal vibration by about two orders of magnitude. This feature of the molecular crystal can be exploited to simplify the model that is used in the MD simulations by freezing the internal degrees of freedom of the molecules.

1.2.2 SF_6

Even though the MD method is a general method capable of solving any many-body problem as equation 1.1, provided the number of molecules is not too large and the potential function u is not too complicated, the advantage of it over some other methods such as the lattice dynamics method[24] becomes obvious only when the system under investigation is highly anharmonic. One such system is the liquid, a state in which the molecules are not confined to the vicinity of any lattice point and the orientations of the molecules are disordered. Another highly anharmonic system is the liquid crystal, a substance usually consisting of long linear molecules which are translationally disordered as in the liquid while their orientations are ordered. The third example is the molecular crystal which has a plastic crystal phase[22, 23]. In this phase, the molecules still occupy the regular lattice sites of a crystal but reorient frequently so that they are, to different extents for different substances, orientationally disordered.

Experiments

SF_6 is one of the substances which has a plastic crystal structure. This is because the molecules of this substance are very spherical so that there is a lower energy barrier to the reorientation. The plastic phase of SF_6 exists between the melting point 223K and 96K at ambient pressure and the structure has a body-centred cubic(bcc) symmetry[18, 19, 20, 21]. In this phase, the SF_6 molecules reorient

rapidly while certain orientational order is still retained. This remaining orientational order comes from the tendency of the S-F bonds of the molecules to align with the three ⟨100⟩ directions of the lattice[17]. When melting happens, this order will disappear completely in the liquid state.

Below 96K, SF_6 experiences a solid-solid phase transition to become truly crystalline. Early studies of the structure of this low-temperature phase through Raman in 1972[16], NMR in 1977[25] and electron diffraction in 1981[26] revealed that the structure of this phase has a symmetry lower than cubic and that there exit two distinct sites in the structure. The solution of this problem about the structure was not finally reached until the year 1988 through neutron diffraction experiments[27, 28]. The experiments showed that below 96K the structure of SF_6 is monoclinic with a space group of C2/m and there are six molecules in a unit-cell. In this monoclinic structure there are two distinct sites and the ratio between the numbers of molecules occupying different sites is 1:2.

Previous MD Simulations

MD simulations have played an active role in understanding the properties of SF_6. The first work on this topic was carried out by Pawley and can be dated back to 1980[31] while the low-temperature structure of the substance was still very much unknown. In this work, the simulated MD system consisted of only 54 molecules and the molecular centres were fixed so that the molecules can only have angular displacements. Even with this much simplified model, the molecular reorientations were observed and some evidence of the correlations between these reorientations emerged. Shortly after this pioneer work much more intensive MD simulations were carried out by Pawley and Thomas[32]. The sample used in those simulations was composed of 4096 molecules. In the simulations the solid-solid phase transition was observed. These simulations greatly helped the neutron diffraction study into the low-temperature structure. However, because of the limitation of the method which is used in the MD simulation, the results concerning the low-temperature structure were not totally in agreement with the more recent neutron diffraction study[28] and the present MD simulations.

In the study of SF_6, there has been an unsolved problem concerning the low-

temperature structure. According to the electron diffraction study[26] and some MD simulations[34], there is some evidence which indicates that a structure, in which some molecules are orientationally disordered while others are ordered, exists between the plastic-crystal transition temperature and an even lower temperature. The phase is known to be the *intermediate phase* of SF_6. The problem has been that this phase did not show up in neutron diffraction experiments. Part of the present work will be devoted to the explanation of this controversy.

1.3 Parallel Computers

The development of the MD method and its applications have always been interlocked with the advances in computer technology. Currently, there are basically three main directions in the development of modern high-performance computers; the first is to develop *parallel computers*, the second is to develop more conventional serial *supercomputers* and the third is to develop some *special purpose computers*. In this section, we are going the introduce two parallel computers on which our present work has been carried out. We will only concentrate on the problems which are related to the implementation of the MD method.

1.3.1 The Distributed Array Processors

Part of the present MD simulations have been carried out on the two DAPs (*d*istributed *a*rray *p*rocessors)[33], DAP-510 and DAP-608, in the Edinburgh Parallel Computing Centre(EPCC). The DAP is a Single-Instruction-Multiple-Data (SIMD) computer. It has a fixed number of processing elements(PEs) arranged on a two dimensional array. These PEs can perform the same operation simultaneously under a single instruction. The data can be stored locally on each PE and can be passed around for communication and input-output. The total number of PEs of the DAP is called 'DAPSIZE' and it has a value of 1024 for DAP-510 and 4096 for DAP-608. These PEs form a 32×32 array for DAP-510 and 64×64 array for DAP-608.

On the DAP the data can be stored and manipulated in the forms of a *vector*, a *matrix* or a *long-vector*. To be specific, for the DAP-510 a *vector* is a one dimensional array consisting of 32 data sets corresponding to the same number of PEs. A *matrix* consists of 32×32 sets of data stored on the 1024 PEs. A *long-vector* also consists of the same sets of data as a *matrix* but the data sets are treated as if they are arranged on a one dimensional chain and the data or the PEs are labeled by only one index running from 1 to 1024. In what follows the appearance of the term *vector*, *matrix* and *long-vector* in italics shall be assumed

to indicate the mode of the DAP data storage.

The programs on the DAP are written DAP-FORTRAN, which resembles FORTRAN but includes commands aimed at implementing parallel computation. For example, in DAP-FORTRAN, a DAP *matrix* is represented as A(,), the element A(i,j) is a data stored in a PE which we label as PE_{ij}. If there are two sets of data stored in *matrices* A(,) and B(,) and we want to calculate the sum of the two numbers on each PE and store the results in another *matrix* C, what we need to do in DAP-FORTRAN is to use the command C(,)=A(,)+B(,).

To simulate a physical system using the MD method, it is necessary to calculate the interactions between the constituent elements such as atoms or molecules. If the coordinate of an atom (or a molecule) is stored on a PE, it is necessary that it can be passed to other PEs where information of other atoms is stored so that the distance between this atom and other atoms can be calculated efficiently. On the DAP the communication between different PEs is carried out through SHIFT commands. For example, if A is a *long-vector* then the command B=SHLC(A,n) will bring the data A(i) on the ith PE to the $(i-n)$th PE where i is any number between 1 and DAPSIZE. This SHIFT operation is cyclic and $(i-n)$ has modulo DAPSIZE. Therefore, the shift command B=SHLC(A,n) is equivalent to the FORTRAN command

```
      DO 10 I=1,DAPSIZE
      J=I+n
      IF(J.GT.DAPSIZE)J=J-DAPSIZE
10    B(I)=A(J).
```

Periodic Boundary Conditions

The architecture of the DAP and the way it carries out communication between different PEs makes it convenient to deal with one-dimensional(1D) cyclic chains of the length of DAPSIZE and two-dimensional(2D) lattices. However, in MD simulations one often needs to model three-dimensional lattices. Pawley and Thomas have shown in their work that even though it is not practical to build a sample

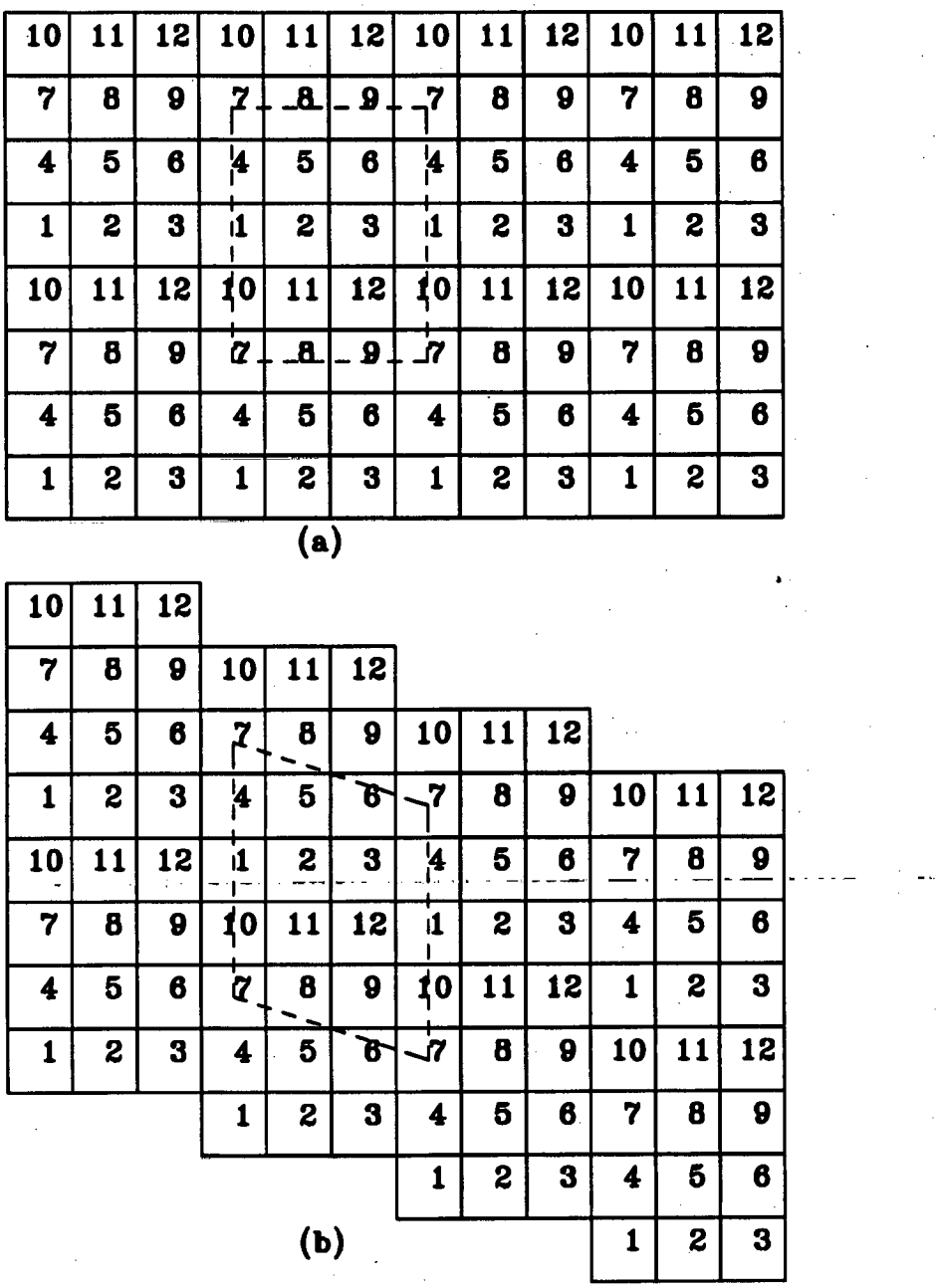

Figure 1.1: The comparison between the straight and skew cyclic boundary conditions for a notional computer with 12 PEs.

with ordinary cyclic boundary conditions, which usually requires that the MD-cell vectors are parallel to the basic vectors of the unit-cell of the lattice of the simulated system, it is possible to build a sample with the *skew cyclic boundary conditions* by using the *long-vector* mode of data storage[35].

Relative Index	Relative Space Vectors
1	(1,0)
-1	(-1,0)
3	(0,1)
-3	(0,-1)

Table 1.1: The neighbour list for the system in figure 1.1(b).

To illustrate this type of boundary condition, we use an imaginary DAP with only 12 PEs to simulate a 2D 3×4 square lattice with cyclic boundary conditions. Figure 1.1(a) shows how the space is filled when the ordinary straight cyclic boundary conditions are applied and figure 1.1(b) shows the situation when the skew cyclic boundary conditions are used. One possible choice of the MD-cell is marked by broken lines in both cases.

From figure 1.1(b) we can see that the relative indices (modulo 12) between a site and its neighbours are exactly the same for any site on the lattice. The relative indices for the four nearest neighbours of a site are easily found to be 1, 3, -1(or 11) and -3(or 9) This universal neighbour relationship means that we can make a single neighbour list which is valid for all the sites. Such a list for the system in figure 1.1(b) is given in table 1.1. In this list, without losing generality, only the nearest neighbours are included. What the list can tell us is that the nearest neighbours of molecule i have indices $i+1$, $i-1$, $i+3$ and $i-3$ modulo 12 (the DAPSIZE). These neighbours have relative space vectors (1,0), (-1,0), (0,1) and (0,-1). Since each pair of molecules only needs to be counted once for the calculation of the intermolecular distance, the second and the fourth lines in the list should be omitted.

In MD simulations, we need to calculate the interactions between neighbouring molecules which often depend only on the relative space vectors or even just on the distance between them. Under the skew cyclic boundary conditions and by using DAP-FORTRAN we can easily calculate these vectors. For example, if the coordinates of the molecules are stored in a *long-vector* A and we want to calculate the intermolecular vectors between the molecules. The neighbours of

Relative Index	Relative Space Vectors
1	(1,0,0)
3	(0,1,0)
9	(0,0,1)

Table 1.2: The neighbour list for a 3D system in figure 1.2.

these molecules have a relative index of n or, in other terms, the neighbours are n places to the right of the molecules in the *long-vector*. The calculation can be carried out by a single command B=A−SHLC(A,n) where B is the *long-vector* which stores the results, the relative space vectors in this case. In doing so, the parallelism of an MD problem can be fully exploited.

If the ordinary cyclic boundary conditions are used and the molecules are still indexed as if their information is stored in *long-vectors*, as in figure 1.1(a), the lists of neighbours are very different for different molecules. For example the relative indices of the nearest neighbours of molecule 1 are 1, 3, 2 and 9 but similar indices for molecule 3 are -2, 3, -1 and 9. The situation is very similar when a three dimensional system is constructed. As a result of this complex list, we cannot implement the model on the DAP without losing much of the parallelism.

The neighbour list for a 3D system is very much the same as in a 2D system. As an example, let us assume a different imaginary DAP with DAPSIZE=25 and give the neighbour list for a system with simple cubic structure in table 1.2. In this list, the relative indices and space vectors are given for 3 nearest neighbours. Because of the symmetry, this list in fact includes all the 6 nearest neighbours. To show how the list works we plot several successive planes of the system in figure 1.2. In the figure, plane (b) is directly on top of plane (a) and plane (c) is on top of plane (b) and so on.

By comparing figure 1.2 with the corresponding neighbour list in table 1.2, the relation between a site and its neighbours is obvious. It is not difficult to find that

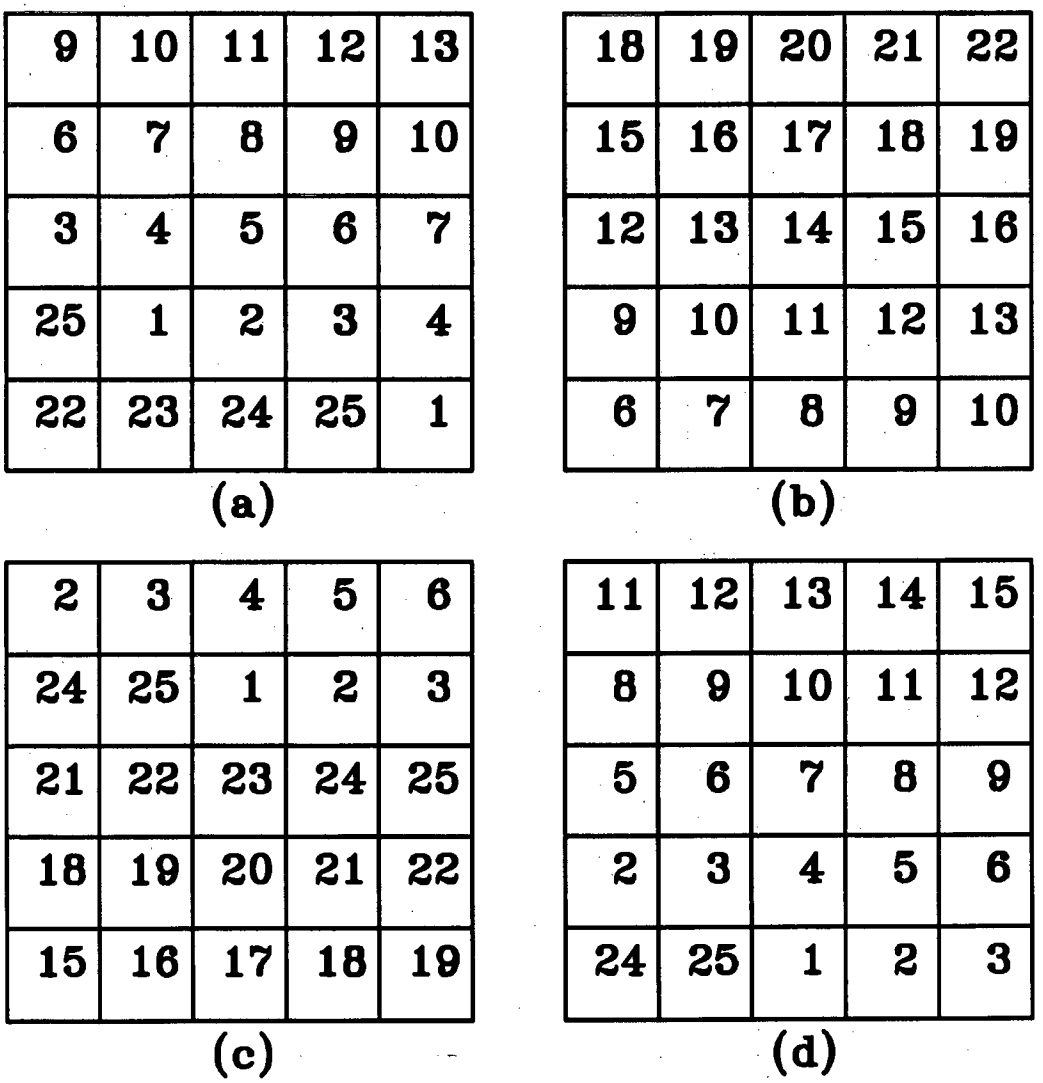

Figure 1.2: Four planes of a system with 25 elements. The skew boundary conditions are applied. The neighbour list for this construct is in table 1.2.

in this system, the basic vectors of the MD-cell may be chosen as

$$\begin{aligned} \mathbf{a} &= (3,-1,0), \\ \mathbf{b} &= (0,3,-1), \\ \mathbf{c} &= (1,2,2). \end{aligned}$$

It is possible to chose other basic vectors but it is not possible to chose one which forms a cubic MD-cell even if one is allowed to change the neighbour list. In fact we prearranged this result deliberately by chosing a DAPSIZE of 25, not a perfect cube, to demonstrate the general situation.

Non-DAPSIZE Simulation

In the above discussion, it was assumed that the number of molecules of the system, N, is the same as the number of the PEs in the DAP (DAPSIZE simulation). In reality, it may be necessary to simulate a system which does not meet this condition (non-DAPSIZE simulation). In the following part of this section, we will discuss how this problem is solved and show that the fixed number of PEs of the DAP is not a serious obstacle to MD simulations.

When the size N is smaller than DAPSIZE, there is no problem of storing the data of the N molecules in the DAP if there are not too many atoms in a molecule. The problem arises when one tries to pass around the data between the PEs using the scheme which has been outlined. The cause of the problem is the existence of the DAPSIZE−N empty PEs. The SHIFT commands treat the whole DAP *long-vector* as a 1D chain, not just those holding the data of the N molecules. Our solution is to arrange the N molecules on a 1D chain as we did for the DAPSIZE simulations and use a simple subroutine which can shift the N elements of a *long-vector* cyclically. This can be done through a combination of the SHIFT command and *logical masks*[35], a type of DAP-FORTRAN commands which can be used to activate only some elements in a *matrix*, *vector* or *long-vector*.

When the system size N is larger than the DAPSIZE, one PE will have to hold data for more than one molecule. Because of the limited memory of the machine,

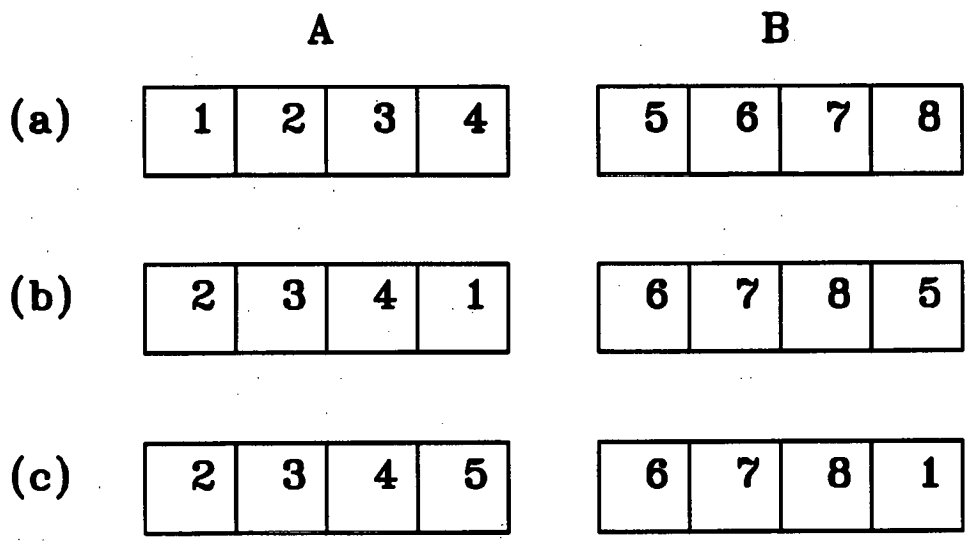

Figure 1.3: Non-DAPSIZE simulation. (a) The 8 molecules are arranged on the 4 PEs. (b) The shift command can only shift A and B separately. Molecule 1 and 5 are in the wrong sites. (c) The required shift of the data.

the size of the system is certainly limited. Apart from this we have found that the DAP can cope with the problem very well. To be specific, we assume that the number of molecules N=2×DAPSIZE and each PE stores the data of two molecules. We then imagine that the N=2×DAPSIZE molecules are arranged on a 1D cyclic chain so the skew cyclic boundary conditions can still be imposed in the same way as in a DAPSIZE simulation. The molecules are arranged so that the data of the ith and the (DAPSIZE+i)th molecules are on the ith PE. Therefore the data of the first DAPSIZE molecules can be represented by a *long-vector* A and the rest DAPSIZE molecules can be represented by another *long-vector* B. The problem now is that the SHIFT command can only applied to A or B separately, it cannot shift the whole chain which has N=2×DAPSIZE molecules cyclically. We now take as an example DAPSIZE=4 and N=8. Figure 1.3 shows what the SHIFT command can do and what is required in the present situation. Once again, the required operation can be achieved by the use of *logical masks.*

Up to now, we have insisted that the molecules in the system should form a cyclic

Relative Index	Relative Space Vectors
$N_1=M_x\times M_y$	(+0.5,+0.5,+0.5)
$N_2=N_1-1$	(-0.5,+0.5,+0.5)
$N_3=N_1-M_x$	(+0.5,−0.5,+0.5)
$N_4=N_3-1$	(−0.5,−0.5,+0.5)
$N_5=1$	(+1.0,+0.0,+0.0)
$N_6=M_x$	(+0.0,+1.0,+0.0)
$N_7=N_4+M_x\times M_y$	(+0.0,+0.0,+1.0)

Table 1.3: The neighbour list for the simulation of SF_6.

chain and then the 3D sample is constructed in a uniform manner. We point out that this is not the only way a 3D system can be implemented on the DAP. For example, if we want to form a bcc system of N molecules and N=2×DAPSIZE, we can place two molecules from a bcc unit-cell on each PE. Then it is the unit-cells that are used to form a cyclic chain. In this method, we need a different neighbour list in which the relative vectors are the relative vectors between unit-cells. In this special case of N=2×DAPSIZE simulation, this method is more efficient because less time is consumed on the operation of *logical masks*. However, we did not use this method because we prefer the previous method which is consistent with simulations of arbitrary number of molecules.

1.3.2 The Simulation of SF_6 on the DAP

In the plastic crystalline phase, the structure of SF_6 is bcc. To implement such a system on the DAP, one possible general neighbour list is in table 1.3. In the table M_x and M_y should be chosen so that the shape of the MD-cell is close to a cube. For AMT DAP-510 which has 1024 PEs and taking into account the fact that there are two molecules in every bcc unit-cell, M_x or M_y are chosen to be integers near $\sqrt[3]{1024/2}$, the *radius* as we will call it, which happens to be 8 in this case. In general, if the sample consists of N molecules, M_x or M_y are chosen to

be approximately

$$\sqrt[3]{N/2}.$$

In the low-temperature truly crystalline phase, the molecules have two orientations corresponding to the two distinct sites in the monoclinic structure. One third of the molecules form a group which we will call molecule 1 (the minority) and the other molecules form the other group which we will call molecule 2 (the majority). Since the proportion between the two groups of molecules is 1:2 the total number of molecules we need to form a periodic 1D chain and thus a single crystal should be a multiple of three. Consequently, we have to carry out non-DAPSIZE simulations. In the early stages of our work, DAP-608 was not available. In order to simulate a system which is reasonably large we chose the system of 3072 molecules. For the sample of this size, the *radius* of the sample is about 11 or 12 and it looks as if we can choose M_x and M_y to be either of them. This is not true because the structure of the crystal will impose some restrictions on the choice of M_x and M_y if a single crystal is to be simulated. For SF_6 , the molecules of the minority form 1D chains along the nearest neighbour direction and these chains are isolated by the molecules of the majority resulting in a honey-comb structure[32]. It is conceivable that not all the choices of M_x and M_y can meet the requirement of forming such a structure. To illustrate this point we choose M_x to be 12 and plot some molecules on the x-y plane in figure 1.4 to see what structure we get. In the figure, each site has two numbers. The upper one is the overall molecular index running from 1 to N and the lower one the type of the molecule (molecule 1 or 2). It can be seen that the minority molecules form 1D chains by joining the next-nearest neighbour along the y direction, a formation which is not consistent with the real structure of SF_6.

From this example, we can see the importance in choosing the neighbour list in order to simulate a single crystal. A neighbour list which meets all the conditions is given in chapter 2.

The DAP and the PR Method

When the skew cyclic boundary conditions are imposed, the MD-cell repetition

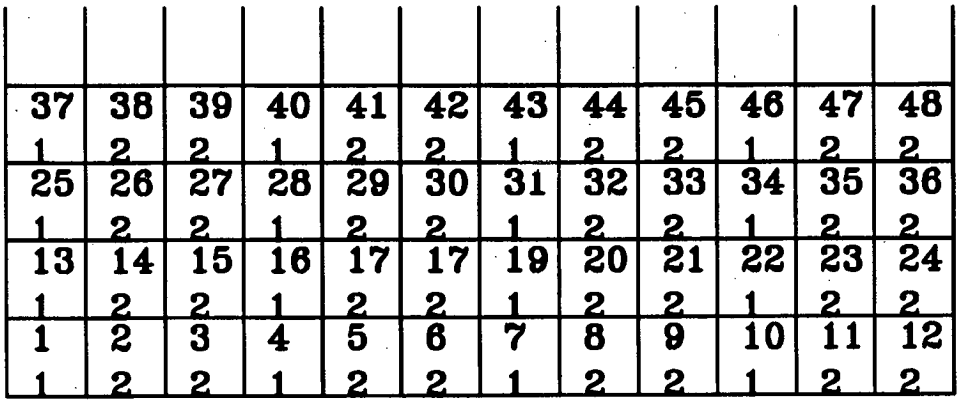

Figure 1.4: A layer of molecules on the x-y plane. The minority molecules form a 1D chain along the next-nearest direction.

vectors are usually not along any basic vectors of the underlying crystal structure. As a result, when the PR method is used the h matrix cannot directly reflect the symmetry of the lattice structure of the system. Therefore, instead of using the MD-cell vectors to define the scaled coordinates, we use vectors which are shorter and more closely related to the crystal structure of the simulated system. The basic unit formed from these vectors can be called a sub-MD-cell. For example, in the plastically crystalline phase the structure of SF_6 is bcc, so a convenient choice of the sub-MD-cell is simply the cubic unit-cell and the three vectors **a**, **b** and **c** of this sub-MD-cell are along the three basic vectors of the bcc unit-cell. When the shape and size of the system change, the sub-MD-cell parameters, and thus the elements of the h matrix which is defined by the sub-MD-cell vectors now, fluctuate correspondingly. If there is any structural change in the system and the structure ceases to be bcc the new structure could be found from the symmetry of the sub-MD-cell and the positions of the molecules in the sub-MD-cell.

Because of the change in definition of the h matrix, the relation between the volume and the h matrix also changes. When the structure is bcc and the sub-MD-cell is chosen as described previously there are 2 molecules in each sub-MD-cell

so that

$$V = \frac{N}{2}\mathbf{a}\cdot(\mathbf{b}\times\mathbf{c}) = \frac{N}{2}V_s \tag{1.15}$$

where N is the number of molecules in the system and

$$V_s = det(h)$$

is the volume of the sub-MD-cell. This change of the relation between the volume and the h matrix does not affect the equations of motion but it does change the relation between the piston mass W and the response of the volume to the pressure change in the system. The frequency of the volume fluctuation will be different from equation 1.11. From the equations of motion, equations 1.8a and 1. , we can deduce the approximate differential equation of the volume fluctuation

$$\frac{d^2}{dt^2}\delta V = \frac{V^2}{W}Tr[(\mathbf{\Pi} - p\mathbf{I})h^{-1^t}h^{-1}]. \tag{1.16}$$

If the sub-MD-cell is near cubic so that $h_{11} \doteq h_{22} \doteq h_{33}$ and $h_{ij} \doteq 0$ if $i \neq j$, we have

$$\frac{d^2}{dt^2}\delta V_s = -(\frac{N}{2})\frac{V_s^{1/3}B}{W}\delta V_s. \tag{1.17}$$

This is the equation of motion of a one-dimensional oscillator and the period of the volume fluctuation becomes

$$\tau = 2\pi(\frac{W}{3BV_s^{1/3}(N/2)})^{1/2}. \tag{1.18}$$

Because the overall shape of the MD-cell is near cubic $V \doteq L^3$. From equation 1.15 and 1.18 the period of the volume fluctuation can be expressed as

$$\tau = 2\pi(\frac{2}{N})^{1/3}(\frac{W}{3LB})^{1/2} = 2\pi\left((\frac{2}{N})^{2/3}\frac{W}{3LB}\right)^{1/2}. \tag{1.19}$$

Comparing this formula with equation 1.11, one can see that in order to obtain a certain value of τ, a larger piston mass is required in the simulations when the sub-MD-cell is used to define the h matrix than in the simulation when the MD-cell basic vectors are used to define the h matrix. If there are two molecules in one sub-MD-cell as in the simulation of SF_6, the difference in the values of the piston mass is a factor of

$$(N/2)^{2/3}.$$

For the simulation of 3072 molecules this factor is approximately 135.

If one wants the relation between the piston mass and the fluctuation period to be the same form as when the MD-cell vectors are used to define the h matrix, we can change the term with W in the Lagrangian to

$$\frac{1}{2}W(\frac{N}{2})^{2/3}Tr(\dot{h}^t\dot{h}).$$

For consistency, the Lagrangian is not changed in the present study. So the volume fluctuation period is calculated through equation 1.19 when the simulations are carried out on the DAP.

1.3.3 The Edinburgh Concurrent Supercomputer

Another parallel computer which we have used to carry out the present work is the Edinburgh Concurrent Supercomputer(ECS). The ECS is a computer system consisting of *transputers* [37]. Each transputer is in its own right a computer with its own CPU, floating point unit, local memory and 4 bi-directional links which can be used to communicate with other transputers or host computers. At present there are more than 400 transputers in the ECS and they are divided into *domains* of different number of transputers. The largest domain now has 132 transputers and the smallest has only one. A transputer can be used as an individual computer or it can be connected to other transputers on the same domain to form transputer arrays. Unlike the DAP which is an SIMD computer in which all the PEs perform the same operation under a single broadcast instruction, the transputers in a array can run different processes simultaneously so the ECS is a Multiple-Instruction-Multiple-Data (MIMD) machine. In general, an MIMD machine is more flexible than an SIMD machine but is also more difficult to use because all the communication sequences and their timing have to be well organized in the program.

In the present MD simulation of SF_6 some work was carried on the ECS. The program was adapted from one originally written by Craven[38] for the simulation of benzene. It suits domains of any number of transputers on the ECS. In the simulation, the transputers are connected to form a simple loop and the number of molecules assigned to each transputer is approximately N/n_t where n_t is the

number of transputers in the domain. It has been found that if N/n_t is not very small the computer time spent on communication is negligible compared to the time spent on calculation and the simulation is very efficient[38]. In our simulation of SF_6, a speed of about 35 Mflops was recorded in the simulation of a sample of 1024 molecules on a domain with 132 transputers. This speed is approximately three times faster than a similar simulation on the DAP-510. For non-DAPSIZE simulations the advantages of using the ECS are more prominent.

Because of the features of the ECS mentioned above, we used the ECS primarily to do the simulations which need very long runs such as surface-initiated melting and the calculation of physical properties using fluctuations. These works will be discussed in chapter 3 and chapter 4.

1.4 Some Details of the Simulation

1.4.1 The Model Molecule and the Potential Function

In the simulation of SF_6, the molecules are treated as rigid bodies and the L-J potential function (equation 1.13) is used for the interactions between the fluorine atoms of different molecules. The S-F bond length is taken as the exact experimental value so it is very much an atom-atom model. However, as a simplification measure, the interactions involving sulphur atoms are assumed to be included in the interactions between the fluorine atoms[31]. So in fact, the model has the features of both the atom-atom and point-point methods. This simplification can reduce the work of calculating the intermolecular forces by about 20% while the main geometric feature of the SF_6 molecule is retained. One possible shortcoming of this model seems to be that the molecule might be slightly less spherical than a real one, though no convincing evidence of this has occurred in our simulation so far.

1.4.2 The Integration Algorithm

To integrate the equations 1.8a, 1.8b and 1.8c numerically, we need an integration algorithm. In this work we use a hybrid Beeman algorithm[36] which divides one iteration into three steps as

$$1)\quad x(t+\delta t) = x(t) + \dot{x}(t)\delta t + \frac{1}{6}(4\ddot{x}(t) - \ddot{x}(t-\delta t))\delta t^2 \tag{1.20a}$$

$$2)\quad \dot{x}(t+\delta t) = \dot{x}(t) + \frac{1}{2}(3\ddot{x}(t) - \ddot{x}(t-\delta t))\delta t \tag{1.20b}$$

$$3)\quad \dot{x}(t+\delta t) = \dot{x}(t) + \frac{1}{6}(2\ddot{x}(t+\delta t) + 5\ddot{x}(t) - \ddot{x}(t-\delta t))\delta t \tag{1.20c}$$

where x is a generalized coordinate. The original Beeman algorithm does not have the step 2 [39]. We need this extra predictor step because in the PR MD method the second derivatives are dependent on the first derivatives as can be seen in equation 1.8a, 1.8b and 1.10. As a result, the second derivatives cannot be calculated from the equations of motion before the first derivatives are known. The first derivatives are calculated again in step 3, but this time the second derivatives at the same time $t + \delta t$ are calculated from the equations of motion using the first derivatives from step 2. The second and the third steps can be iterated more than once to gain higher accuracy. This algorithm has been used successfully in the MD simulation of n-butane[36, 40]. Both in the work of n-butane and the present work on SF_6, it is found that steps 2 and 3 only need to be iterated once to get satisfactory accuracy.

Some other commonly used integration algorithms are, for example, the Verlet[41] and leapfrog[42] algorithms. In these algorithms, as in the Beeman[39] algorithm, the highest order of the time increment δt is two[43]. It has been found that the trajectories obtained through these three algorithms are the same if the initial conditions are identical, but the calculation of the kinetic energy is different[44, 45, 46]. Some comparisons of these algorithms in simulations have been made only on some simple models such as the 1D oscillator[44] and the atomic liquid[46]. It seems that the Beeman and leapfrog methods tend to overestimate and the Verlet method underestimates the kinetic energy[46]. This problem becomes serious only when the timestep is large. Because of this, Amini and co-workers suggested some methods of improving the calculation of the kinetic energy in MD simulations[46].

The drawbacks of their method are that the computer storage has to be increased and the instantaneous kinetic energy and the potential energy are not calculated simultaneously. In the present simulation we use equation 1.20c to define the velocity and the kinetic energy directly, and the results are satisfactory.

1.4.3 Cut-off and Corrections

In order to save computer time, the intermolecular forces used in MD simulations usually have a cut-off distance r_c beyond which the interactions are ignored. This can be a good approximation especially for the simulation of molecular substances because of their short-distance inter-molecular forces. As a compensation to this approximation, correction terms can be added when the potential energy and the stress tensor are calculated. These corrections are calculated by assuming a uniform distribution of the molecules beyond r_c and ignoring the term of repulsive force. The cut-off correction of the potential energy is

$$\delta\phi = -\frac{24N\pi(4\epsilon\sigma^6)}{Vr_c{}^3} \tag{1.21a}$$

for each molecule and the cut-off correction for the diagonal terms in the stress tensor is

$$\delta\Pi_{ii} = \frac{2N\delta\phi}{V}. \tag{1.21b}$$

The corrections for the three diagonal terms are the same and for the off-diagonal terms the corrections are zero if the molecular density distribution of the system is isotropic.

The ways of imposing the cut-off are different in the programs on the DAP and the ECS. Consequently there is a small difference in calculating the corrections. On the ECS, there is a cut-off distance which can be chosen for each simulation run so the calculation of the corrections is a straightforward use of equations 1.21a and 1.22a On the DAP, however, the cut-off is realized through the use of a fixed neighbour list. Any neighbours which are not in the list are ignored in the calculation of the forces and torques, so it is not necessary to have an extra cut-off distance parameter. To calculate the corrections the cut-off distance can be

defined as

$$\frac{4\pi}{3}r_c^3 = 15\frac{V_s}{2} \tag{1.22}$$

because each molecule has 8 nearest and 6 next-nearest neighbours and the cut-off distance is defined as the 'radius' of the cluster of the molecule and its 14 neighbours. The potential energy and the stress tensor corrections now become

$$\delta\phi = -\frac{128\pi^2(4\epsilon\sigma^6)}{15V_s^2} \tag{1.23a}$$

and

$$\delta\Pi_{ii} = -\frac{4\delta\phi}{V_s}. \tag{1.23b}$$

For SF_6 the typical values of these corrections are about 2(kJ/mol) for the potential energy, which is about 10% of the total potential energy at 150K, and 0.7kbar for the stress tensor.

In an attempt to make the simulations on the DAP and the ECS as similar as possible, the cut-off distance on the ECS is chosen so that in the simulations of the solid phase only the nearest and the next-nearest neighbours are included in the neighbour list. If the simulation on the DAP has been carried out, the cut-off distance to be used in the simulation on the ECS can be calculated from equation 1.22. For example, at about 150K, the cut-off distance calculated from the equation is about 7Å. Figure 1.5 shows the radial distribution function (r.d.f) based on the simulation on the ECS and from which we can see that nearest and the next-nearest neighbours have a very clear separation from the more distant molecules at about 7Å, the use of this cut-off distance on the ECS is justifiable.

1.5 Early Runs

In the PR MD method the total Hamiltonian becomes

$$\mathcal{H} = \frac{1}{2}\sum_i m_i \dot{s}_i^t G \dot{s}_i + \sum_{i<j} u(r_{ij}) + \frac{1}{2}WTr(\dot{h}^t\dot{h}) + pV \tag{1.24}$$

and is conserved[11] though the total energy E=U+K is not conserved. In the equilibrium state, the term with $\dot{h}$ is small so the Hamiltonian approximately

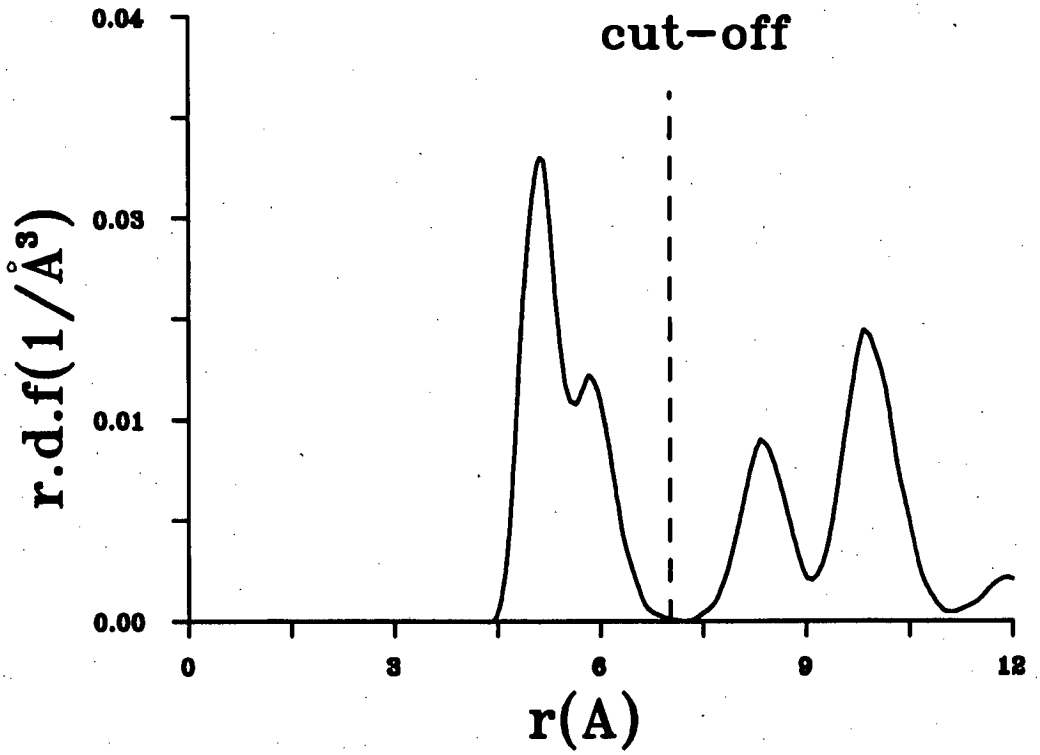

Figure 1.5: The radial distribution function (r.d.f) and the cut-off distance at about 150K.

equals the enthalpy

$$H = E + pV.$$

When in the equilibrium state and at zero pressure, the $\dot{h}$ term and the pressure term vanish and the total energy should be almost identical to the Hamiltonian and thus very close to being constant. In figure 1.6, we show the time evolution of the potential energy U, the internal pressure p and the deviation of the total energy from its initial value in a test run on the DAP. In the test run, the initial value of the lattice parameter a was 5.786Å and this corresponds to a static lattice energy of -4.8458kcal/mol or -20.26kJ/mol if the four-fold axes of the SF_6 molecules are aligned with the axes of the three cubic unit-cell vectors. In this run the timestep was set at 0.015ps, the piston was 20,000 a.m.u($a$tomic $m$ass $u$nit), the external pressure was zero and the total number of molecules was 3072. From the figure we can see the following features.

- After about 1ps in simulation time, the potential energy has become noticeably lower than the initial value, which is the minimum value when the

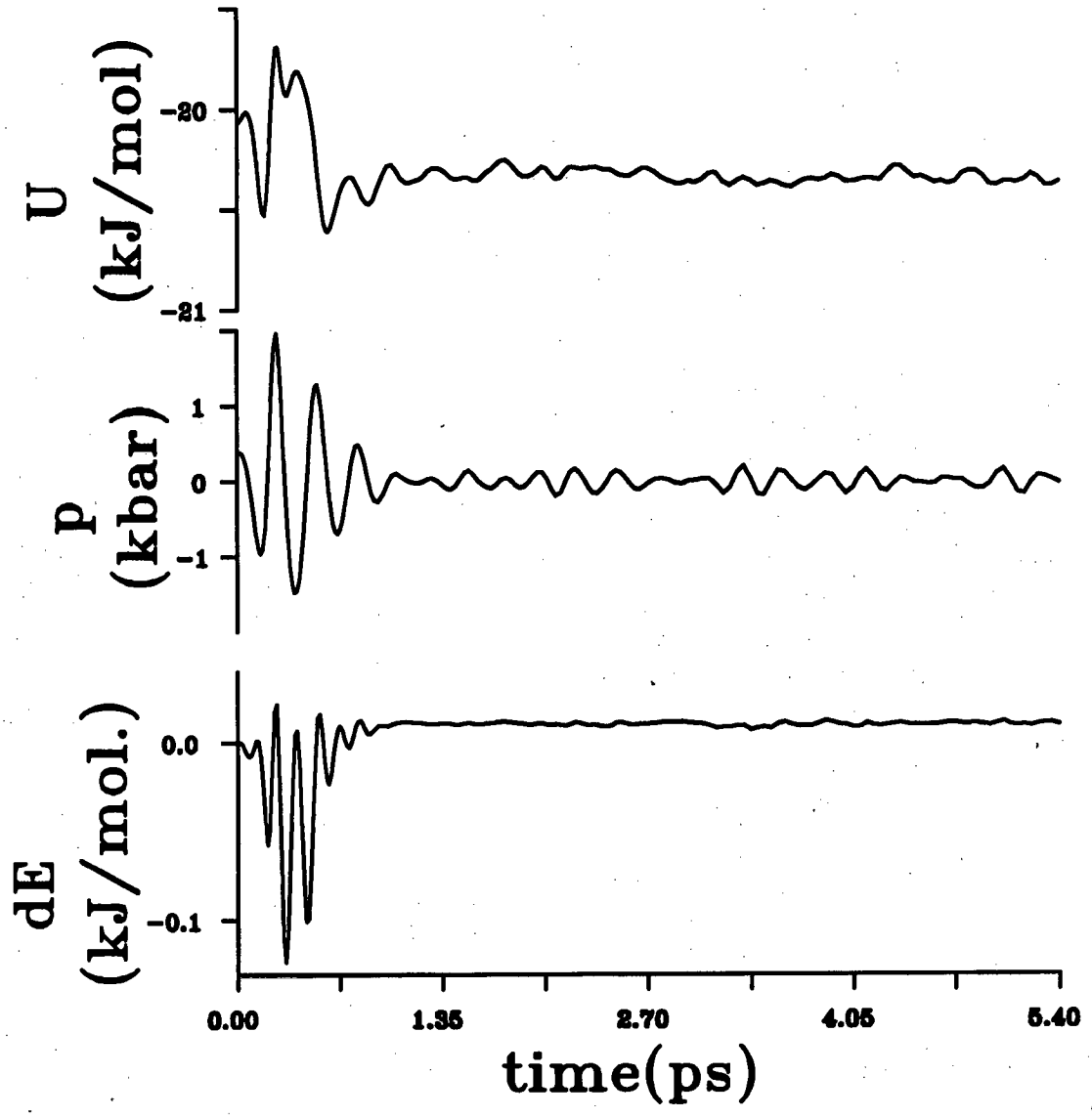

Figure 1.6: The time evolution of some properties starting from the unphysical situation described in the text. dE=E(t)−E(0)

lattice and molecules are static and the the S-F bonds of the molecules are aligned with the bcc unit cell axces. This shows that when the molecular orientations become dynamically disordered the system becomes more stable.

- The pressure only fluctuates around zero and the amplitude decays quickly. This is exactly what we need in this (HPN) MD simulation because the required pressure is zero in this particular run.
- There is large deviation of the total energy from the initial value in the early stages of the run and this is caused by the term with $\dot{h}$ in the Lagrangian in equation 1.7. From the figure it is evident that the influence of this term on the total energy is negligible after about 1ps.

Figure 1.7 shows the configurations of some molecules in the x-y plane at the end of the run. The molecules are on a lattice but the orientations are disordered, the microscopic feature of a plastic crystal.

The Volume Fluctuation

One of the problems of the PR method is to choose the value of the piston mass W. In the following part of this section we first investigate the relation between W and the frequency of the volume fluctuation based on the formulae given previously. Then we prove that in order for the integration algorithm to be stable there is a lower limit of choosing W.

Figure 1.8 shows the results from two runs with different choices of the piston mass. The figure shows that when W is 320,000a.m.u, the period of the volume fluctuation, τ, is about four times the period when W is 20,000a.m.u. This is in agreement with equation 1.18 which indicates that the period is proportional to the square root of W. From equation 1.18 we can also calculate the value of the periods if the bulk modulus is known. In chapter 4 we will see that the bulk modulus is about 40kbar when the temperature is around 170K. By substituting the value of the bulk modulus into equation 1.18, the period is calculated to be about 0.35ps and 1.4ps for the two values of the piston mass respectively. These results are very close to the corresponding values estimated from figure 1.8.

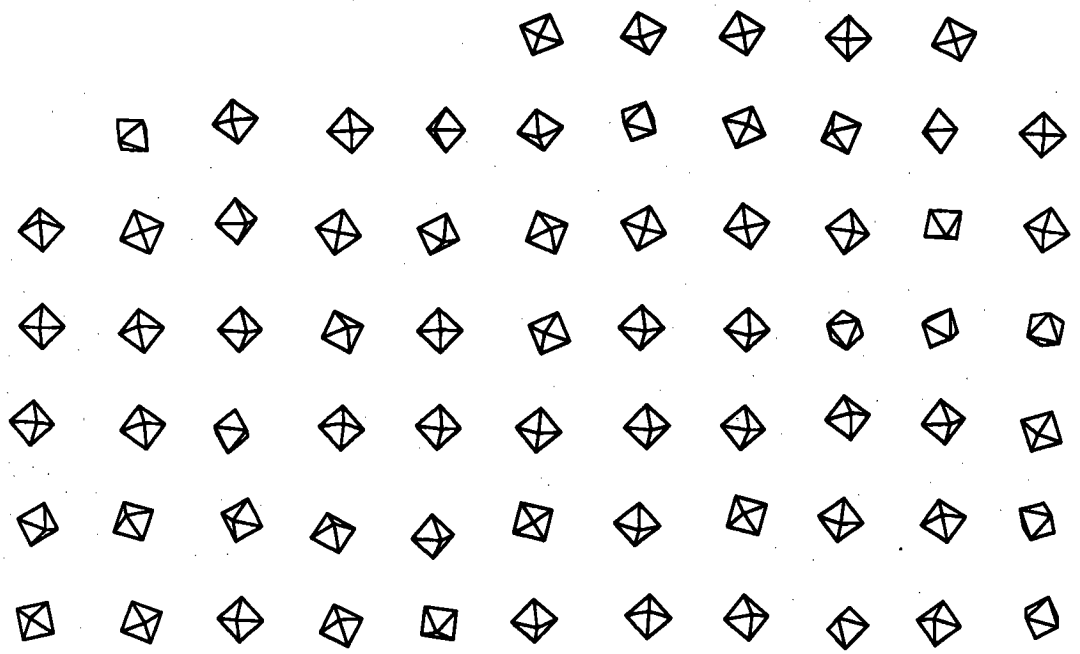

Figure 1.7: Snapshot of some molecules at the end of the test run. The molecules are on the x-y plane.

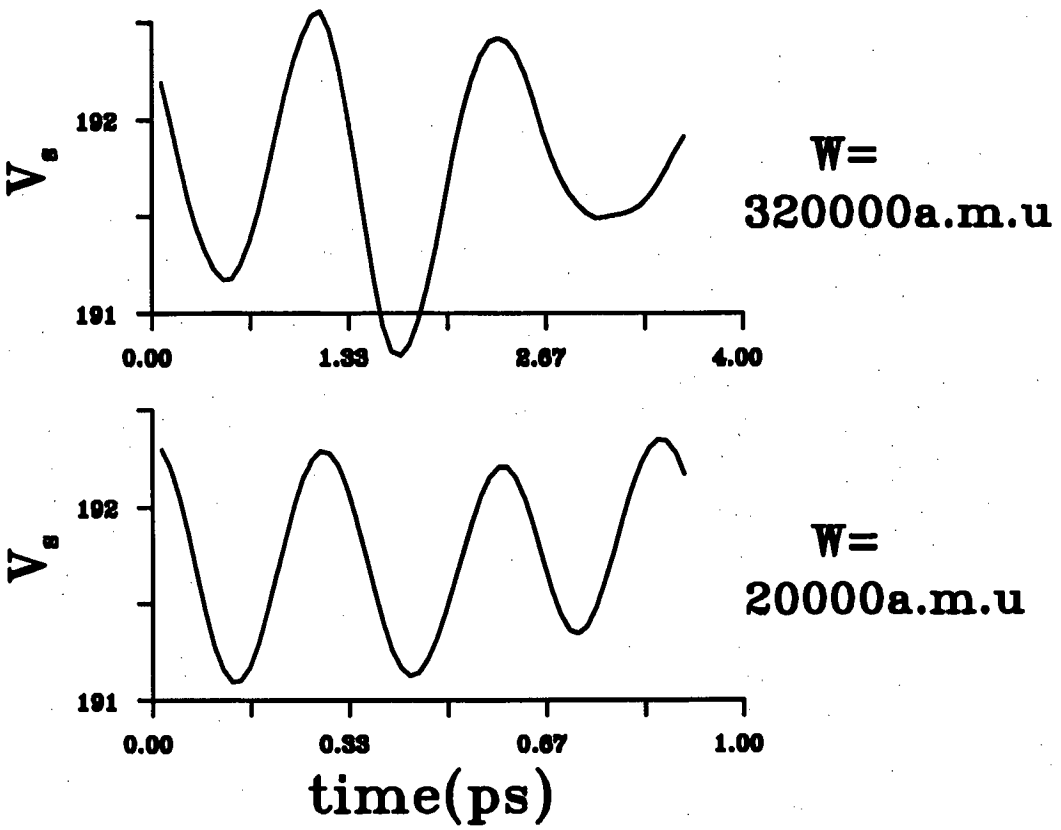

Figure 1.8: Comparing the periods of volume fluctuations under different piston mass W.

Because the parameter W is adjustable and the fluctuation of the MD cell is relatively simple compared to the molecular movements, we can test the stability of the integration algorithm by varying the ratio between the period of the volume fluctuation and the timestep. It was found that when this ratio is less than 4 the system becomes very unstable. This outcome is not very far away from the result of a test on a 1D oscillator which suggested that the similar ratio is 2[42].

The result from our test also suggests that the value of W should not be too small. For a system of any number of molecules and the timestep for the simulation is δt, W should satisfy the inequality relation

$$\tau > 4\delta t, \tag{1.25}$$

where τ is defined in equation 1.18. For the system under discussion, this becomes approximately

$$W > 3 \times 10^6 \delta t^2, \tag{1.26a}$$

where the unit of δt is ps and the unit of W is a.m.u. When δt=0.015ps, this lower limit of W is 675a.m.u.

If the h matrix is defined by the basic vectors of the MD-cell, the above formula becomes

$$W > 2.2 \times 10^4 \delta t^2. \tag{1.26b}$$

When δt=0.015ps, this lower limit of W is approximately 5a.m.u.

1.6 The Aims

The aims of the present MD simulations of SF_6 can be summarized as follows.

- To study the low-temperature structure of SF_6 and try to explain the controversy over the intermediate phase. Through this study we also demonstrate the ways of simulating single crystals on the DAP.
- To investigate the applicability of the PR MD method in searching for unknown structures.
- To exploit the MD method to study the melting of SF_6 – an example of the application of MD to the study of nonequilibrium processes.
- To calculate the elastic properties and other properties, especially their behaviour near phase transitions. The method is to use the fluctuations of some other more readily available properties such as the MD-cell matrix, volume and temperature.

Chapter 2

The Low-temperature Structure

2.1 Introduction

This chapter is a study of the low-temperature phase and the solid-solid phase transition in SF_6 through the PR MD method. Experiments have shown that between 96K and the melting point, which is 223K, the SF_6 molecules are translationally ordered with a bcc structure but orientationally disordered[17]. In this phase the molecules librate with large amplitude and frequently reorient between their symmetric positions. When the temperature is below 96K, the orientational disorder is frozen out and the structure shears to become truly crystalline with a symmetry lower than bcc. Not long ago, some neutron diffraction experiments on SF_6 revealed that this true crystalline phase has a monoclinic structure with space group C2/m, the structure having two unidentical sites accounting for one-third and two-thirds of the molecules[28]. The molecules occupying inequivalent sites have both different orientations and different environments. Later in this chapter we refer to these two groups of molecules as the minority (or molecule 1) and the majority (or molecule 2). We will find that these two groups of molecules have very different thermal motions.

About the low-temperature structure of SF_6 there has been a controversy. On the one hand, neutron powder diffraction results show that the substance has only a monoclinic structure[28]. On the other hand, an electron diffraction experiment[26]

showed some evidence of the existence of another phase at temperatures between 96K and about 50K. This phase, the intermediate phase as we will call it, has a structure of trigonal symmetry. In this phase, the minority molecules become orientationally disordered and the majority remain ordered. Below 50K, both the two experiments agree with very similar results. MD simulation[34] has also achieved an intermediate phase which is in agreement with the electron diffraction experiment. In those MD simulations, a modified constant-volume method was used, whereby the system could be kept at a certain pressure but shear stress could still develop so any possible structural changes would be hindered. In the present work, we use a stress-free MD. One purpose of this simulation was to look for the intermediate phase and try to explain the difference between the two experimental results. In doing so, we will illustrate that the transitions studied in MD simulations do not need to be between two perfect single crystals. Our conclusion is that the PR[10] technique has aided the discovery of the developing phase to a considerable extent, and that its use for such model prediction is totally justified.

Part of the work described in this chapter has been written into two papers[51, 52].

2.2 Details of the Simulation

2.2.1 The Implementation

The simulations were performed on an AMT DAP with 1024 PEs. Since the ratio between the numbers of molecule 1 and molecule 2 is 1:2 the total number of molecules in a sample has to be a multiple of three so that the system can make a single crystal. Because of this requirement and of our desire to have a large system, a sample of 3×1024 molecules is used and the skew boundary conditions are carefully chosen. One choice of the neighbour list corresponding to the system with 3072 molecules is as given in table 2.1 (see chapter 1 for the meaning of the table). The PEs are used as a one-dimensional cyclic string to implement the skew cyclic condition, each PE containing information for three molecules. From

Relative Index ρ	Relative Space Vectors $\mathbf{v}$
121 (31)	(+0.5,+0.5,+0.5)
120 (30)	(−0.5,+0.5,+0.5)
110 (26)	(+0.5,−0.5,+0.5)
109 (25)	(−0.5,−0.5,+0.5)
1 (1)	(+1.0,+0.0,+0.0)
11 (5)	(+0.0,+1.0,+0.0)
230(56)	(+0.0,+0.0,+1.0)

Table 2.1: The neighbour list for the systems of 3072 molecules, using the skew boundary conditions. The relative index of the neighbour list for a system of 384 molecules is also given (in the brackets).

the table, the three basic vectors of the MD-cell can be worked out as

$$\begin{aligned} \mathbf{u} &= (11, -1, 0), \\ \mathbf{v} &= (-0.5, 10.5, -0.5), \\ \mathbf{w} &= (5, 7, 13). \end{aligned}$$

Here the unit corresponds to bcc unit cell.

As a result of the skew boundary conditions the shape of the MD-cell is clearly not orthogonal even in the bcc phase. Since the list also determines the boundary conditions it is designed in such a way that a single crystal can be formed in both the plastic and the truly crystalline phase. This is important because we would like to observe the transition between single crystals in the two phases.

To investigate possible finite-size effects smaller systems have also been simulated. The program for the sample of 3072 molecules is easily adapted to simulate these systems. For smaller systems, the neighbour lists have to be different; as an example the neighbour list for a system of 384 molecules is given in Table 2.1.

The potential function which governs the interactions of SF_6 molecules is the two-parameter L-J pairwise potential function (see equation 1.13). The value of σ was first estimated as 2.7Å, based on the experimental data about the bcc structure

of SF_6[31] and was later improved to a value of 2.859Å using new experimental data [27]. The value of ϵ is 2.34kJ/mol and the S-F bond length is 1.566Å. In the present work these two values will be used and a comparison of the results will be given.

2.2.2 The Structure

As is well known, the structure of a model system can often be studied by the molecular packing analysis[48]. Given the model potential(s), the structure may be obtained by analyzing the potential energy variation when the packing parameters are being adjusted. The stable structure is then considered to be the one with the lowest potential energy. This method is useful especially at low temperature when the Gibbs free energy might be close to the internal energy. Naturally, this method has some limitations. First of all, as it is a static method it does not give any information about the thermal motion of the constituent molecules. Secondly it is a zero temperature approximation so the study of the temperature dependence of the structure is either difficult or impossible. Thirdly, the success of the method depends much on the knowledge of the structure. If the structure is not well understood, many configurations have to be tested in order to find the one which really has the minimum potential energy. In the MD method, the first two difficulties do not arise because temperature is naturally embedded in the method. As for the third one we will show that it still exists within a practical simulation time-scale, but the problem does not seem to be very serious, at least for SF_6.

In order that the system quickly enters the targeted thermodynamic equilibrium state, the initial structure should not be too far away from the true structure determined by experiments. However, it is also interesting to see how the PR method makes it possible to simulate the structural change of a bulk sample. This is important because, firstly, experimental data is not always available or sufficient and, secondly, a model may not always very good so that the best structure for a model may be quite different from the true structure. So, instead of making the initial structure completely the same as the monoclinic structure, we started

from a configuration which resembles the true structure in terms of the molecular orientations but not the lattice structure. In fact, the molecular centres were placed on a bcc lattice.

The simulations were performed for the two σ values and the results for σ=2.859 are shown in table 2.2. As for the SF bond length, a value of 1.566Å, which can be compared with the neutron diffraction data in [28], has been used in the simulation at all temperatures. The system starts from a bcc lattice with the three basic vectors aligned with the three axes of the laboratory coordinate system, which is fixed in space throughout the simulation. In the course of the equilibration stage the bcc lattice becomes distorted and so does the shape of the MD-cell. For the sake of convenience, the bcc system will still be used for defining cell vectors. For example, the three cell vectors of the single monoclinic crystal can be expressed in the scaled coordinates system throughout the simulation as

$$\mathbf{a} = (1, -1, 2), \quad \mathbf{b} = (-1, -1, 0), \quad \mathbf{c} = (1, -1, -1)/2.$$

If we use the laboratory system the cell vectors will change a little from

$$\mathbf{a} = (1, -1, 2)a, \quad \mathbf{b} = (-1, -1, 0)a, \quad \mathbf{c} = (1, -1, -1)a/2,$$

where a is the bcc unit-cell parameter in the plastic phase, to become

$$\mathbf{a} = (5.06, -5.55, 11.76)\text{Å}, \quad \mathbf{b} = (-6.10, -5.61, 0)\text{Å}, \quad \mathbf{c} = (2.59, -2.82, -2.94)\text{Å},$$

at 85 K in the truly crystalline phase.

In figure 2.1, the total energy, the pressure and the MD-cell parameters are plotted as functions of time in the early stage of the simulation run. This figure shows the process of the system evolving from the initial pseudo-bcc structure to the monoclinic structure. In the first 1.5ps or so, there is much uncertainty in the transformation, and the MD-cell parameters, the pressure and the total energy oscillate in large amplitudes. After this stage the monoclinic structure prevails and the splits of the cell dimensions and the angles become certain, the pressure becomes very near zero and the total energy becomes much lower than in the initial state. In this run, the temperature was kept at a constant value of about 75K by rescaling the velocities every four timesteps, one timestep being 0.01ps. According

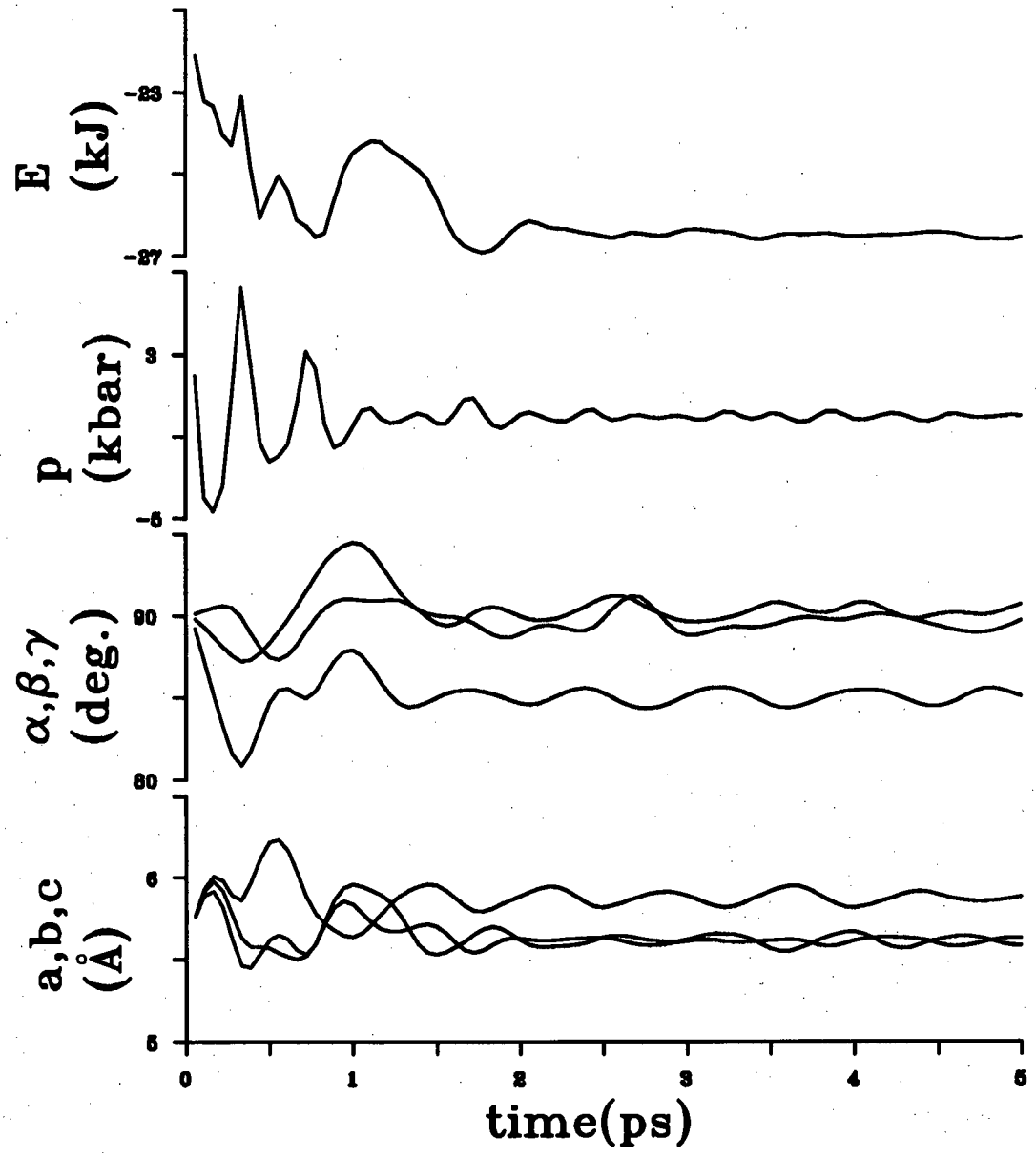

Figure 2.1: The evolution of the total energy, pressure and the MD-cell parameters in the first 5ps of the run. The monoclinic structure is formed after about 1.5ps.

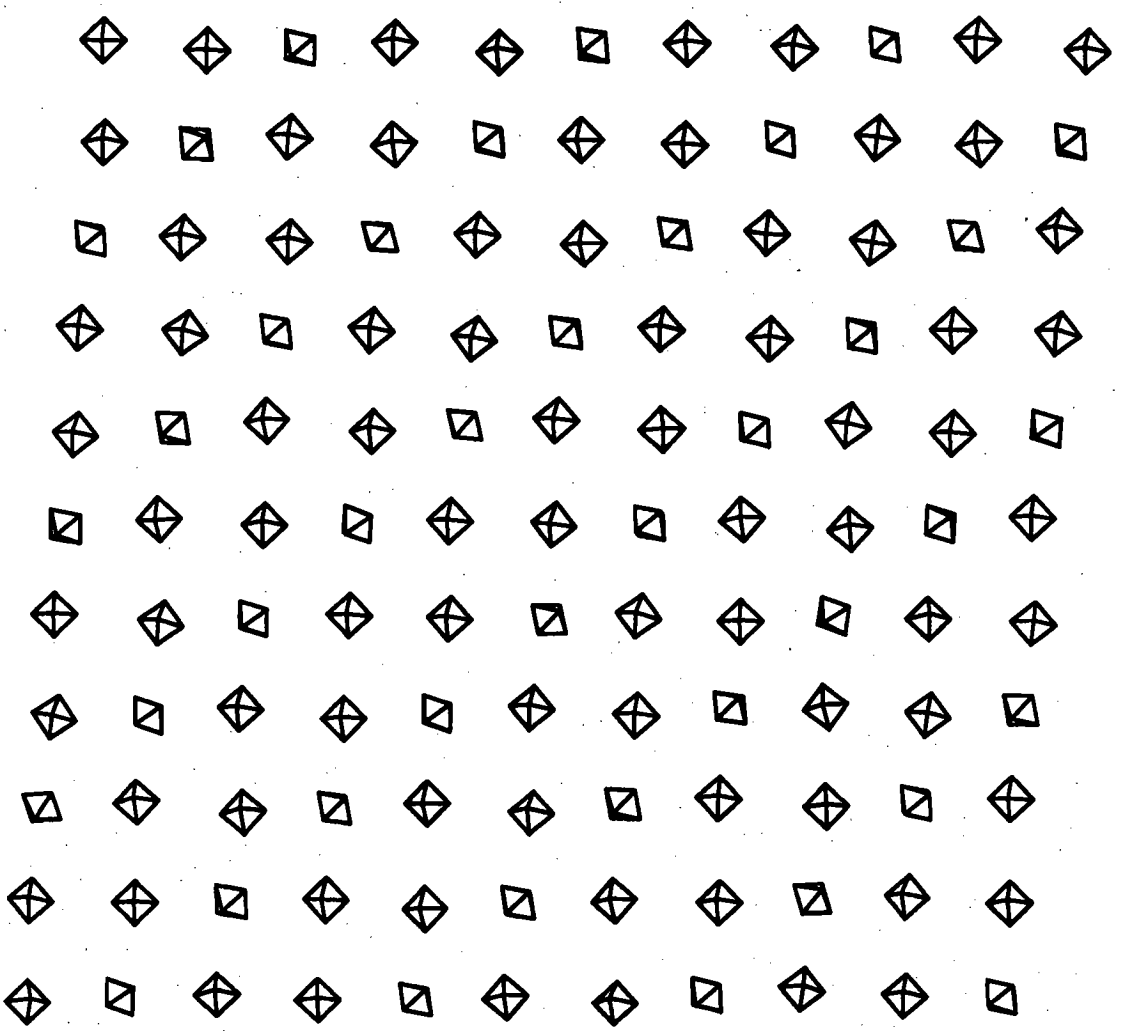

Figure 2.2: One layer of molecules from a single crystal at 85K. These molecules lie in the x-y plane of the laboratory coordinates system.

to our experience, if this procedure is changed one may get other structures other than the monoclinic one. This problem will be dealt with later in this chapter.

Figure 2.2 shows a layer of molecules, which are drawn as octahedra, on the x-y plane in the low-temperature phase. The molecules are well ordered both in their positions and orientations. According to their orientations the molecules can be classified into two groups–molecule 1 and 2. This ordering remains until the MD temperature reaches above 140K. A hysteresis of about 15K was observed, a phenomenon which, to our knowledge, has not yet been reported experimentally. Thus the simulated system has a higher crystal-to-plastic transition temperature than the true system even if the hysteresis is taken into account. Further adjustment of the potential parameters may be effective in fitting the transition temperature to the experimental value but it may not be so attractive as other aspects of the model may be affected to the worse. Besides, the phase transition temperature is difficult to locate precisely in MD simulations. If the transition from the monoclinic phase to the plastic phase happens between single crystals the small size of the MD sample and its unrealistic purity may result in seemingly much higher transition temperature which cannot be explained by the possible hysteresis in a first order phase transition.

In the simulations the orientation of a molecule is represented by a unit quaternion[53]

$$q = (q_0; q_1, q_2, q_3). \tag{2.1}$$

In terms of the components of a quaternion the rotation matrix which links the molecular body coordinate system to the space coordinate system becomes

$$R = \begin{pmatrix} q_1^2 - q_2^2 - q_3^2 + q_0^2 & 2(q_1q_2 - q_3q_0) & 2(q_1q_3 + q_2q_0) \\ 2(q_1q_2 + q_3q_0) & -q_1^2 + q_2^2 - q_3^2 + q_0^2 & 2(q_2q_3 - q_1q_0) \\ 2(q_1q_3 - q_2q_0) & 2(q_2q_3 + q_1q_0) & -q_1^2 - q_2^2 + q_3^2 + q_0^2 \end{pmatrix}.$$

The rotation matrix can also be expressed in terms of the more easily understandable Euler angles and by comparing the two different expressions the relations between a quaternion and the euler angles are found to be

$$\begin{aligned} q_0 &= cos\frac{\theta}{2}cos\frac{\psi+\phi}{2}, \quad q_1 = sin\frac{\theta}{2}sin\frac{\psi-\phi}{2}, \\ q_2 &= sin\frac{\theta}{2}cos\frac{\psi-\phi}{2}, \quad q_3 = cos\frac{\theta}{2}sin\frac{\psi+\phi}{2}, \end{aligned} \tag{2.2}$$

Temperature(K)	18	23	75	85
Lattice parameters				
a(Å)	13.760(2)	13.77(2)	13.928(9)	13.96(1)
b(Å)	8.193(1)	8.20(1)	8.2696(6)	8.2849(5)
c(Å)	4.7736(8)	4.778(7)	4.8214(4)	4.8320(4)
α(deg.)	89.999(3)	89.993(3)	90.00(6)	89.997(9)
β(deg.)	95.434(5)	95.41(5)	95.15(9)	95.08(1)
γ(deg.)	90.00(4)	89.997(3)	89.987(6)	89.990(8)
Unit-cell volume(Å^3)	535.7(3)	537.1(2)	553.10(4)	556.71(6)
Euler angles(deg.)				
molecule 1				
θ_1	−30.8(2)	−30.9(2)	−31.3(5)	−31.3(5)
δ_1	0.07	0.04	0.33	0.21
molecule 2				
θ_2	47.3(2)	47.6(2)	48.4(3)	48.4(4)
δ_2	0.04	0.05	0.16	0.12
Centre of mass				
molecule 2				
x(Å)	4.379(9)	4.384(8)	4.4429(5)	4.4560(6)
y(Å)	0.00002(8)	0.0002(1)	0.0003(3)	0.0004(4)
z(Å)	1.9904(8)	1.991(4)	1.9959(2)	1.9969(3)

Table 2.2: The temperature dependence of the MD structural parameters for the monoclinic phase of SF_6. The space group is C2/m, bond length = 1.566Å, σ = 2.859Å. The centre of mass of molecule 1 is at the origin. δ_i is the angle between the unique axis of the monoclinic cell and the diad axis of the molecules which becomes zero in the thermodynamic limit. The euler angles ϕ_i and ψ_i are equal to the ideal symmetry-fixed values within statistical error.

where q_i is the ith component of the quaternion and the euler angles are defined as in[47]. The order of applying the rotation operation corresponding to the three euler angles is ϕ, θ and ψ. If a different definition (convention) is used the above relations will change as the reader will find in [49]. In the simulation, the quaternions are referred to the laboratory system. In the above formulae, however, the quaternion represents the molecular rotation about orthogonal axes **X**,**Y**, **Z** related to crystal lattice **x**, **y**, **z** by $\mathbf{X}\|\mathbf{x}$, $\mathbf{Y}\|\mathbf{y}$ and $\mathbf{Z}\|\mathbf{X}\times\mathbf{Y}$ where **x** , **y** and **z** are the vectors along the three monoclinic unit-cell axes. The euler angles ϕ and ψ have the values 0° and 45°(misprinted as 90° in [28]) respectively as required by the symmetry. Our measurements are consistent with these values to within the limits of error as evidenced by δ_i in table 2.2, and the atomic positions in fractional units are listed in table 2.3. The value of δ_i in table 2.2 is the deviation of the molecular diad axis from the unique axis of the monoclinic unit-cell and these two axes should be in line with each other if the structure is ideal. Therefore δ_i can be used as a measurement of the system's deviation from the monoclinic structure. The δ_i's can be evaluated as follows.

The ideal orientation of a molecule occupying one of the two distinct sites in the monoclinic structure is represented by a quaternion q_e. One of the diad axes coincides with the unique axis of the monoclinic unit-cell. The orientational difference between this ideal molecule and the mean quaternion value , q_m, which represents the mean orientation of a group of molecules, can be calculated from

$$\Delta q = \left((1 - \Delta q_1^2 - \Delta q_2^2 - \Delta q_3^2)^{1/2}; \Delta q_1, \Delta q_2, \Delta q_3\right) = q_m q_e^{-1} \tag{2.3}$$

and Δq can also be termed as

$$\Delta q = (cos(\delta'/2); sin(\delta'/2)\mathbf{l}). \tag{2.4}$$

This expression means that if the molecule representing the mean orientation of the group of molecules is rotated by an angle of δ' about axis **l**, the molecule will have the ideal orientation as represented by q_e.

Combining equations 2.3 and 2.4, and noting that δ' is small because q_m and q_e are close to each other, δ can be expressed as

$$\delta' = 2(1 - (1 - \Delta q_1^2 - \Delta q_2^2 - \Delta q_3^2)^{1/2})^{1/2}. \tag{2.5}$$

In general the rotation axis **l** is not perpendicular to the unique axis of the monoclinic structure so that δ' is not the angle between the diad axes of the ideal molecule and the molecule representing the mean orientation of the group of molecules. If the angle between **l** and the unique axis is λ then it can be shown that

$$sin(\delta/2) = sin(\delta'/2)sin(\lambda). \tag{2.6}$$

Because δ and δ' are very small this can be reduced to

$$\delta \approx \delta' sin(\lambda). \tag{2.7}$$

In figure 2.3, the monoclinic unit-cell is plotted based on the data in table 2.2 and 2.3. The molecules at the eight corners and the C-centres of the cell are molecule 1 and the rest are molecule 2. From this figure the packing of all the atoms in the unit-cell is clear. The temperature dependence of the parameters from the simulation and the neutron diffraction experiments are shown in figure 2.4. The agreement between the MD results and the neutron diffraction data is good and the improved σ clearly gives a more accurate set of lattice constants.

To assess the change in the shape of the monoclinic unit-cell with temperature, we can introduce three strain components e_1, e_2 and e_3[28]. They are defined by the unit-cell parameters as

$$e_1 = 1 - \frac{4\sqrt{2}c}{(a+\sqrt{3}b)}, \quad e_2 = tan(\beta - 90), \quad e_3 = \frac{\sqrt{3}b - a}{\sqrt{3}b + a}. \tag{2.8}$$

The results are given in table 2.4, from which one can see a similar trend in the structural deformation as shown by neutron diffraction experiments[28]. The parameter e_1 has the least temperature dependence and e_3 is closely proportional to $(e_2)^2$.

Temperature(K)		18	23	75	85
Molecule 1	x	-0.0651	-0.0650	-0.0641	-0.0640
F	y	-0.1352	-0.1350	-0.1339	-0.1336
	z	0.1198	0.1199	0.1202	0.1204
	x	-0.0678	-0.0678	-0.0673	-0.0672
F	y	0.0000	0.0000	0.0000	0.0000
	z	-0.2826	-0.2822	-0.2783	-0.2773
	x	0.0651	0.0650	0.0641	0.0639
F	y	-0.1352	-0.1351	-0.1339	-0.1337
	z	-0.1198	-0.1200	-0.1202	-0.1203
Molecule 2	x	0.3320	0.3320	0.3319	0.3320
S	y	0.0000	0.0000	0.0000	0.0000
	z	0.4188	0.4187	0.4156	0.4149
	x	0.3921	0.3920	0.3902	0.3898
F	y	-0.1352	0.1351	-0.1339	-0.1336
	z	0.5905	0.5903	0.5877	0.5870
	x	0.2720	0.2721	0.2736	0.2740
F	y	-0.1352	-0.1351	-0.1339	-0.1337
	z	0.2472	0.2470	0.2436	0.2428
	x	0.4086	0.4086	0.4090	0.4092
F	y	0.0000	0.0000	0.0000	0.0000
	z	0.1960	0.1963	0.1984	0.1990
	x	0.2720	0.2721	0.2736	0.2740
F	y	0.1352	0.1351	0.1339	0.1337
	z	0.2472	0.2470	0.2436	0.2428
	x	0.3921	0.3919	0.3902	0.3898
F	y	0.1352	0.1351	0.1339	0.1337
	z	0.5905	0.5903	0.5876	0.5870
	x	0.2555	0.2555	0.2548	0.2546
F	y	0.0000	0.0000	0.0001	0.0000
	z	0.6417	0.6410	0.6329	0.6308

Table 2.3: Fractional atomic positions. Bond length=1.566Å, σ=2.859Å. The S atom of molecule 1 is at the origin.

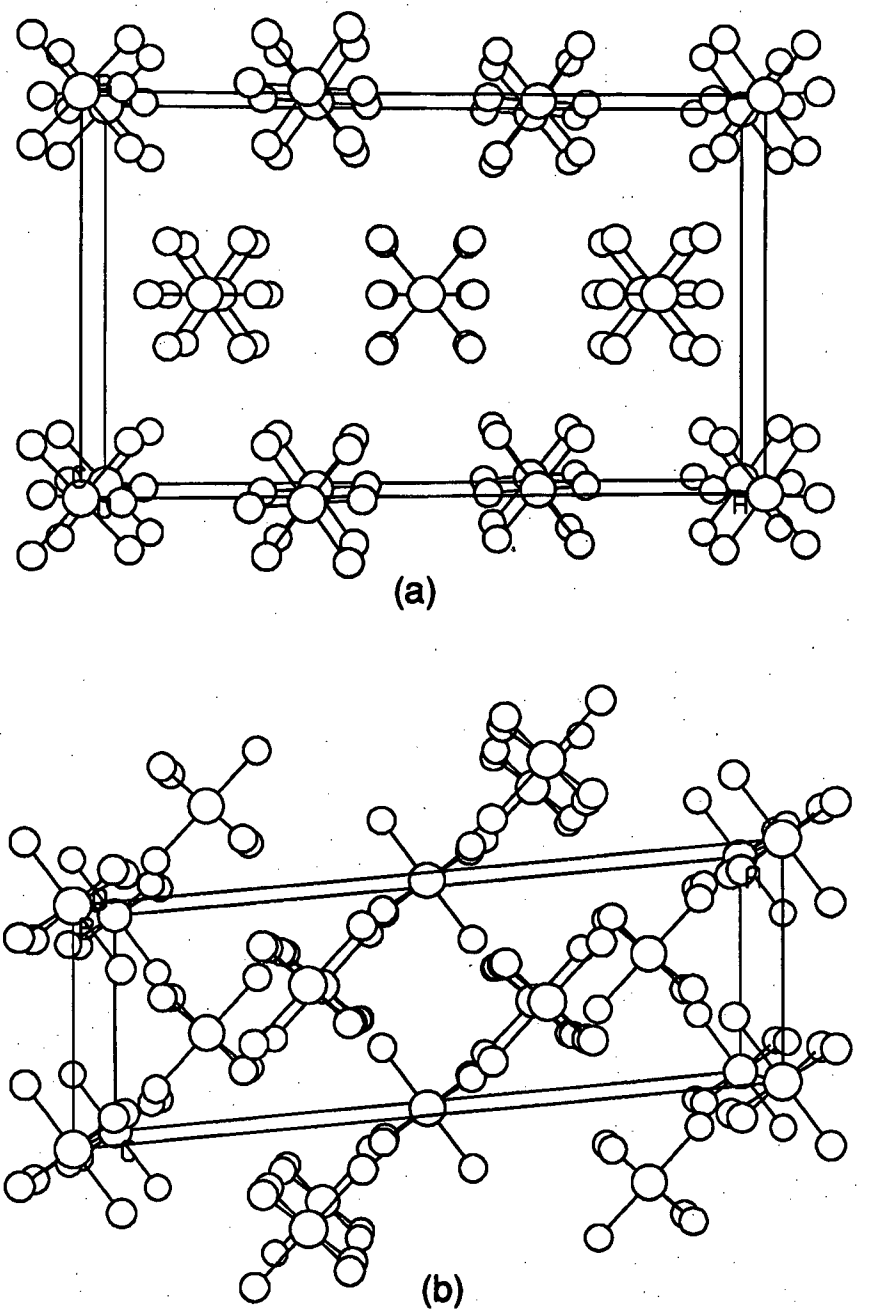

Figure 2.3: The unit-cell of the low-temperature phase of SF_6. In (a) the projection is along c axis and in (b) the projection is along the b axis.

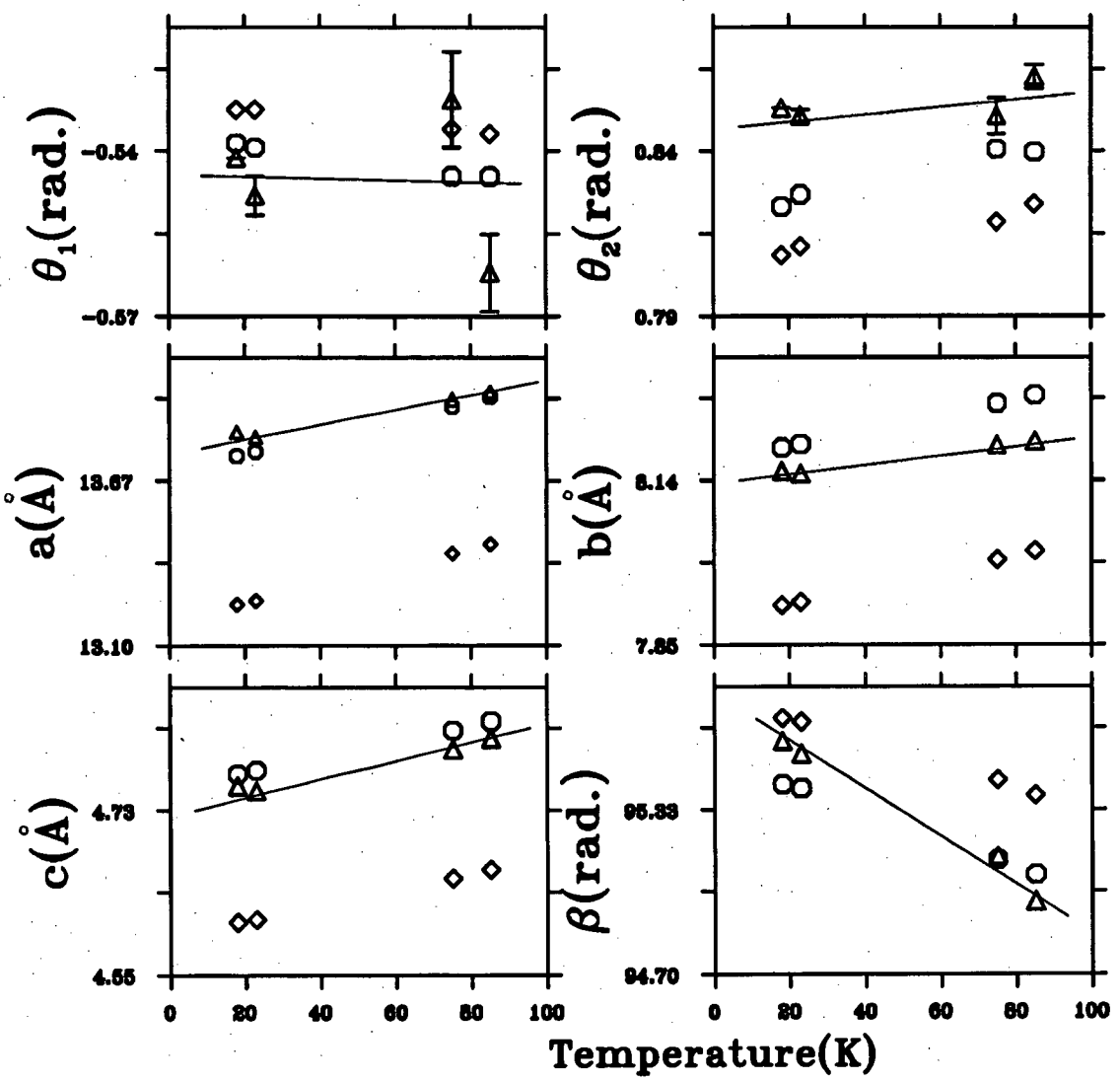

Figure 2.4: The temperature dependence of the monoclinic unit-cell parameters. $\triangle$ derived from neutron scattering data from which the best fit straight lines are given, $\diamond$ $\sigma = 2.7$Å, $\circ$ $\sigma = 2.859$Å. θ_1 and θ_2 are the second Euler angles for molecule 1 and molecule 2 .

T(K)	$e_1(10^{-4})$	$e_2(10^{-4})$	$e_3(10^{-4})$	e_2^2/e_3
18	338.6(5)	951(1)	154.0(2)	5873
23	338.1(5)	947.5(9)	152.8(3)	5906
75	346(1)	901(2)	140.0(5)	5799
85	345(1)	889(2)	137.2(5)	5760
95	348(1)	875(2)	133.0(7)	5757
115	347(1)	842(2)	123.9(7)	5710
135	340(2)	774(3)	110.4(9)	5426

Table 2.4: The temperature dependence of the strain components.

2.2.3 The Thermal Motions

The translational and librational thermal motions of the molecules can be studied via the T-tensors and L-tensors. These tensors are defined as

$$T_{ij} = < dr_i dr_j > \tag{2.9}$$

$$L_{ij} = < d\theta_i d\theta_j > \tag{2.10}$$

where dr_i and $d\theta_i$ are the deviations of the molecular centre position and orientation from the equilibrium values, i and j are cartesian indices. The method of calculating $d\theta_i$ is similar to that used to obtain Δq_i from equation 2.3, the difference being that q_e is replaced by the mean quaternion and q_m is replaced by the quaternion of an individual molecule.

As an example of the advantages of simulating a single crystal, these tensors are easy to calculate for any groups of molecules because of the simplicity in determining the identity of the molecules and the lack of any defects in the sample. The T-tensors and L-tensors at 85K are listed in table 2.5.

In table 2.6, the L-tensors are diagonalized and the principal axes are represented by their direction cosines which refer to three different systems. From the table we can see that the principal axes are not lined up with molecular symmetry axes for either molecule 1 or 2, but for molecule 1 they are very close to the monoclinic unit-cell axes.

	molecule 1			molecule 2		
$T(10^{-3}Å^2)$	11.0	−1.72	0.342	10.75	−0.138	−0.357
		11.4	−0.037		11.9	0.401
			10.0			14.3
$L(10^{-3}rad.^2)$	7.13	−1.70	−2.64	4.72	−0.509	0.085
		10.4	1.43		4.94	−0.083
			7.49			4.74

Table 2.5: The T-tensors and L-tensors at 85K. They are referred to the laboratory coordinate system.

	molecule 1			molecule 2		
$L(10^{-3}rad.^2)$	4.4			4.3		
		9.1			4.7	
			11.5			5.4
A	0.721	0.370	0.583	−0.797	−0.078	0.599
	0.670	−0.591	−0.448	−0.568	−0.245	−0.786
	0.176	0.714	−0.678	0.208	−0.966	0.151
B	0.744	0.430	−0.512	−0.772	0.063	0.632
	0.211	0.576	0.790	−0.617	0.162	−0.770
	0.634	−0.695	0.338	0.151	0.985	0.087
C	0.145	0.972	−0.183	0.112	−0.747	0.655
	−0.984	0.124	−0.126	0.971	0.223	0.090
	−0.111	0.112	0.987	−0.223	0.689	0.689

Table 2.6: The diagonalized L-tensors(L) and the direction cosines of their principal axes(A, referring to the laboratory system, B referring to the molecular body system and C referring to the monoclinic unit-cell) at 85K.

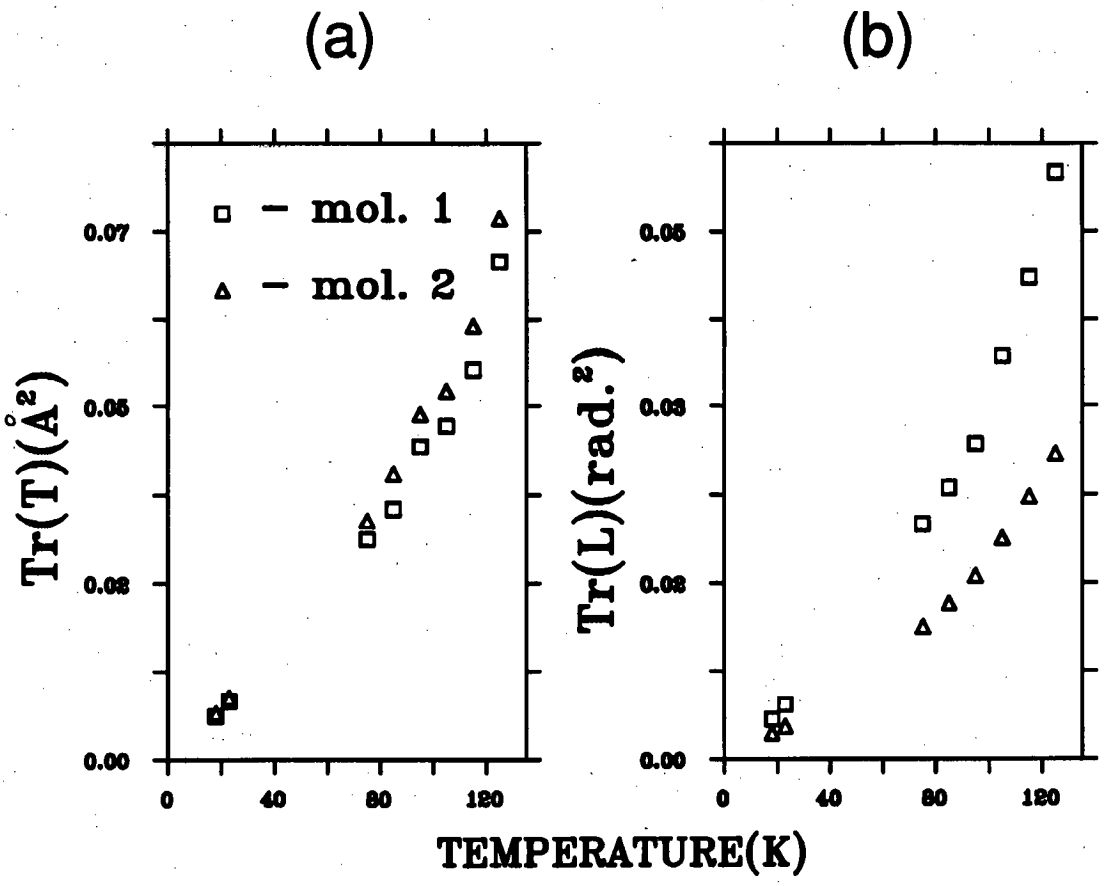

Figure 2.5: The temperature dependence of the traces of the T-tensors and L-tensors.

The temperature dependence of the traces of the tensors are plotted in figure 2.5 These traces represent the translational and librational mean-square deviations of the molecules from their mean positions. These results show that the molecules on the two distinct symmetry sites exhibit quite different behaviour, the minority molecules have significantly larger librational deviations but surprisingly marginally smaller translational deviations than the majority molecules. This demonstrates the different restraints the molecules experience at different sites in the crystal.

In order to understand further the difference between the behaviour of the two sets of molecules, the mean *single-molecule potentials*(SMPs)[50] were calculated. To obtain these potentials, we take a configuration and rotate one molecule about a

molecular symmetry axis and calculate the potential energy between the molecule and the rest of the system. This process is repeated for all the molecules to get the mean potentials and the mean-square deviations. These potentials and deviations are then averaged over a number of configurations to give the SMPs. As may be predicted, it has been found that the SMPs are very different for the two sets of molecules and are rather anisotropic. Figure 2.6 shows the SMPs and the corresponding mean-square deviations about ⟨100⟩, ⟨010⟩ and ⟨001⟩ molecular axes, these axes are along the S-F bonds and thus are three-fold symmetry axes of a model molecule.

First we see that for the majority molecules, molecule 2, the barrier is nearly isotropic. For the minority molecules, molecule 1, the SMPs about ⟨100⟩ and ⟨001⟩ are not very different from those of the majority molecules, but the SMP about ⟨010⟩ is much lower than any of the others. The flatter ⟨010⟩ potential well for molecule 1 is consistent with the larger thermal motion compared to that of molecule 2.

2.2.4 Molecular Reorientation

In the crystalline phase, the molecules are orientationally ordered and only librate about the equilibrium positions. However, we have found that when the temperature is near the plastic-to-crystalline transition point, some reorientations have been observed in the MD simulation. Moreover, most of the reorientations are of the minority molecules.

The meaning of a reorientation of SF_6 can be illustrated as follows. One can imagine that a molecule rotates away from its equilibrium orientation along one of its 4-fold (3-fold) axis. The rotation angle is θ, which is usually very small in crystalline phase. A reorientation happens when θ exceeds 45° (60°). When this happens a reorientation event can be recorded and the rotation is redefined by an angle of $90° - \theta$ ($120° - \theta$). Because of the symmetry of the molecule, this operation does not change the actual molecular orientation at all. For more details about the definitions of molecular reorientations and their relations with the quaternion

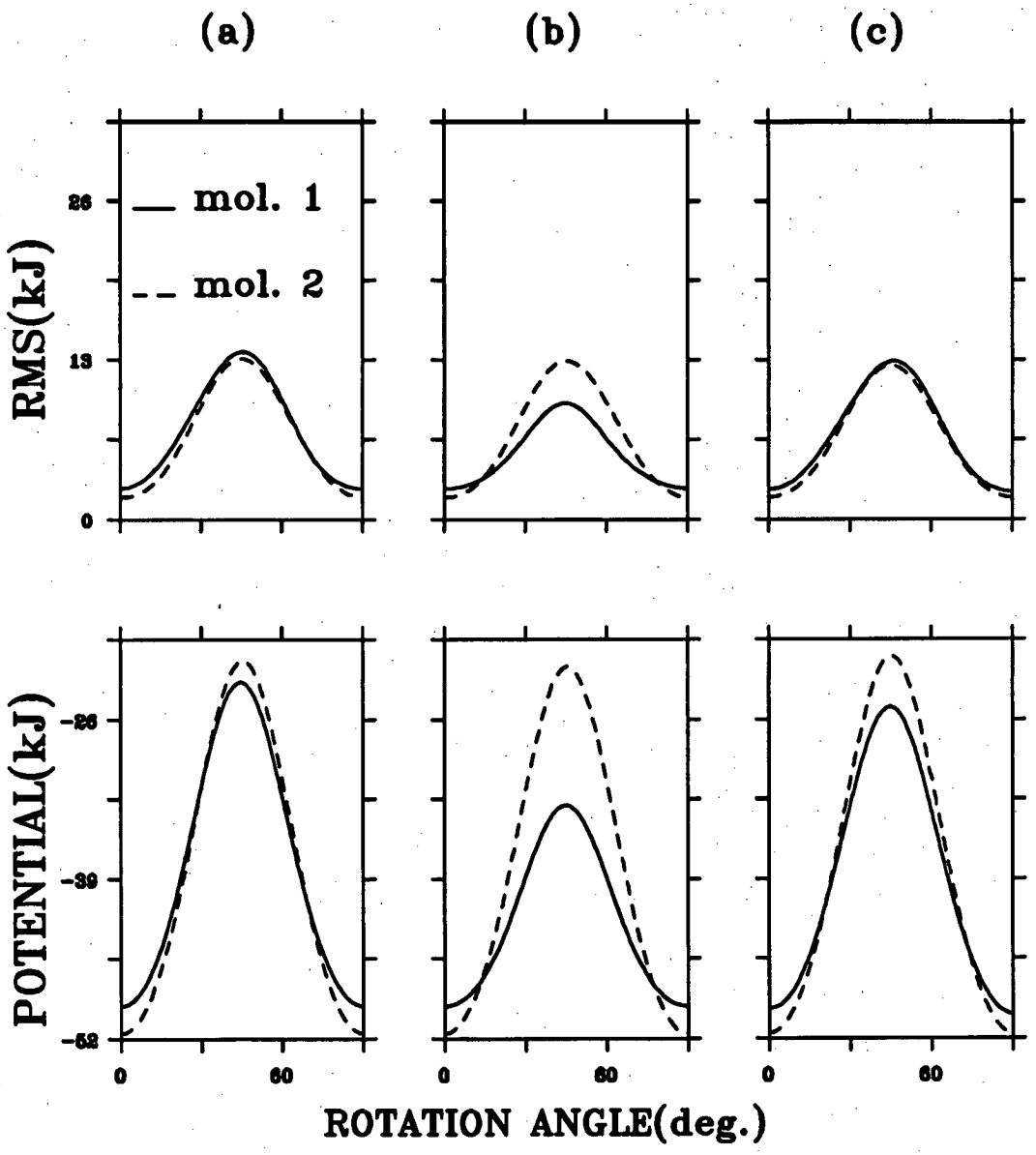

Figure 2.6: The mean single-molecule rotational potential and the corresponding root-mean-square(RMS) potential energy about the ⟨100⟩ (a) , ⟨010⟩ (b) and ⟨001⟩ (c) 4-fold molecular symmetry axes at 125K.

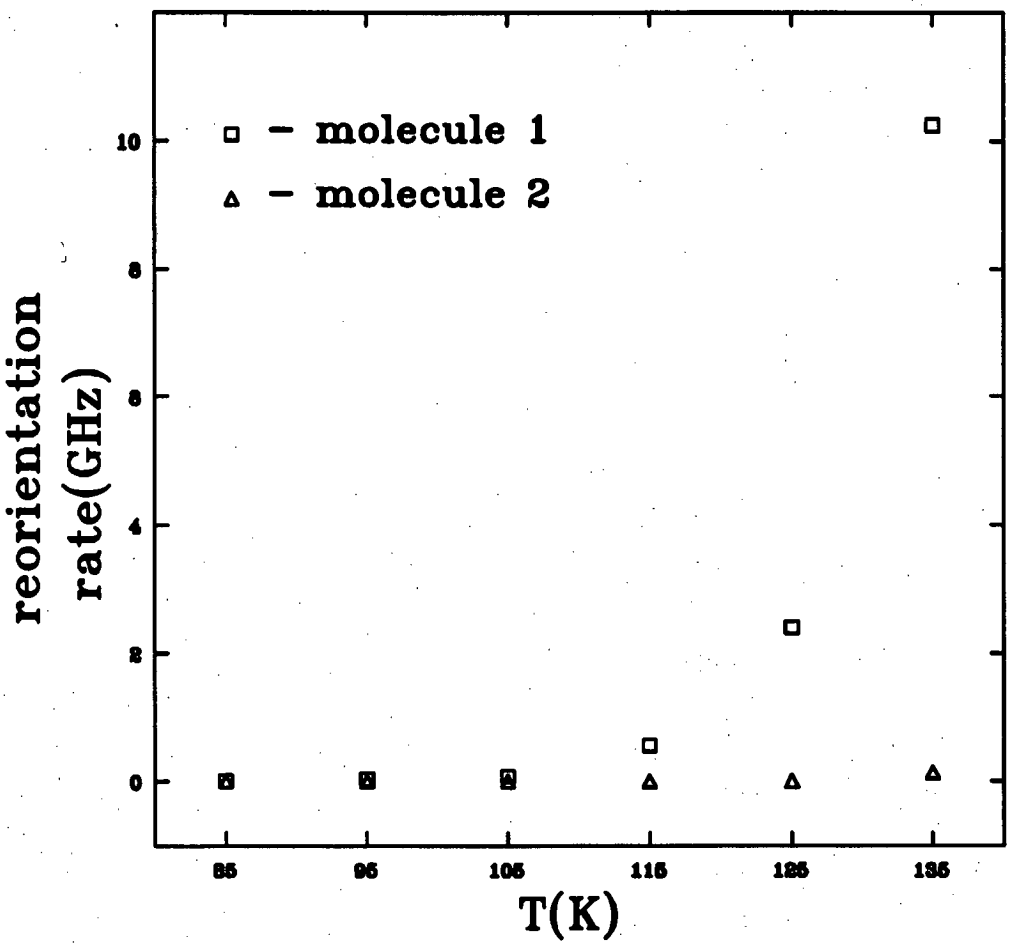

Figure 2.7: The temperature dependence of the reorientation rates in the crystalline phase.

representation the reader is directed to[56]. Compared with the reorientation test in the plastic phase, the major difference is that in the crystalline phase there exist two groups of molecules of two different equilibrium orientations so the test should be applied to the two groups separately.

Figure 2.7 shows the reorientation rates of the two sets of molecules at several temperatures. The minority molecules have a much higher reorientation rate than the majority. The reorientation rate for the majority molecules is close to zero until quite a high temperature. From the above discussion about the SMPs, it is reasonable to deduce that they are related to the reorientation rates. The

	⟨100⟩	⟨010⟩	⟨001⟩
95K	0	1	0
105K	0	7	0
115K	4	48	1
125K	15	191	22
135K	114	757	113

Table 2.7: Reorientation distribution among the three four-fold axes for molecule 1. The data are collected in 90ps simulation time. During this period only one reorientation event was recorded for molecule 2 at 135K.

lower potential barrier for molecule 1 means that it needs less activation energy to reorient. This can be further justified by table 2.7 which shows that most reorientations are those about the ⟨010⟩ axis, the axis about which the smallest potential barrier was observed.

The difference between the maximum and the minimum value of the SMP about ⟨010⟩ axis is about 50% lower for molecule 1 than for molecule 2. If the potential energy barrier to reorientation is estimated as the mean difference between the maximum and the minimum of the SMPs about the three 4-fold axes, this barrier is found to be about 30% lower for molecule 1 than for molecule 2. This result is qualitatively in agreement with the NMR experiments on SF_6 carried out by Garg[25], but in this NMR study the number proportion between the two groups of molecules was estimated as 1:3, not the correct value 1:2.

The Mechanism of Molecular Reorientation

There are two different explanations for the mechanism of molecular reorientations in molecular solids. One is the *classic rotor model*(CR) and the other is the *activated state model*(AS)[58]. In the CR model, the molecules are considered as oscillators in potential wells. Between these wells are energy barriers to both the librational and the translational movements so for most of the time a molecule will oscillate near the bottom of the potential well. Occasionally the molecule may acquire enough kinetic energy, because of the thermal fluctuations, to get

on top of the librational barrier. Since the molecule and the lattice interact with each other the molecule may lose some energy and fall into an adjacent well. This process is the molecular reorientation in terms of the CR model. If this model is right we should be able to describe the temperature dependence of this process by the Arrhenius expression of rate process

$$k = Ae^{-dE/RT}. \tag{2.11}$$

where k is explained as the orientation rate or the rate of a molecule crossing over the energy barrier dE at temperature T. The pre-exponential factor A should be explained as the oscillation frequency of the molecule in the potential well[57] in the context of the CR model. The meaning of equation 2.11 is as follows. A molecule oscillates at a frequency A in the potential well so it approaches the barrier with the same frequency. The exponential factor is the probability of the molecule acquiring enough energy to cross the potential barrier.

To apply equation 2.11 to the reorientation of SF_6, A can be calculated through

$$A = 4\sqrt{dE/2I} \tag{2.12}$$

where dE is the energy barrier and I is the moment of inertia of the molecule[59, 58, 60]. This formula gives the frequency of an oscillator in a potential well of the height dE. In our calculation this energy barrier is estimated as the potential barrier calculated from the SMPs at the corresponding temperature.

At 125K, the calculated reorientation rate for molecule 1 is about $1.3\times10^{8}s^{-1}$ while the recorded value in the simulation is about $2\times10^{9}s^{-1}$. There is an obvious yet not very large discrepancy in the two values if it is compared with a similar value for hexafluorobenzene[58], for which the discrepancy is about 3 orders of magnitude. This result suggests that for SF_6 the mechanism of the molecular reorientation in the crystalline phase is close to what is described by the CR model.

In the AS model, the reorientation of a molecule is thought to be caused by the cooperative movements of the molecule and its surrounding neighbours. According to this model, when an orientation happens a local volume expansion in the surrounding area is accompanied to allow the molecule to have enough space or

favourable configuration to reorient. If this is the case, equation 2.11 can still be used but the pre-exponential factor A will be different from that in the CR model and cannot be determined by the oscillation frequency of the molecule in the potential well. The energy barrier dE can no longer be explained as the potential barrier. For more details about this model interested readers are directed to [58, 57] and the references therein.

From the above discussion it is reasonable to believe that the molecular reorientation can roughly be described by the CR model, but the mechanism suggested by the AS model may also plays a minor role.

2.2.5 Single-Molecule Dynamics

The microscopic properties of a simulated molecular crystal are very complicated because of the great number of degrees of freedom of the system. In order to extract useful information about the molecular movements various correlation functions are often calculated to describe the general patterns of the molecular movements. For example, the single-molecule dynamics can be studied through the auto-correlation functions of the translational velocities $\mathbf{v}$ and the angular velocities ω:

$$Z(t) = \frac{< \mathbf{v}(t+t_0) \cdot \mathbf{v}(t_0) >}{< |\mathbf{v}(t_0)|^2 >}, \tag{2.13}$$

$$C(t) = \frac{< \omega(t+t_0) \cdot \omega(t_0) >}{< |\omega(t_0)|^2 >}. \tag{2.14}$$

The means are calculated over different initial times t_0. Once these functions are calculated, the Fourier transformation of them can be done and the resulting power spectrum $Z(f)$ and $C(f)$ are the densities of states of the translational and librational motions. The variable 'f' in $Z(f)$ and $C(f)$ is the frequency.

The auto-correlation functions can be calculated for any group of molecules. This is significant for the study of the low-temperature phase of SF_6 because we have already known that the behaviours of molecules at different symmetry sites are very different. As an example, the calculated $C(t)$ and $C(f)$ are plotted in figure 2.8. The power spectrum in the plastic phase is also plotted for comparison. It

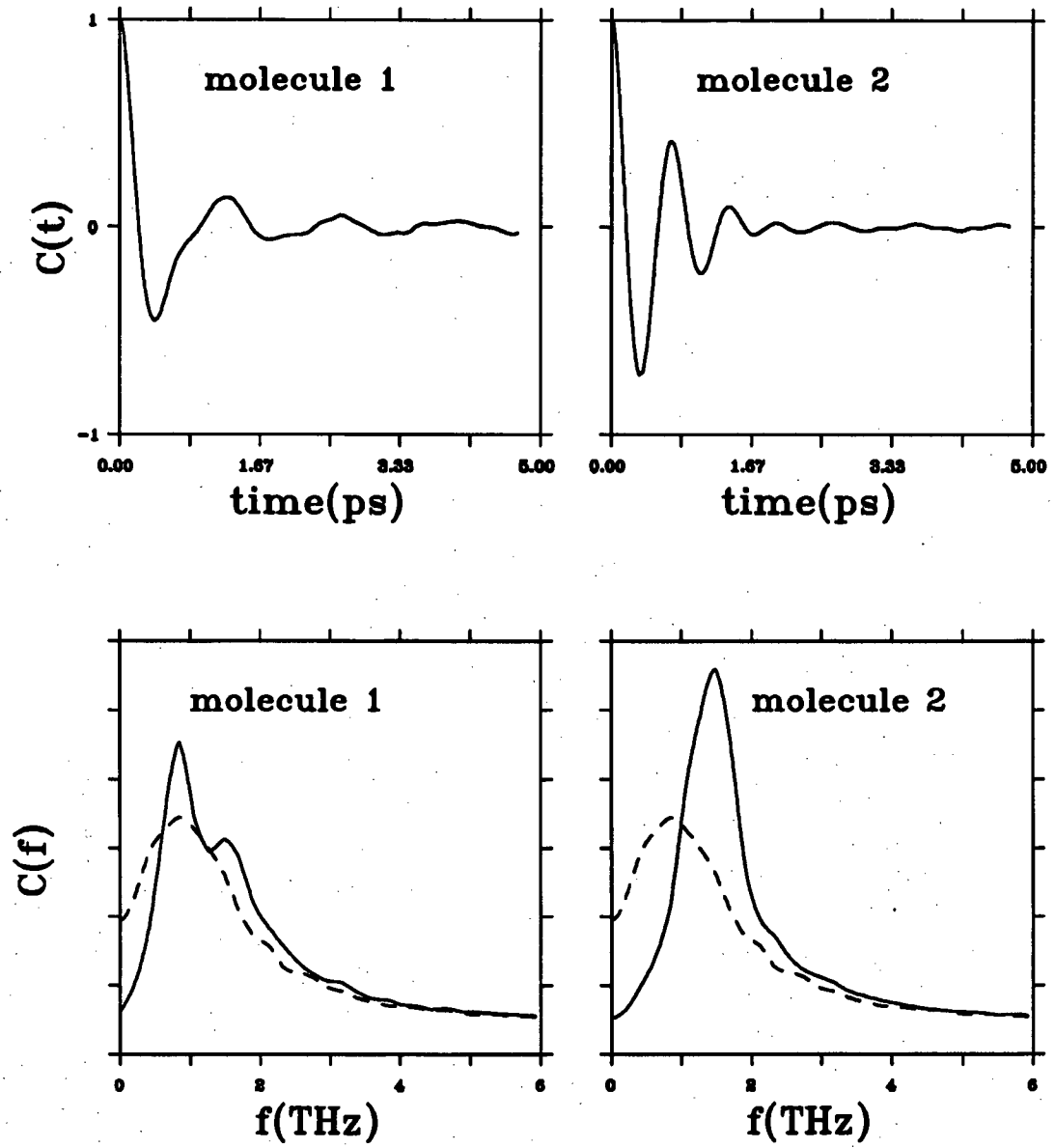

Figure 2.8: The angular auto-correlation functions, C(t), and their Fourier transformations, C(f), in the crystalline phase at 125K. The dashed lines in the C(f) plots are the results for the plastic phase at 150K.

is obvious that the two groups of molecules are very different dynamically. From the $C(f)$ plots we can see that there are two peaks in the spectrum for molecule 1 and only one for molecule 2. The higher peak in the spectrum for molecule 1 is at a frequency markedly lower than that for molecule 2 but very close to the single peak of the spectrum for the plastic phase. More interestingly the lower peak in the spectrum for molecule 1 is at almost the same frequency as the peak of the spectrum for molecule 2. These features suggest that in general the minority molecules (molecule 1) librate at lower frequencies than the majority molecules (molecule 2). The minority molecules have two major librational frequences. Perhaps the existence of these two frequencies is caused by their highly anisotropic environment as indicated by the SMPs. If we compare the spectrum in the crystalline phase with that in the plastic phase we find that the lower frequency mode of molecule 1 is the closest to the mode of the plastic phase indicating that even in the crystalline phase the librational motion of molecule 1 resembles that in the plastic phase. This property is consistent with the fact that some reorientation happens in the crystalline phase.

The auto-correlation function $Z(t)$ and its spectrum $Z(f)$ have also been calculated. It has been found that for the translational motions, the difference between the two groups of molecules are not so distinct as for the librational motions, though the frequency of the translational mode for molecule 1 was found to be a little higher than that for molecule 2. This result is also consistent with other analyses described in this chapter.

2.3 A Metastable Structure

2.3.1 The Structure

We mentioned in section 2.2 that at the beginning of the simulation run the centres of molecules were arranged on a perfect bcc lattice. This is chosen because it is the lattice structure which exists at higher temperature. Consequently, the system can be regarded as being supercooled. When this system relaxes, the structure changes

until the free energy becomes minimum. In the early stages of this structural change, the strain in the sample is usually large compared to the strain in the the equilibrium state. This leads to large fluctuations in the shape and volume and complicates the kinetics of the transition. In terms of free energy, the destination is not unique as the free energy may be regarded as a field of a hyperspace in which there may be some local minima corresponding to the metastable states. These states are not stable against the true structure. Nevertheless, according to Ostwald's 'Law of Stages' the supercooled state usually does not transform to the most stable state directly. Instead, it may first transform into a metastable state which is just a small improvement in stability[23]. So there may be much competition between the most stable state and the metastable states. As a result, a metastable structure may occur and stay for so long that in MD simulations with any practical time-scale it can be interpreted as stable. In fact, this is exactly what we encountered at the beginning of our simulation when the system stablized at a trigonal structure, not the expected monoclinic structure. This trigonal structure has a molar potential energy that is about 0.5% higher than that of the monoclinic structure and is very stable. Later we found that it can be annealed only when the temperature is very close to the solid-solid phase transition point of the model.

Figure 2.9 shows a layer of molecules in the x-y plane. As in the monoclinic phase, the molecules are translationally ordered and have two different orientations in the trigonal. The ratio between the numbers of the two groups of molecules is 1:2 as usual. Comparing figure 2.9 with figure 2.2 one can see that the relative orientations of the two groups of molecules in figure 2.9 differ from those in the monoclinic structure, and the MD-cell shapes are also different.

To show the relative configuration of the two groups of molecules, a 'dot-plot' method can be used. The method is to imagine the sample at the centre of a very large sphere, and project all the SF bonds until they intersect the sphere. The distributions of the resulting points on the sphere show the molecular orientations as modified by thermal motion, and it is these distributions which are to be analyzed. The intersecting points on the sphere can be projected and plotted onto a plane using e.g. the Lambert equal-area projection. In a truly crystalline phase, the molecules have only one or a small number of equilibrium orientations so that

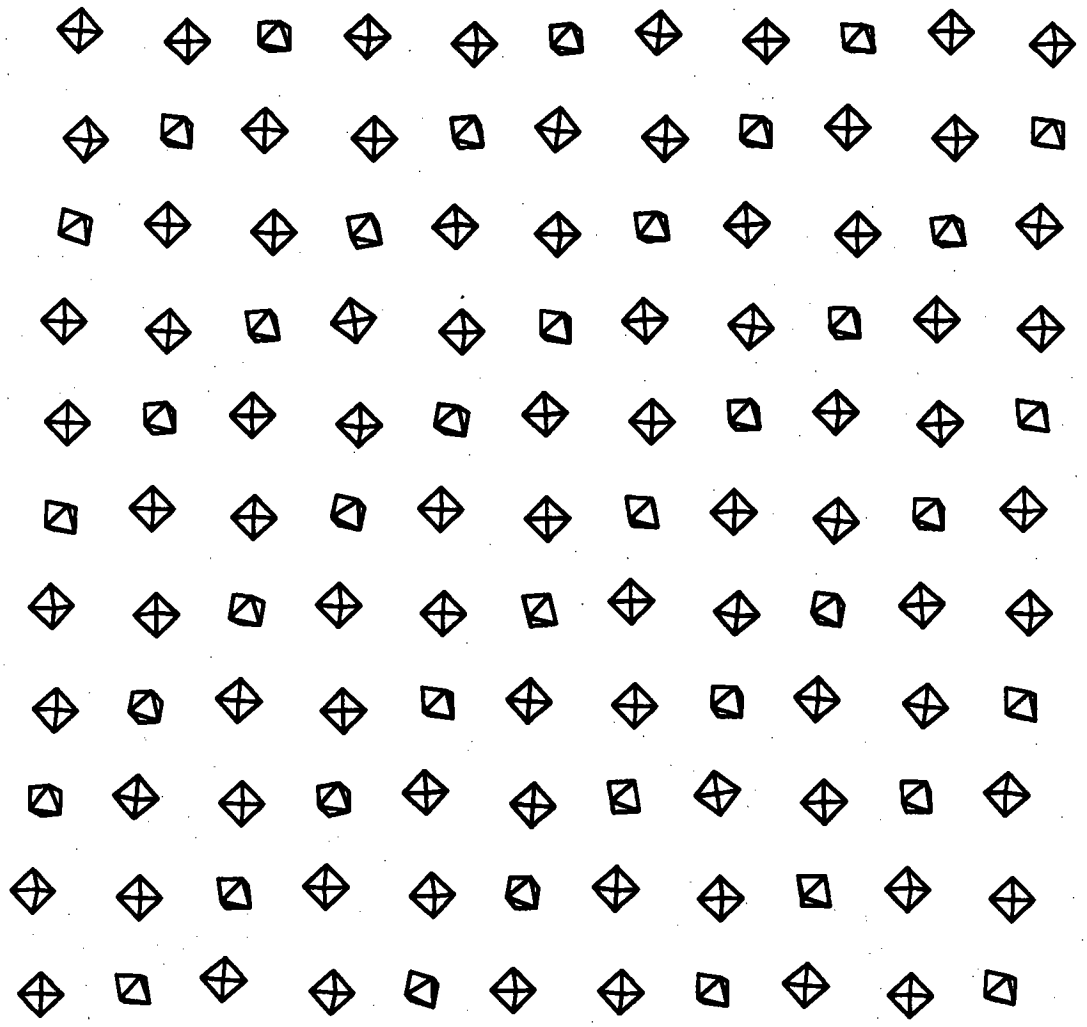

Figure 2.9: The molecule configuration of the metastable trigonal structure of SF_6. These molecules lie in the x-y plane in the laboratory coordinate system.

the dot-plot will show the discrete clusters of the points. The relative orientations among these molecules can be measured geometrically[54]. In the plastically crystalline or liquid phase the points are distributed more evenly, showing little or no order. This method can be applied in a cluster or bulk simulation[54].

In figure 2.10 are two dot-plots at two different temperatures. At 130K the structure is trigonal and at 140K it is monoclinic. The orientations of the two groups of molecules are different in both phases but the relative orientation between the two groups of molecules in the monoclinic phase is different from the trigonal. This difference in the relative orientations can be described by a rotation between molecule 1 and 2 along an axis near ⟨110⟩ direction. By measuring the the angles between those S-F bonds it was found that this difference is about 28°. This change of relative orientation alters the relations between the symmetry elements of the two groups of molecules. In the monoclinic structure, there is only one two-fold molecular axis that is common to the two groups of molecules and this axis is the unique axis of the monoclinic unit cell whereas in the trigonal structure a three-fold symmetry axis of a group of molecules coincides with a three-fold symmetry axis of the other group of molecules.

Since the equilibrium orientations are readily found for any group of molecules, we can develop the dot-plot method into plotting the symmetry elements. In this method the rotational symmetry axes of a group of molecules are calculated from the equilibrium value of the quaternions and then these axes are treated and plotted in the same way as the SF bonds in the dot-plot method. In this way, the relations between the two groups of molecules are revealed very easily without actually measuring the angles between those SF bonds.

The usefulness of the symmetry-plot method is well illustrated by figure 2.11 in which are the symmetry element plots for the trigonal and monoclinic structures. The relation between the rotation symmetry axes of the two groups of molecules is very clearly displayed.

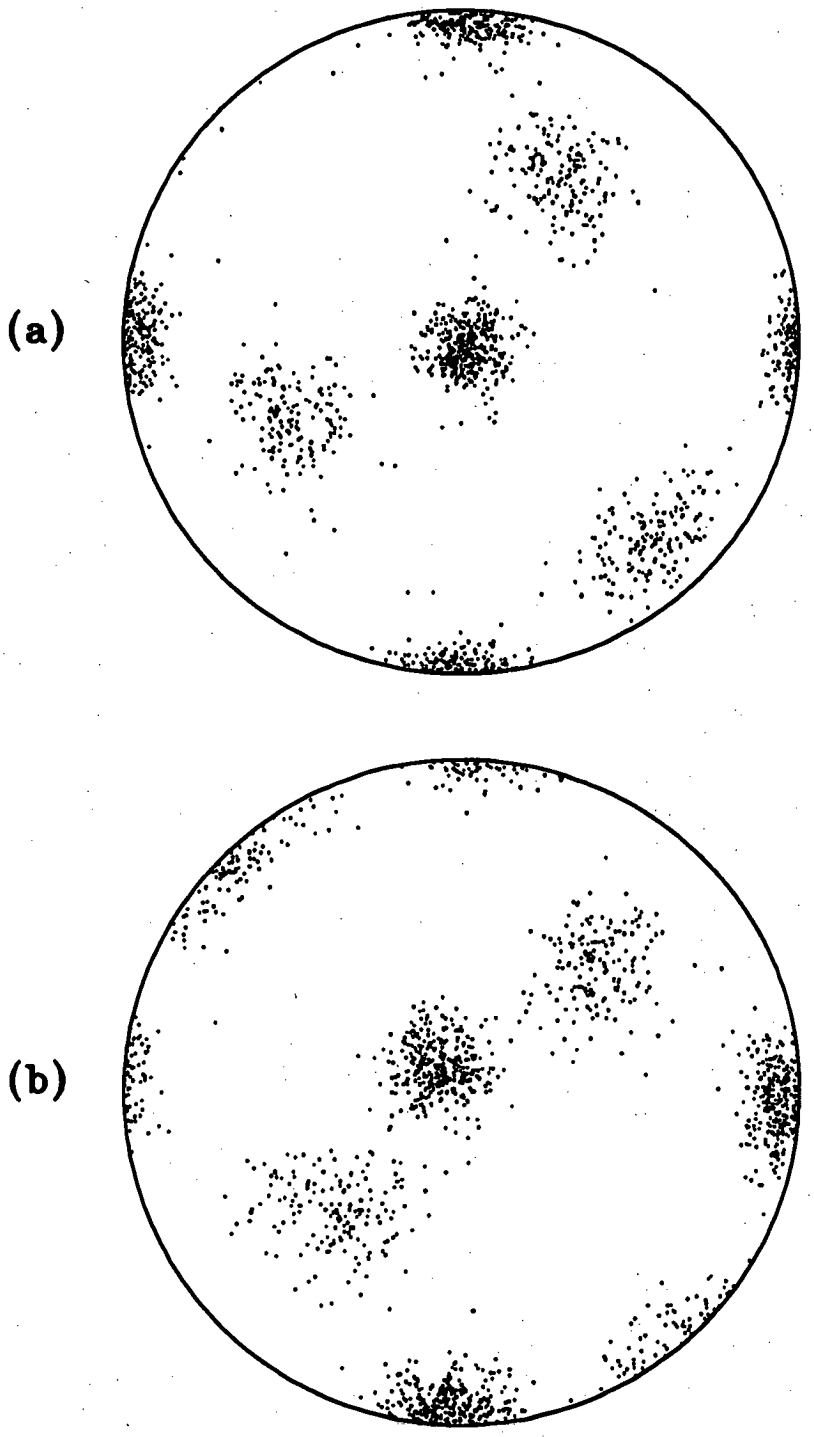

Figure 2.10: Dot-plots for (a) the trigonal structure at 130K and (b) the monoclinic structure at 140K. The difference is in the relative orientation of the two groups of molecules.

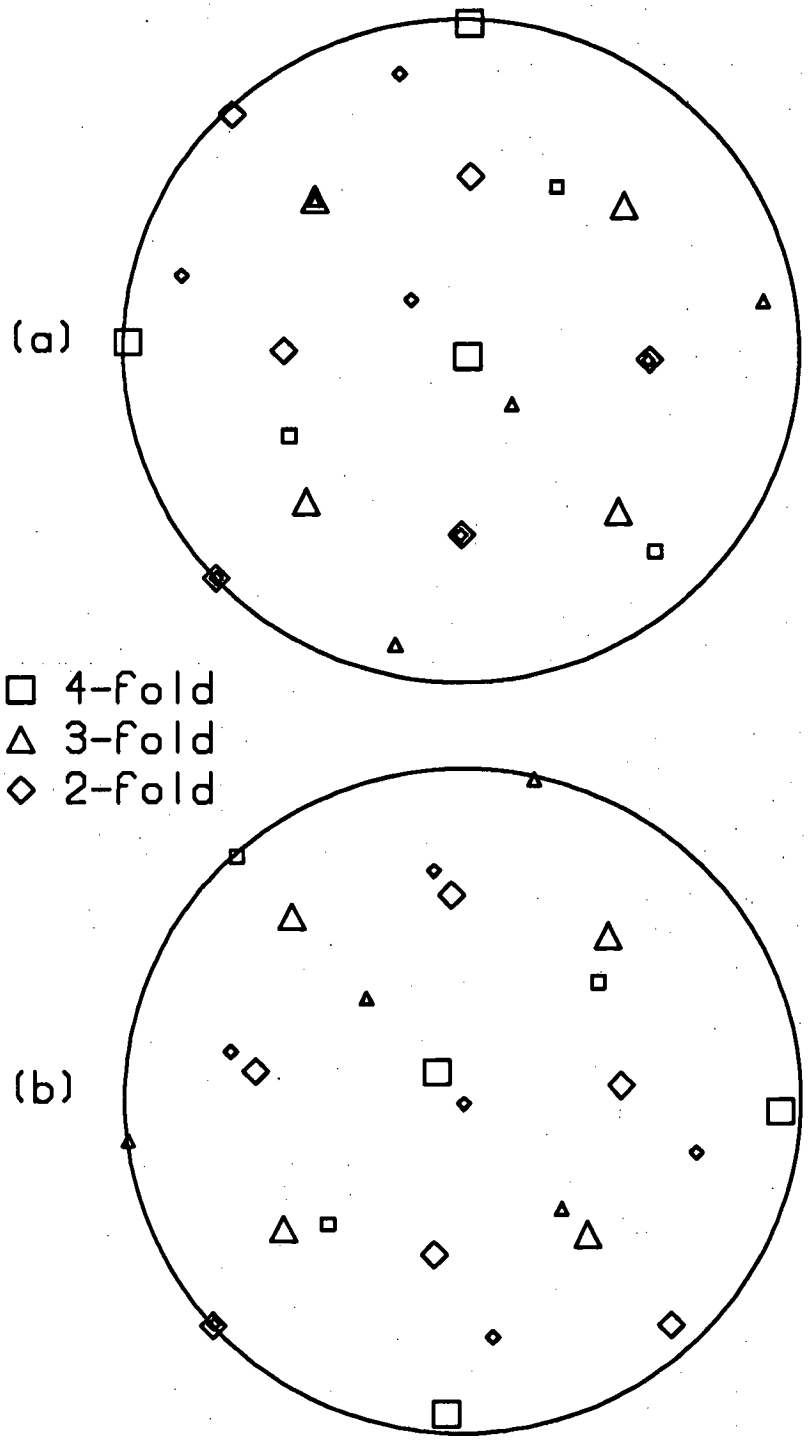

Figure 2.11: The molecular symmetry element plots for (a) the trigonal and (b) the monoclinic structures. In the trigonal structure, the two groups of molecules have a common three-fold axis. Larger symbols are for molecule 1 and smaller symbols are for molecule 2.

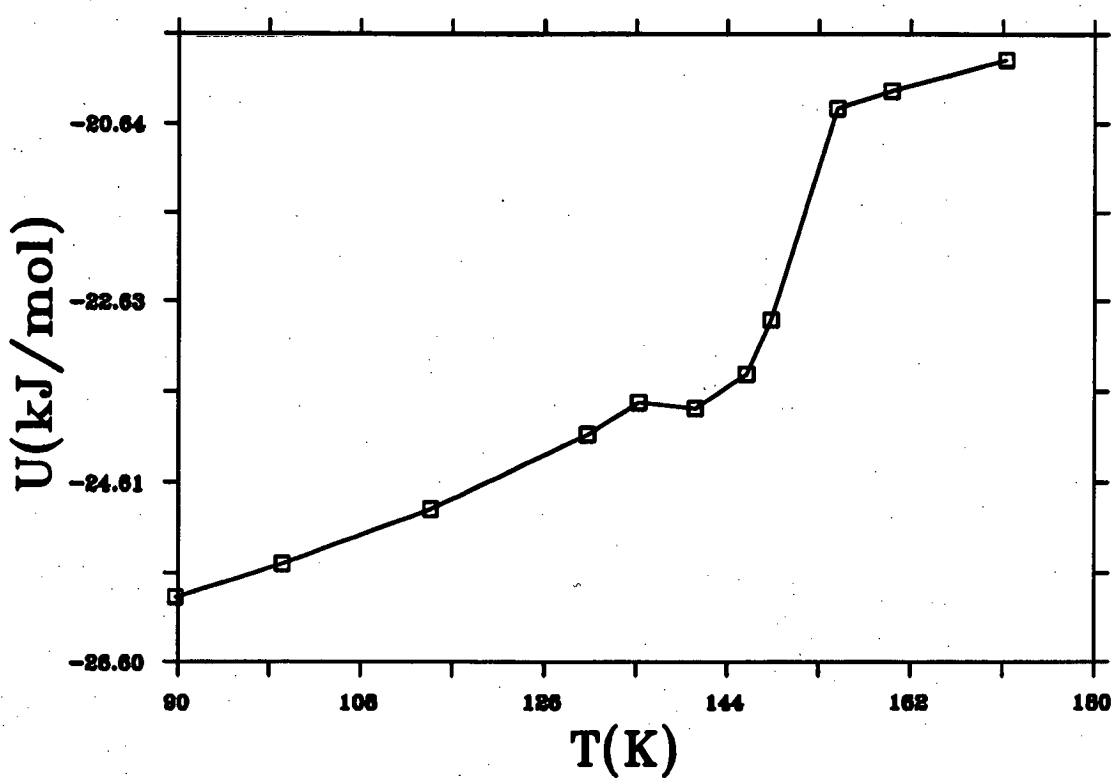

Figure 2.12: Temperature dependence of potential energy in a heating process. The unusual decrease at about 135K is the sign of a structural transition.

2.3.2 The annealing of the metastable structure

To observe the behaviour of the trigonal structure under the influence of temperature, the temperature of the system was increased step by step. The potential energy, the MD-cell matrix and the molecular configurations were monitored in the process. It was found that this structure became unstable at about 140K as the result of a structural transition and this was followed by another structural transition at about 145K.

Figure 2.12 shows the changes of the potential energy in the heating process. At

about 140K the potential energy drops abnormally on increasing temperature. The range of temperature of this abnormality is not wide because it is soon followed by a sharp rise which indicates a major transformation in the structure. Figure 2.13 shows how the parameters of the MD-cell matrix change with time during the process described above. Again it shows two transitions. The first transition is sharp but the second is more complicated. This may have been caused by some metable structures. The identification of the bcc structure is straightforward because it is the structure for which the lengths of the three cell vectors are the same and the three angles between any two of the vectors are all 90°. In this structure the disorder in the orientation is revealed by the dot-plots. The second structure was later determined as the monoclinic structure discussed early in this chapter. The first structure was determined to have trigonal symmetry.

Upon cooling the system from 145K the monoclinic structure persists, though it was found that the monoclinic phase has lower potential energy than that of the trigonal when the temperatures are the same for the two systems. We thus conclude that the monoclinic structure is more stable than the trigonal one and the latter is only a long-life metastable structure. It is noticeable that the annealing happens only when the temperature is approaching the monoclinic-to-cubic transition temperature demonstrating the large energy barrier between this metastable structure and the stable structure.

In this section, by reporting the trigonal structure we emphasize one of the problems in MD simulations, namely the presence of metastable structures. Fortunately, for the SF_6 this structure can be annealed to obtain the true structure. In a more general situation different initial configurations and simulation procedures should be tried to overcome such obstacles in order to find the most stable structure. Finally, we mention that the trigonal structure discussed in this section is not the intermediate phase[26, 34] in which one third of the molecules are orientationally disordered while the rest are ordered.

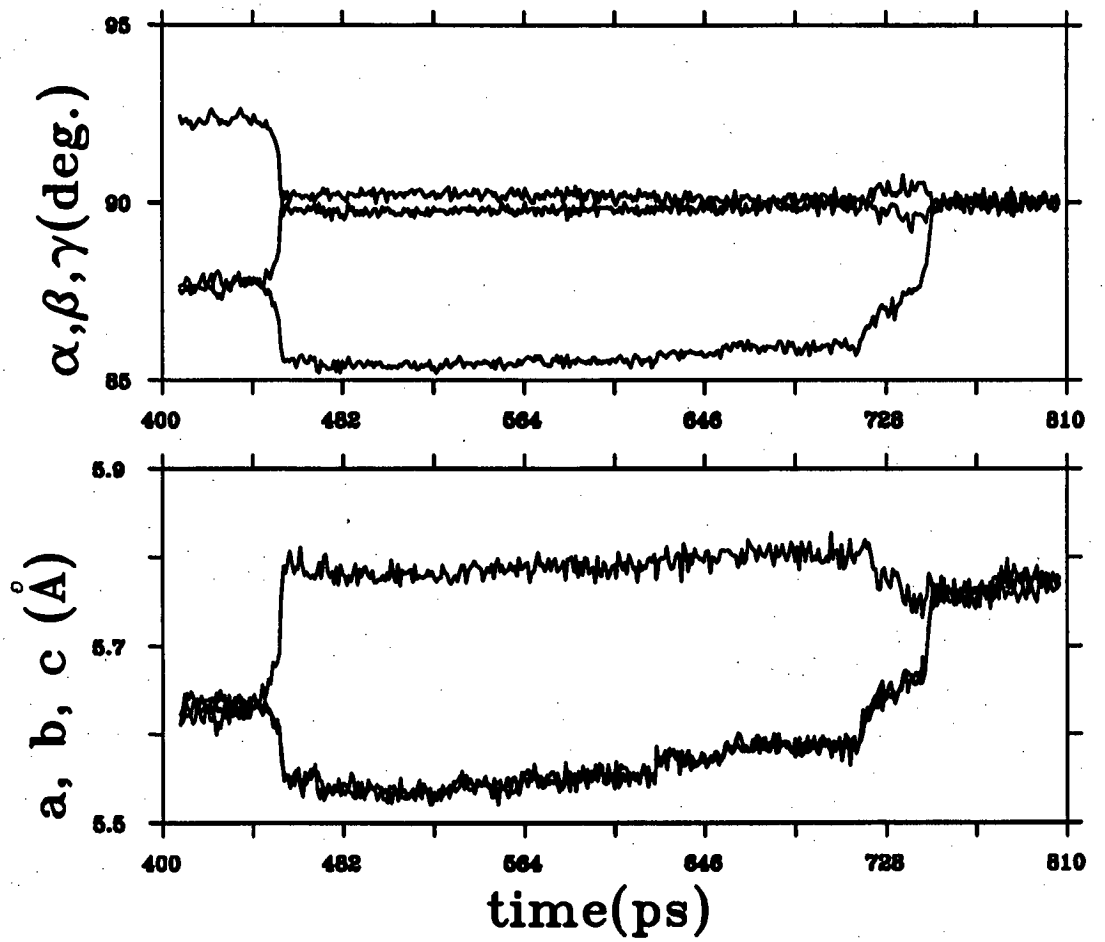

Figure 2.13: MD-cell parameters as functions of time. In the process of the the simulation, the temperature is increased gradually from 140K to about 150K and the system changes from the trigonal to the monoclinic and then to the bcc structure.

2.4 Phase Change on Cooling

As demonstrated in the previous sections, when using the PR technique, transitions between two single crystals can happen within a reasonable simulation time. Another but earlier example of such a transition is that of rubidium changing from fcc to bcc under the effect of pressure[10]. Until now, we seem to have got what we need for a structural change in the MD simulations. But, as it will be explained later, this could have resulted from finite-size effects in a small carefully chosen system. In this section a result which cannot be a finite-size artefact will be presented. We will illustrate that the transition does not need to be a transition between two perfect single crystals. Meanwhile, we will show that the controversial 'intermediate phase' does not now appear in the transition from the bcc plastically crystalline phase to the low-temperature phase.

2.4.1 PR method and Boundary Conditions

In a traditional constant-volume MD simulation of a solid substance, the shape and volume of the MD-cell are fixed. In order to keep the pressure in the sample balanced with the external pressure, the lattice parameters have to be readjusted when the pressure deviates from the required value[32]. Though the procedure is useful it does not remove the shear stress in the system. The PR method allows the shape as well as the volume to change in response to the imbalance between the internal stress of the system and the external pressure. In this way, the pressure is held constant and there is no shear stress. This property of the method can be very important when structural change is involved in the simulation because this is the situation where significant shear stress develops. In this situation, if the PR method is used the shear stress of the system is constantly relieved and the structural deformation of the system as a whole may happen smoothly.

When we use the PR method to study the structural deformation of solids, the constraints from boundary conditions are very important. Only when a structure is compatible completely with the boundary conditions can the system form a

single crystal. Otherwise, the structure can only form as a polycrystalline system, or it may not be able to form at all if the system is too small. If the structure of the substance being simulated is known, one can choose suitable cyclic boundaries so that a single crystal can be formed. In the simulation of a structural transformation, only when the structures of both phases are compatible with the boundary conditions can the transition between two perfect single crystals occur. The correlation between the boundary conditions and the possible structure of the system is thus very strong, and this may well give rise to spurious phenomena.

In the MD simulation of Rb by Parrinello and Rahman[10], the two structures of Rb were both compatible with the boundary conditions. It was observed that the system could change from fcc single crystal to bcc single crystal. In the light of the above discussion, one might ask if the transition observed is simply an artefact of the constrained system.

In a constant-volume MD simulation, however, shear stress will develop in a structural change and this stress can only be relieved through the nucleation of a number of crystallites that have different orientations, and this can only happen provided that the sample is large enough. In Pawley and Thomas's[32] MD study of SF_6 the sample used has as many as 4096 molecules forming roughly $13\times13\times13$ body-centred unit-cells. In the simulation, the pressure is kept constant by adjusting the lattice parameter. The result from the low-temperature simulation shows that the sample is large enough for multiple nucleation to occur. In some relatively big crystallites the crystal structure is very close to the structure obtained from neutron powder diffraction[27]. However, though the sample is big enough to allow some crystallites to develop, a large proportion of molecules are involved in the grain boundaries so that the effect from these grain boundaries has to be taken into account.

2.4.2 Domain Structure

Having achieved the low-temperature structure of SF_6, we increased the temperature of the system gradually. The system remained in the monoclinic structure

until the temperature reached about 140K, and above this temperature the system became a plastic crystal of bcc structure. When the temperature was close to the transition some reorientation events were recorded for molecule 1 but there was no sign of an intermediate phase.

We then cooled the system from the plastic phase at about 120K to about 90K and kept the system at this temperature by extracting energy from it until it was equilibrated. The process was carried out for systems of 3072 and 1536 molecules. In both cases, we found that the shapes of the systems change when temperature decreases and the resulting systems become big crystals with grain boundary defects. The structure of the crystallite is the same as that for the single crystal. In figure 2.14 we can see the MD-cell deviates gradually from bcc structure of the plastic phase.

Figure 2.15 shows a section of molecules and their relation to a monoclinic unit-cell. Obviously, these molecules have basically two orientations and the whole pattern is well ordered. Comparing the molecular configurations in this figure to that in figure 2.2, one can see that the two structures are identical. In figure 2.15, the dimension b of the monoclinic cell is in the plane of the molecules depicted, and the sketched cell is deliberately tilted slightly to give a 3D aspect.

Figure 2.16 shows many more molecules on the same plane as in figure 2.15. In the diagram, the 8 columns of molecules on the left are repeated on the right shifted down one row because of the skew cyclic boundary condition. The ordering is displayed by the lines joining the minority molecules. This result is from the system of 1536 molecules and the MD-cell consisted of $8\times8\times12$ bcc cells. Another run for the system of 3072 molecules gave a similar result, the only difference being the orientation of the crystallites.

Although our simulation was carefully set up so that the phase transition could take place from one single crystal to another single crystal, this did not in fact occur as the system was cooled from the plastically crystalline phase. The transition is expected to be initiated by a fluctuation which acts as a nucleation centre. Such a fluctuation can occur with a possible 12 orientations, three of which correspond to the lower phase single crystal. In the few independent cases we have studied,

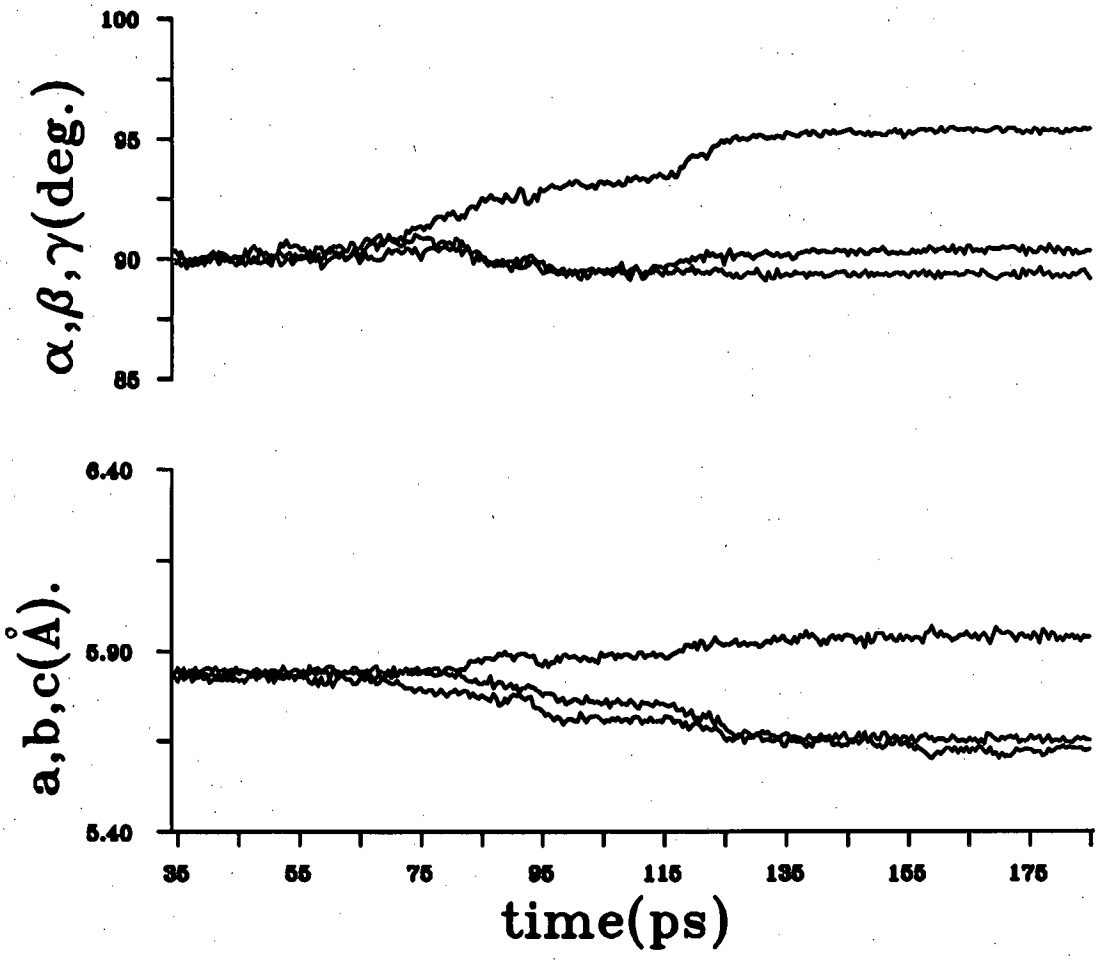

Figure 2.14: The deformation of the bcc structure to a low-temperature phase during a cooling process from 120K to 90K. The velocities of molecules were rescaled a number of times to remove energy from the system. The cell dimensions a, b, c and angles α, β, γ are the MD-cell parameters, not the monoclinic parameters.

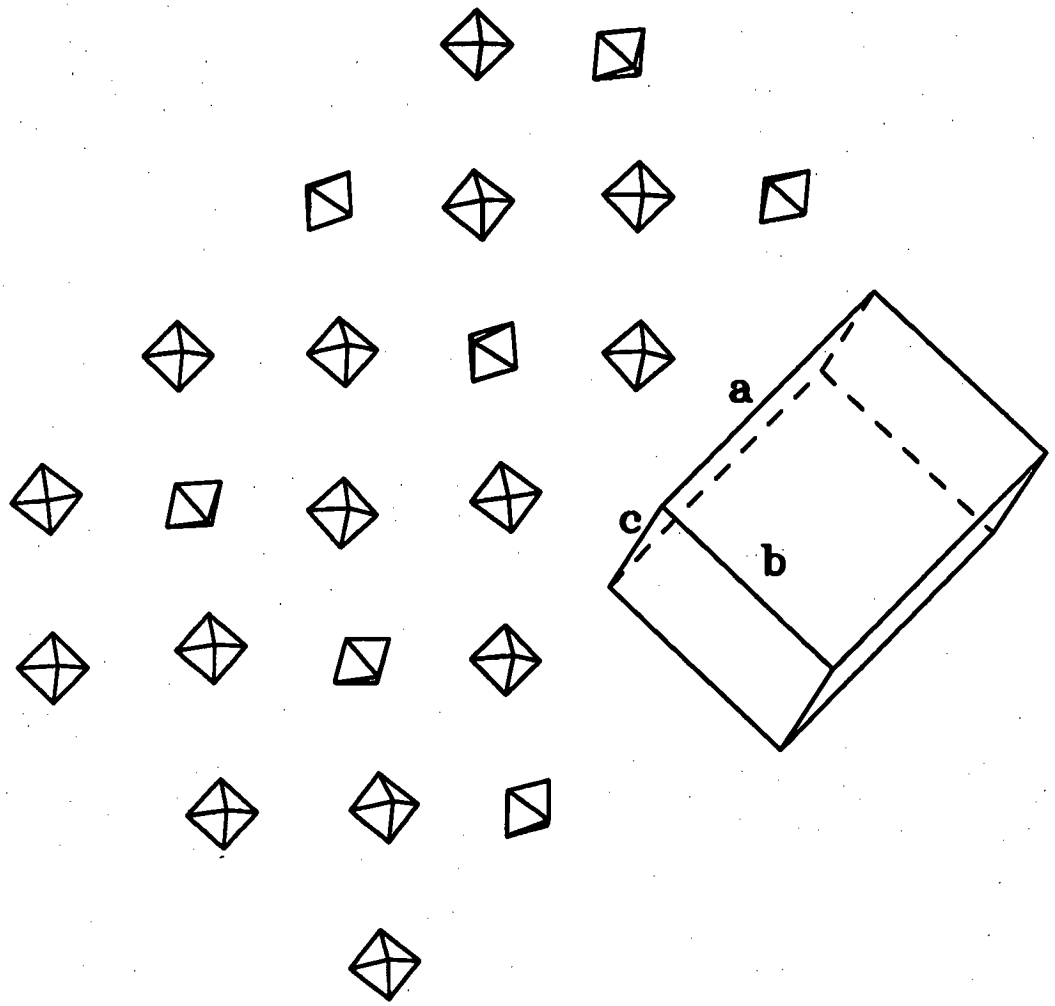

Figure 2.15: A section of ordered molecules and their relation to the monoclinic cell.

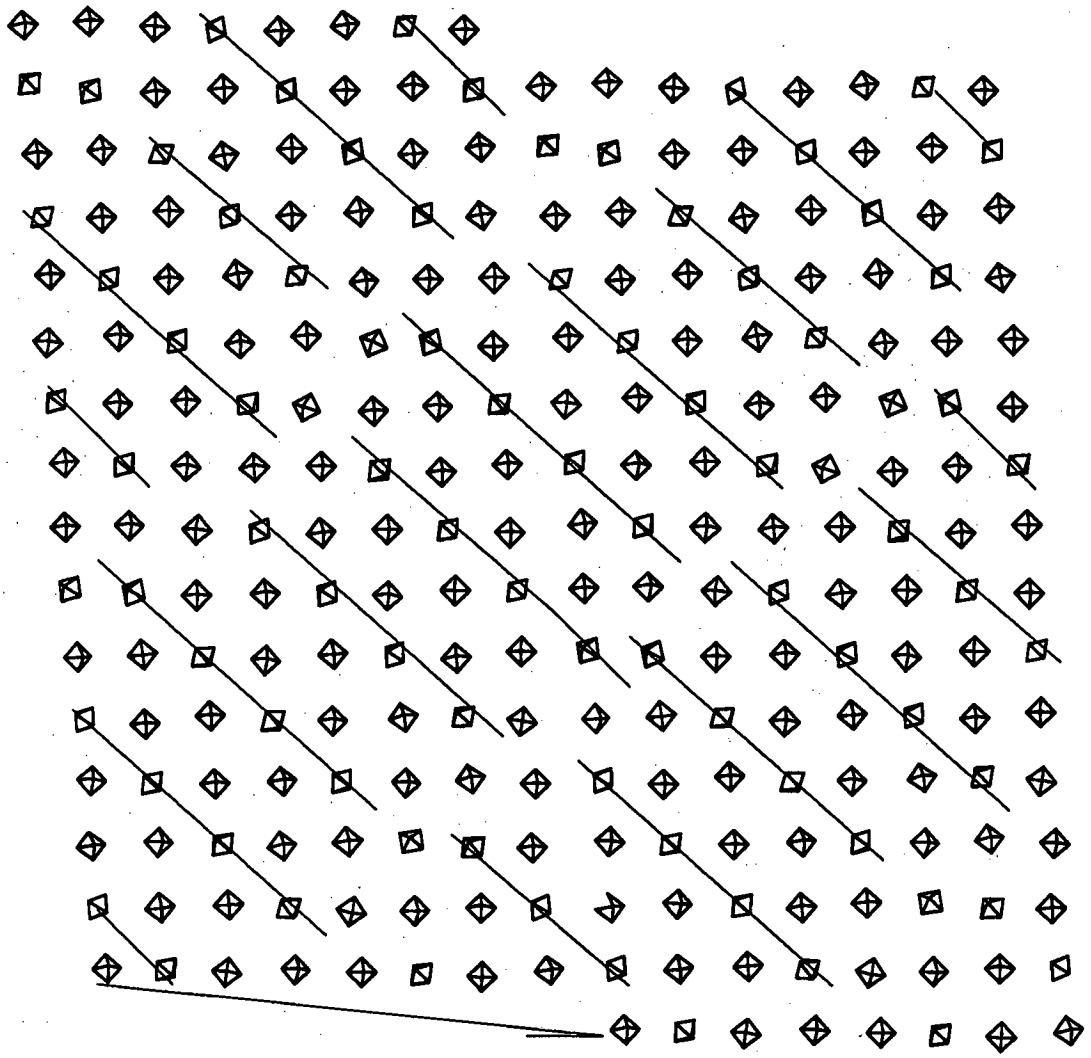

Figure 2.16: Crystallites and grain boundaries at low temperature. The system consists of 1536 molecules. The repetition of the eight columns on the left is due to the skew cyclic boundary conditions, the arrow showing the repetition vector.

the fluctuation which determined the growth of the dominant grain has not been of the particular orientation just described. The system shape then shears as the dominant grain grows, giving a result with some molecules involved in a grain boundary. The PR method thus allows the whole system to grow with one crystal orientation, the boundary conditions being satisfied by the inclusion of a single grain boundary. From figure 2.16 it is clear that this grain boundary develops at right angles to a crystal axis, thus minimizing the number of molecules involved in the defect. It is of interest that in the few cases we have studied, the axis perpendicular to the grain boundary has always been the b-axis, which is the unique axis of the elusive intermediate phase.

2.5 SF_6 under High Pressure

In the previous sections, the simulations were all carried out under zero pressure. When high pressure is applied, the lattice spacings are expected to change and this change will lead to the changes in the crystallographic and dynamic properties of the system. In the simulation, we increased pressure on the system at 85K in the monoclinic phase to as high as 60kbar. In this process, the lattice parameters changed gradually with the pressure and no drastic structural transformation was observed. This result suggests that the monoclinic structure is stable under very high pressure.

High-pressure simulations have also been carried for samples in the plastic phase and it was found that the plastic-to-crystal transition point was affected by the pressure. In one instance, a sample at 180K transformed into crystalline phase when the pressure reached above 8kbar. Further work has to be done before more details of the phase diagram is available.

2.6 Summary and Discussion

The simple rigid-body model with a two-body L-J potential gives a remarkable representation for the condensed phases of SF_6, especially when the optimum value of σ is used. The structure can be studied to very good accuracy. The T-tensors, L-tensors and the SMPs are readily found and this helps the study of the thermal motion and reorientation in this anharmonic system. For the true SF_6 crystalline phase, the molecules at different symmetry sites have very different SMPs and thus exhibit different thermal motions and reorientation rates. These differences are crucial for the understanding of the structural phenomena. On warming the crystal, molecules 1 gain far more librational energy than would be expected in a typical molecular crystal, giving an incipient instability. This instability manifests itself in the transition to the plastic crystal.

It is a valuable exercise to examine why an incorrect conclusion was made concerning the low-temperature phase originally predicted by MD[32]. It could be argued that the crystallites in the simulation were distorted from the monoclinic symmetry as a result of their small size. Although this was certainly true, the underlying symmetry was probably sufficiently well represented for a discovery of the true structure to be possible given a good analysis technique. Such an analysis would have involved an exhaustive automatic search program, but it is now clear that a result would have been far more evident had a full PR simulation been done[51, 52] as in the present work.

A later simulation of a cluster of SF_6 molecules[54] yielded an isolated single crystal which afforded a more accurate possible analysis of the bulk structure at the centre of the cluster. An analysis through the calculated powder diffraction pattern was a possibility, though such analyses are very difficult[27]. However, there was one analysis, based on the dot-plot method, of the cluster result which pointed to the monoclinic structure which was unfortunately mistaken for an anomaly[55].

For this method to have been successful with the earlier (EVN) MD simulation result a single crystallite would have had to be isolated from the MD configuration, requiring the hand of the experimenter. Such intervention however would not be

necessary using PR even if the system has a domain structure as happened when the system was cooled from the plastic phase to the crystalline phase.

The fact that no intermediate phase has been found in our present simulation is contrary to the earlier MD simulation of SF_6 [34], where a zero pressure method was used. This different behaviour might be related to the different grain boundary structure. In the system of 1536 molecules we used in this work, there are roughly 25% of the molecules involved in the single grain boundary, whereas in the earlier work about 40% of the molecules are involved in the various grain boundaries. This indicates that there is more energy associated with grain boundary defects in the original study, an energy which is frozen in because further annealing is not possible. The transition from the plastic phase to the crystal phase was found in the earlier work by Dove and Pawley[34] to be a two-stage process in which the first stage was a distortion to give the trigonal intermediate phase. Further cooling led to a second shearing of the structure to give the monoclinic phase, originally thought to be triclinic. Each of these first-order processes involves a latent heat which we can relate to the defect energy of the molecules in the grain boundaries.

Our suggestion is that the intermediate phase is maintained in the simulation where shearing of the MD-cell is not allowed and the various grain boundaries do not have the chance to anneal out. In the real system as studied by electron diffraction the production of the sample is such that a very rapid cooling takes place to a temperature above 50K, permitting the first stage of the transition but not the second. The intermediate phase is therefore a metastable phase which is frozen in.

Below 50K in the (EVN) MD simulation[34] the second shearing takes place and the system experiences the transition from the intermediate phase to the monoclinic phase while the domain boundaries still exist. This is in agreement with the electron diffraction experiments at these low temperatures. In the sample used for neutron scattering the low-temperature crystalline phase is reached in one step even at the higher temperatures, as the cooling is sufficiently slow that grain boundary annealing can take place along with the second shearing.

We have seen quite clearly in the present simulation study that grain boundary annealing can take place on cooling the plastic phase sample, giving behaviour more characteristic of the bulk neutron diffraction sample than the very thin electron diffraction sample. The fact that the whole MD sample can shear with the PR method results from the finite-size artefact introduced by using a small system with cyclic boundaries. This greatly facilitates the annealing and thus the simulation search for new phase transitions. This 'finite-size annealing' does not, however, generate an artefact, but this must lead to a caveat if the low-temperature phase always grows as a perfect single crystal, as for very small samples[10]. In the MD simulations of phase transitions we should, perhaps, add that care should be taken in the choice of periodic boundaries so that a transition between two perfect single crystals is not possible, or at least not the only possibility.

Chapter 3

The melting of SF_6

3.1 Introduction

Melting is the process by which a solid changes into liquid. In the framework of the theory of thermodynamics this phenomenon can be described clearly in terms of the Gibbs free energy which is defined as

$$G = U - TS + PV = H - TS \tag{3.1}$$

where U is the internal energy, S is the entropy of the system and H is the enthalpy.

In general, a state of a thermodynamic system is stable only when the Gibbs free energy is lower than that of any other states. If two states have the same Gibbs free energy, they will coexist. These arguments can be applied to melting. At a certain temperature at which the solid form of a substance is the most stable state, the free energy in this state is lower than in the liquid state. When the temperature increases the free energy falls for both states. Because the liquid state has a higher degree of disorder than the solid state it also has a higher entropy. From equation 3.1 and the other thermodynamic relations we have

$$\left(\frac{\partial G}{\partial T}\right)_p = -S. \tag{3.2}$$

implying that the free energy decreases faster for the liquid state[62]. The result is that at a certain temperature T_m the free energy in the two states will be

identical and the two states will coexist. When the temperature is increased even further, the system will become completely liquid. This process is melting and the temperature T_m is defined as the melting point[61].

Melting is a very common phenomenon and is also one that has not yet been fully understood. While the thermodynamic theory of melting has long been established, there has not been any complete theory on how a solid with an ordered arrangement of atoms(or molecules) transforms into a liquid in the process of melting. The macroscopic thermodynamic theory is based on heat measurement and does not give details of the molecular movements and the influence of the crystal structure of the specific system under investigation. There have been, however, some attempts to address this issue. For example, in 1910 Lindemann attributed melting to the emergence of the vibrational instability of the atoms on the lattice in the solid phase as the temperature increases[71, 64].

In the present work, rather than discussing various theories about melting, MD simulations will be used to study the melting of SF_6 with various boundary conditions. These correspond to the bulk, cluster and slab MD simulations. A bulk sample is an infinite system that is realized by applying full periodic boundary conditions to the finite MD-cell. A cluster is a sample with free boundaries. A slab can be formed by applying periodic boundary conditions to the MD-cell in only two directions leaving two free surfaces. The MD method has been used to study melting for some time[66, 67]. The advantage of this method is twofold. Firstly it can give a microscopic picture of the phenomenon and secondly, unlike the Monte Carlo method, the dynamics of the process can be studied.

3.2 Melting in a Bulk Sample

A simulation of the melting of the bulk sample was carried out on the ECS. The sample consisted of 8×8×8 bcc unit-cells and the total number of SF_6 molecules was therefore 1024. PR MD method was used to allow the volume to expand as the temperature is increased. The simulation started from 100K and the total energy was then increased gradually by scaling the velocities of the molecules.

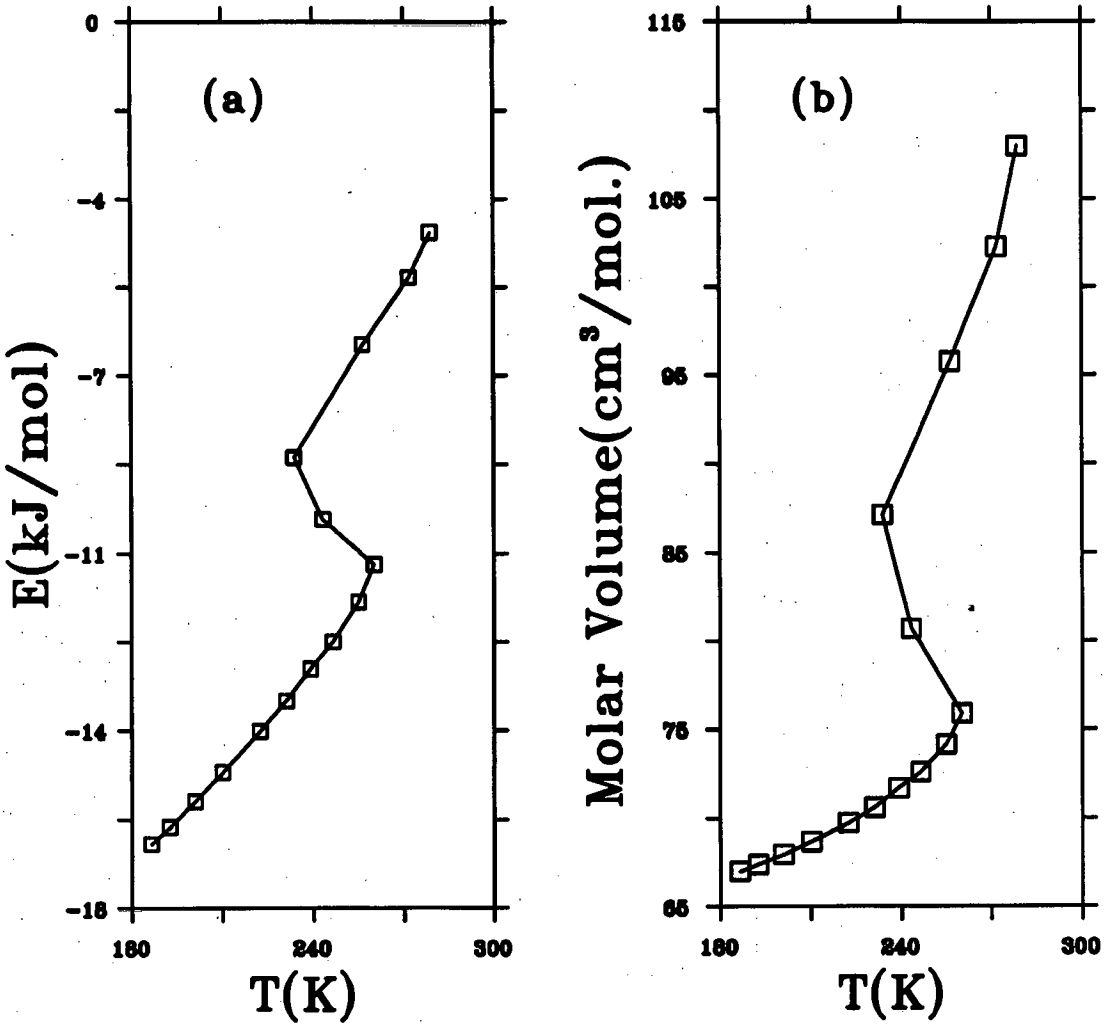

Figure 3.1: The simulation of the melting in the bulk. Figure 3.1(a) shows that the temperature drops when melting happens and figure 3.1(b) shows the change of the molar volume as the temperature increases.

Each scaling period was 25 timesteps and after each scaling period, the system was left free to evolve for 2400 timesteps to equilibrate, each timestep is 0.01ps. This procedure was repeated many times until the temperature reached about 280K. Part of the results are shown in figure 3.1.

The curve in figure 3.1(a) shows the change of the temperature as the total energy is increased and the curve in figure 3.1(b) shows the molar volume as a function of temperature. The sudden drop of the temperature at about 265K is regarded as an indication of melting. When melting happens, the molecules become trans-

lationally disordered and the potential energy begins to increase. Consequently the temperature drops to make up the amount of energy needed to increase the potential energy. The increase of the molar volume in the liquid phase is another sign of the change in the environment of the individual molecules. These discontinuous changes of thermodynamic properties are a feature of the first order phase transition. Here it is necessary to mention that when the simulation of a bulk sample is carried out on the DAP as previously described, melting can also be observed. The only problem is that the scheme which was designed to simulate the crystalline state is not suitable to simulate a liquid. The reason for this is that in the liquid state, molecular diffusion is inevitable and molecules are no longer confined to the vicinity of the lattice points. The method of using a fixed neighbour-list will thus fail. The present simulations were carried out on the ECS and the neighbour-list was determined by the cut-off distance method and was updated constantly so that the liquid phase can still be simulated[38].

From the simulation of the bulk sample, the melting point can be estimated to be between 265 to 270K. However, in the simulation, melting was achieved by heating the system so there is the possibility of *superheating* i.e. the substance is heated above the melting point T_m but remains solid. (If it is cooled below T_m and remains liquid it is then said to be supercooled.) The existence of these hysteresis processes can certainly affect the determination of the melting point of a solid by melting or by cooling. In reality, it has been found that it is easy to supercool a substance whereas it is difficult to superheat it. In the present molecular dynamics studies, the situation might be different. The main reason is that no defects have been introduced into the model whereas in reality defects such as dislocations, surfaces etc. are very common. As a result, the melting point determined by the MD simulation of a perfect bulk sample may not be the *genuine* melting point defined by the behaviour of the free energy in the liquid and solid states.

One of the problems arising from the superheating is the reliability of the MD study of the properties near melting. If the real melting point is not known, the conclusions drawn from the study near melting may turn out to be the properties above the thermodynamic melting point. So, even if one is not interested in the

melting behaviour of the model it is still necessary to know the melting point.

The most direct method of finding the melting point would be to calculate the free energies of the solid and liquid phases. The melting point can then be determined by the definition in the theory of thermodynamics. However, the calculation of free energy for a molecular system is by no means easy[65, 67] and no method has been developed to calculate the free energy of a system which has a plastic phase and a solid-solid phase transition as in SF_6. In the following section we discuss the MD simulation of melting process of a slab. This study will lead to a practical method to determine the melting point of the SF_6 model.

3.3 Surface-initiated Melting

Surfaces play a very important role in melting. It has been found experimentally that when the surface effects are suppressed superheating can be observed[68]. It has also been found experimentally that on the (110) surfaces of Pb, liquid films begin to form at a temperature 25% lower than the experimental bulk melting point. The thickness of the films increases rapidly as the temperature approaches the melting point[69]. This discovery is in agreement with the theoretical prediction by Lipowsky and Speth(LS)[72]. According to the LS theory, the surface properties are very different from the bulk properties which change discontinuously during a first order phase transition such as melting. Instead, similar to the situation in a second order transition, surface properties may behave continuously or diverge during such a transition. When a surface is present a liquid-like film will form on it. The thickness of a liquid-like film diverges as

$$-ln(T_m - T)$$

where T is the temperature and T_m is the bulk melting point[72, 74].

Recently some work has been done to use the MD method to simulate systems with surfaces, or other extrinsic defects such as grain boundaries and voids[67, 65, 70, 73]. The results all seem to support the LS theory.

The basic idea of the method is to implement the simulation of a system with surface(s) and study its behaviour at various temperatures. According to the LS theory, different thicknesses of liquid films will form at different temperatures. If the temperature is very near or even higher than the melting point the thickness is in fact infinite. In this case, melting is observed to start first on the surfaces and then progress further into the deeper part of the system. This process can be described as the propagation of a liquid-solid interface and the velocity of this propagation depends on the temperature. The higher the temperature is, the faster is the melting process. Propagation velocities at different temperatures can be found from the simulation and the melting point T_m can be evaluated by extrapolating the interface propagation velocity to zero[72, 74].

This method is simple and helps to understand the dynamic aspects of the melting process and has been used to determine the melting point of silicon [67] and benzene [84] and to estimate the upper bound of the melting point of aluminium[73]. So far as we know, the present work on SF_6 is the first case of applying the method to an orientationally disordered crystal. This can be significant because when a molecular crystal melts, there is usually more than one mechanism involved. From the ordered crystalline phase to the disordered liquid phase the system will lose both the translational order and the orientational order. In the case of a plastic crystal most of the orientational order has already been lost in the solid-solid transition, if there is such a transition, so when melting happens the main change will be due to the loss of the translational order only. Therefore the melting of this special crystal may be different from that of an ordinary one and the problems encountered in the study are considered illuminating for the studies of other similar substances.

3.3.1 Details of the Simulation

The first step of the simulation was to carry out a simulation at 180K using fully periodic boundary conditions and the PR constant pressure method[10]. The system was then heated over a range of temperatures from 180 to 260K step by step and after each step the temperature was increased by 10K. At each increase

in temperature the system was left for 36ps to equilibrate. The mean MD-cell matrices at different temperatures were recorded at this stage as well. Since liquids cannot resist shear stress, the PR method was no longer suitable and therefore the MD-cell matrix was replaced by the mean values calculated in the first stage of the simulation. The samples were then left to equilibrate for a further period of time.

In the second phase of the study, the periodic boundary conditions along the z direction were removed to form a slab with two free surfaces perpendicular to the z axis. The system was maintained at the original temperature for 8000 timesteps (80ps). As the sample begins to melt, the potential energy rises and the temperature decreases. To keep the sample at a fixed temperature, the molecular velocities were rescaled at every 20 timesteps. It has been observed in a test run, that when the sample is heated to 250K and the total energy is kept constant, the melting proceeds for a short time and then stops because of the fall in temperature.

In order to study the process of the surface-initiated melting, the sample is divided into different planes that are parallel to the surfaces of the sample. The Planar Structural Factors(PSFs) are used to monitor the extent of disorder in the planes. The PSF of the jth plane is defined as

$$S_j(\mathbf{k}) = \frac{1}{N_j}\sqrt{(\sum_i^{N_j} cos(\mathbf{k}\cdot\mathbf{r}_{ji}))^2 + (\sum_i^{N_j} sin(\mathbf{k}\cdot\mathbf{r}_{ji}))^2} \tag{3.3}$$

where $\mathbf{k}$ is a wave vector in the plane, $\mathbf{r}_i$ is the space vector of the ith molecule and N_j is the number of molecules in the jth plane. Here it can be seen that when the molecules are at lattice sites, the PSF is unity and when the molecules are disordered the PSF should vanish, assuming the number of molecules is not too small. If the number of molecules in a plane is too few the fluctuation can be very large.

There are two ways of defining a plane in the sample. It can be either a plane with all the molecules lying on one or several lattice planes, or a slice of the sample defined by the molecular positions along the z direction. In the first case, the number of molecules in a plane is fixed but in the second case the number fluctuates especially on the planes near the surfaces where the molecules are most

disordered. In this case we only use the former definition because it was found that if the sample is cut into slices some slices may contain very few molecules at melting and this causes large fluctuations in the PSFs. Increasing the thickness of the slices can partly solve the problem but it also hinders the investigation of the details of the process.

The MD-cell we used consisted of 1296 molecules formed by 6×6×18 bcc unit-cells. The equilibrium unit-cell vectors are parallel to the edge of the MD-cell, so there are 36 (001) planes along the z direction each containing 36 molecules. One of the reasons why the MD-cell shape was chosen in this way was to have as thick a slab as possible, thus reducing the possible interaction between the two surfaces and giving a longer period of surface melting. The wave vector in the PSF was chosen as $(1,0,0)/a$ where a is the bcc lattice parameter. This wave vector is a reciprocal lattice vector of a two dimensional square lattice but not the three dimensional bcc lattice. Hence if a plane is not a plane in the lattice of the crystal but is a slice of the sample, one must choose other $\mathbf{k}$ values like $(2,0,0)/a$ since a slice of the sample may consist of molecules from more than one lattice plane. Larger wave vectors also makes the PSF more sensitive to the distribution of the molecules in the plane. For the wave vector $\mathbf{k} = (1,0,0)/a$ it was found that the PSF is about 0.90 in the solid phase and 0.25 in liquid phase. Therefore, when the PSF of a plane is smaller than 0.4 it could be regarded as melted. The exact value of this criterion is not important so far as it is larger than the value of PSF in the liquid state and sufficiently smaller than the value in the solid state.

3.3.2 Results

The Liquid Films

The PSFs were calculated every 80 timesteps (0.8ps). The runs lasted for a total of 8,000 timesteps or 80ps at each temperature. Results show that when the temperature is between 180 to 200K most parts of the sample remains solid with only some liquid or partially disordered planes on the surfaces. Below 190K only one plane of molecules can be identified as liquid(PSF $<$ 0.4). Figure 3.2 shows

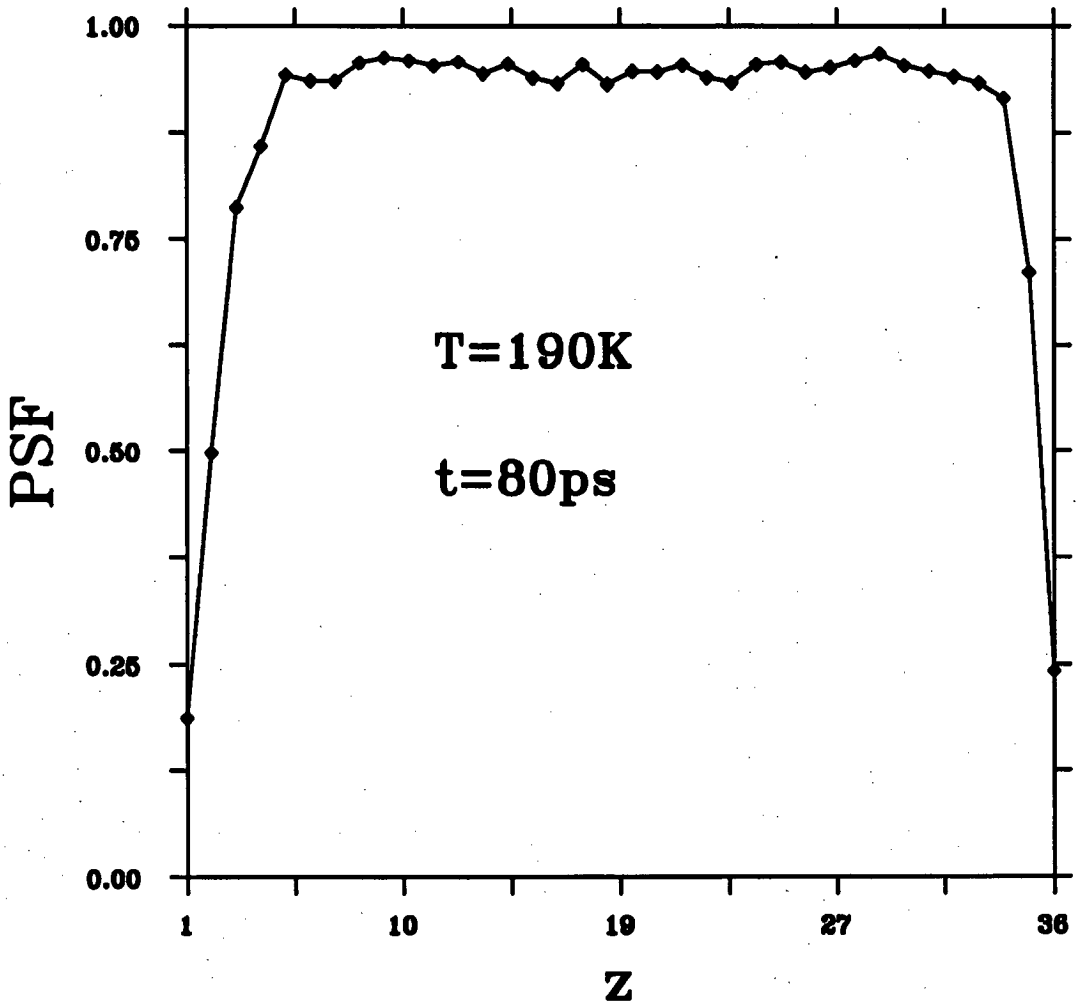

Figure 3.2: The PSF profiles at 190K after a run of 80ps.

the PSF profile at 190K at the end of a 80ps run. At 200K, there are 2 or even 3 planes that have melted, a result that is in agreement with a cluster simulation[54]. At 210K, liquid films are also present but apparently are not in equilibrium with the solid part even towards the end of the run. (Later in this chapter one can find that this happens because 210K is very close to the melting point when surfaces are present. Therefore, given enough time the liquid film at 210K will become thicker and may even lead to the melting of the whole sample.)

PSFs can only give the information of the molecular disorder within the planes perpendicular to the z axis so the molecular density distribution perpendicular to the planes is also worth calculating. Such a density distribution function was

calculated at 210K at the end of a simulation of 40ps and is shown in figure 3.3. From this figure one can see that some planes on the surface do not retain much planar structure whereas those in the middle of the sample can still be identified positively. Calculations at different temperatures and at different stages of the simulations were also made and compared with the PSFs and it was clear that when the molecules are disordered within the plane they are also disordered along z.

The Melting Point

Figure 3.4 shows the total width of the liquid films as a function of time at temperatures from 210 to 250K. Since there are two surfaces in the system the width is in fact the sum of the widths of the two films on both surfaces. The speed of melting is closely related to the temperature. At temperatures above 210K, the system becomes liquid in a period that is much smaller than the total duration of a run. The next step of the simulation should be the evaluation of the velocities of the propagation of the solid-liquid interface from the time-dependent width of the liquid films, from which the melting point can be obtained. However, this is not always easy. As is shown in the figure, the width of the films as functions of time are not linear or the linear parts are very short. Therefore, the method as used for the determination of the melting point of silicon[67] does not seem to work very well. It was thus desirable to try to identify the cause of this problem and try to solve it.

Multi-nucleation

From the work presented in [67, 84, 73], melting of silicon, benzene or aluminium slabs starts from the surfaces and progresses into the middle of the sample. The surfaces serve as the nucleation centres. We have found that this is not the case for SF_6. For this substance not only does melting start from the surfaces it also happens in the middle of the sample when the rest of the sample is still solid. This is shown clearly in figure 3.5 which includes the PSF profiles at four different instants of the melting process at the temperature of 220K.

In order to determine why nucleation also happens in the middle of the system,

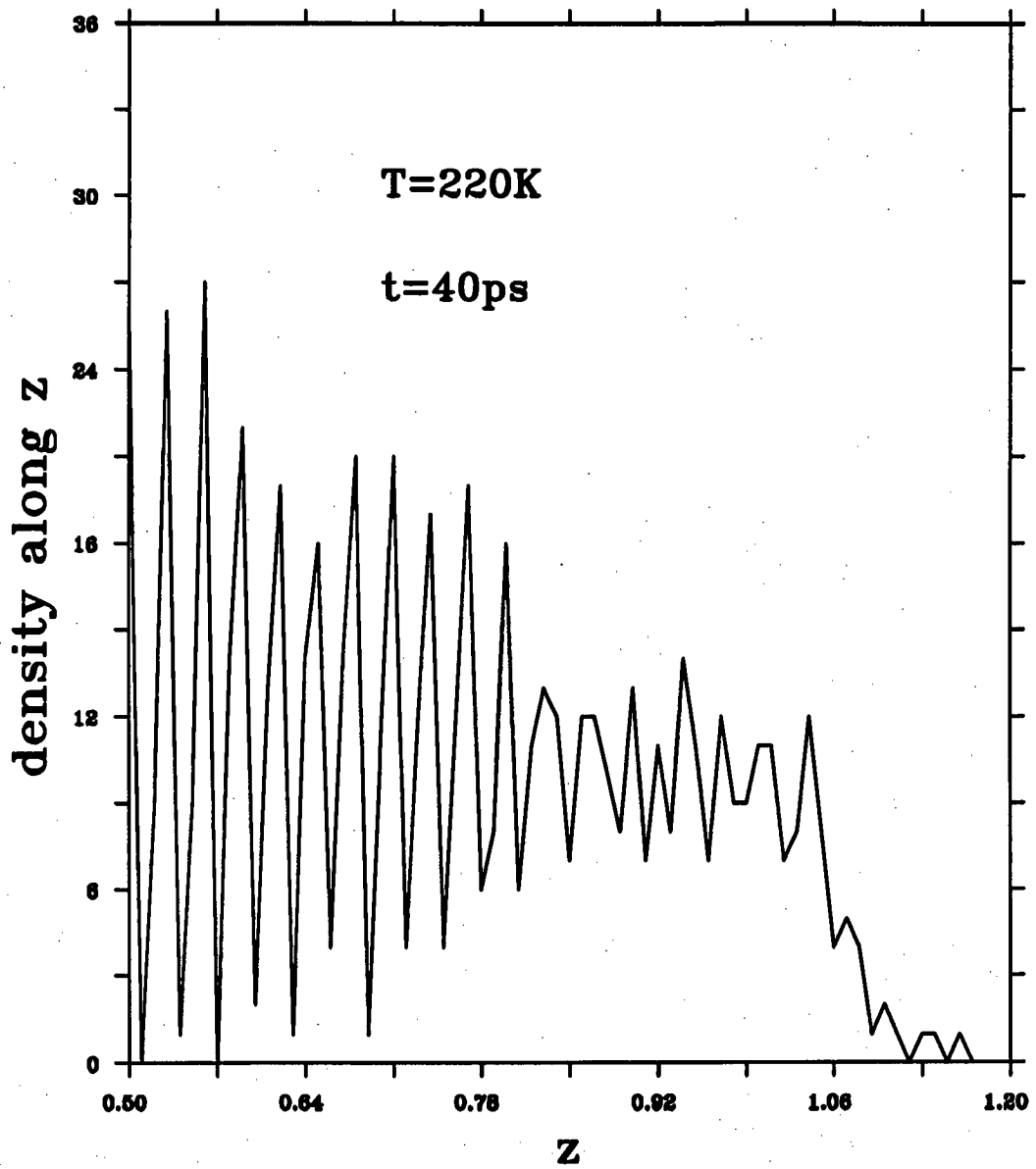

Figure 3.3: The instantaneous molecular density distribution along z axis at 210K. The planes on the surfaces show greater extent of disorder along the z direction while the rest of the sample retains the original periodic structure.

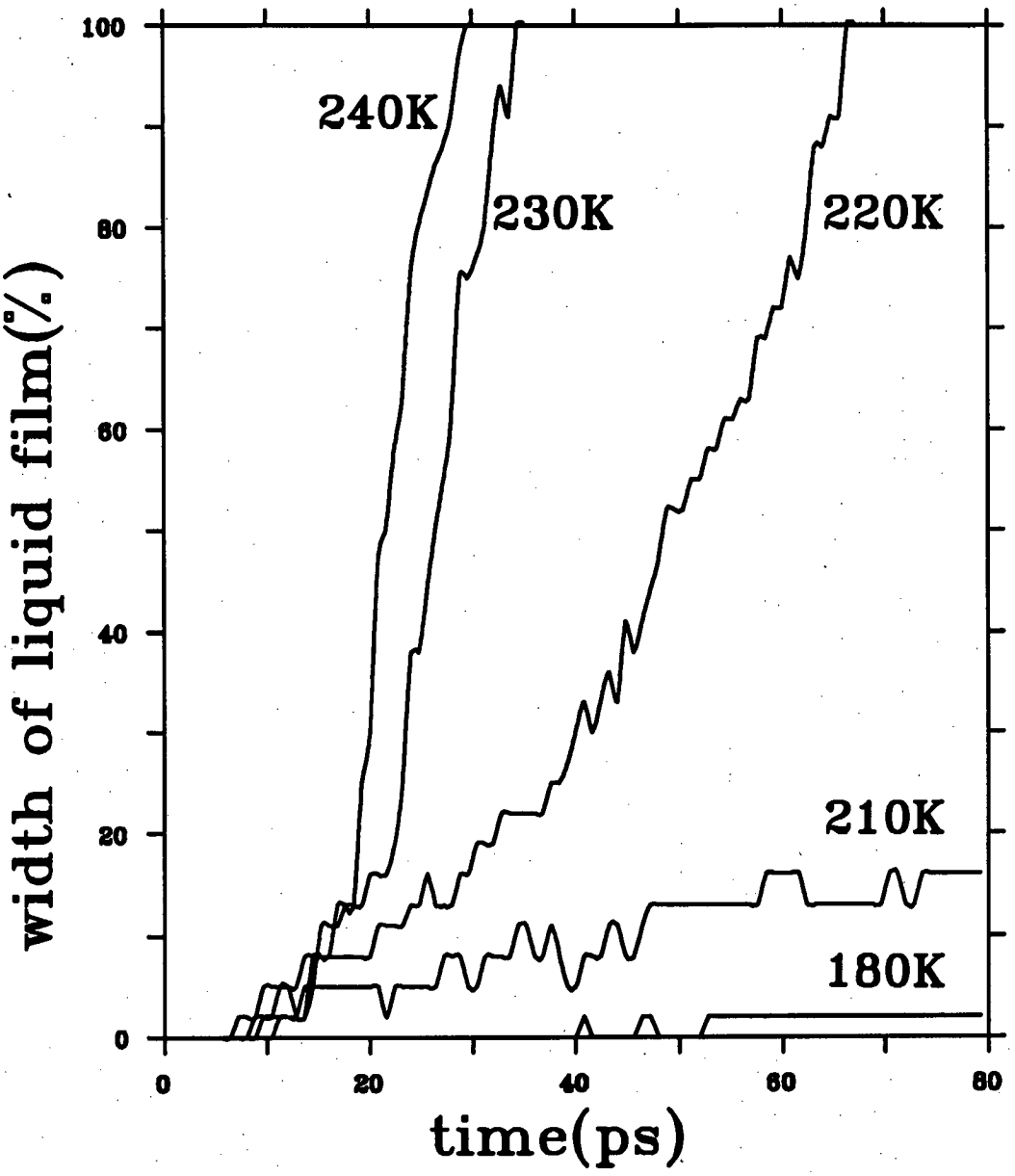

Figure 3.4: The width of liquid films as functions of time. The rate of melting is temperature dependent.

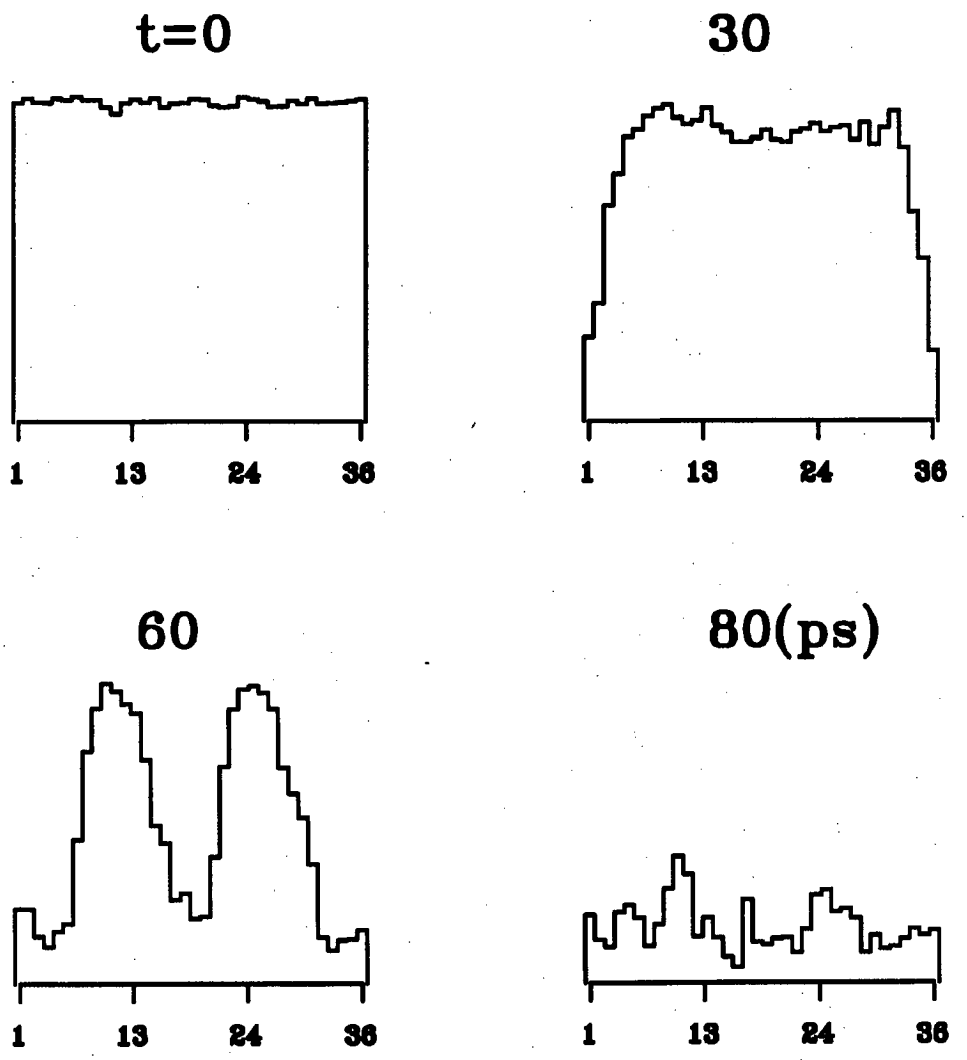

Figure 3.5: PSF profiles at 220K. Melting starts not only from the surfaces.

we define another quantity that is related to the PSFs. We will call the new parameter *Disorder Factor*(DF) and it is expressed as

$$DF = (1 - (\sum_{j}^{P} S_j^2(\mathbf{k})/P)^{1/2}) * 100 \tag{3.4}$$

where P is the number of planes in the sample.

From the definitions of DF and the PSF, DF=100 if the system is completely disordered and DF=0 if the sample is completely ordered and there are an infinite number of molecules in the planes. Some fluctuations are expected for any limited number of molecules and if the number of molecules is very small neither DF or PSF is well-defined.

The DFs are calculated at temperatures from 180 to 210K and the results are plotted in figure 3.6(b). At higher temperatures the major characteristics of the DFs are very similar, the width of the liquid films plotted in figure 3.4 suggesting that the main contribution to the disorder of the whole system comes from the melted parts.

Figure 3.6 also contains a plot of the potential energy. It is interesting to see that the potential energy fluctuates almost periodically. The higher the temperature, the greater the period is. The oscillation persists and the amplitude declines very slowly. Meanwhile, similar oscillations can be observed in the DF plot, but in a less conspicuous way. This periodic oscillation in the DFs becomes clearer when they are calculated with the outermost several planes removed. Figure 3.7 shows the DF of the whole sample (solid line) and the DF without the outermost 7 planes at a temperature of 210K. From the figure, it is clear that the central part of the sample experiences a periodic oscillation and this oscillation seems to die down slowly just as happens with the potential energy. The permanent disorder in the system comes from the planes on the surfaces and these planes form liquid films. It can be concluded that, for temperatures below 210K, melting only occurs on the surfaces. The change of the disorder can also be monitored by the PSF profiles at different times. Figure 3.8 shows two PSF profiles at 210K, one is calculated at 18ps when the potential energy is at its first maximum and the other is calculated at 34.6ps when the potential energy is at the next minimum. The figure shows

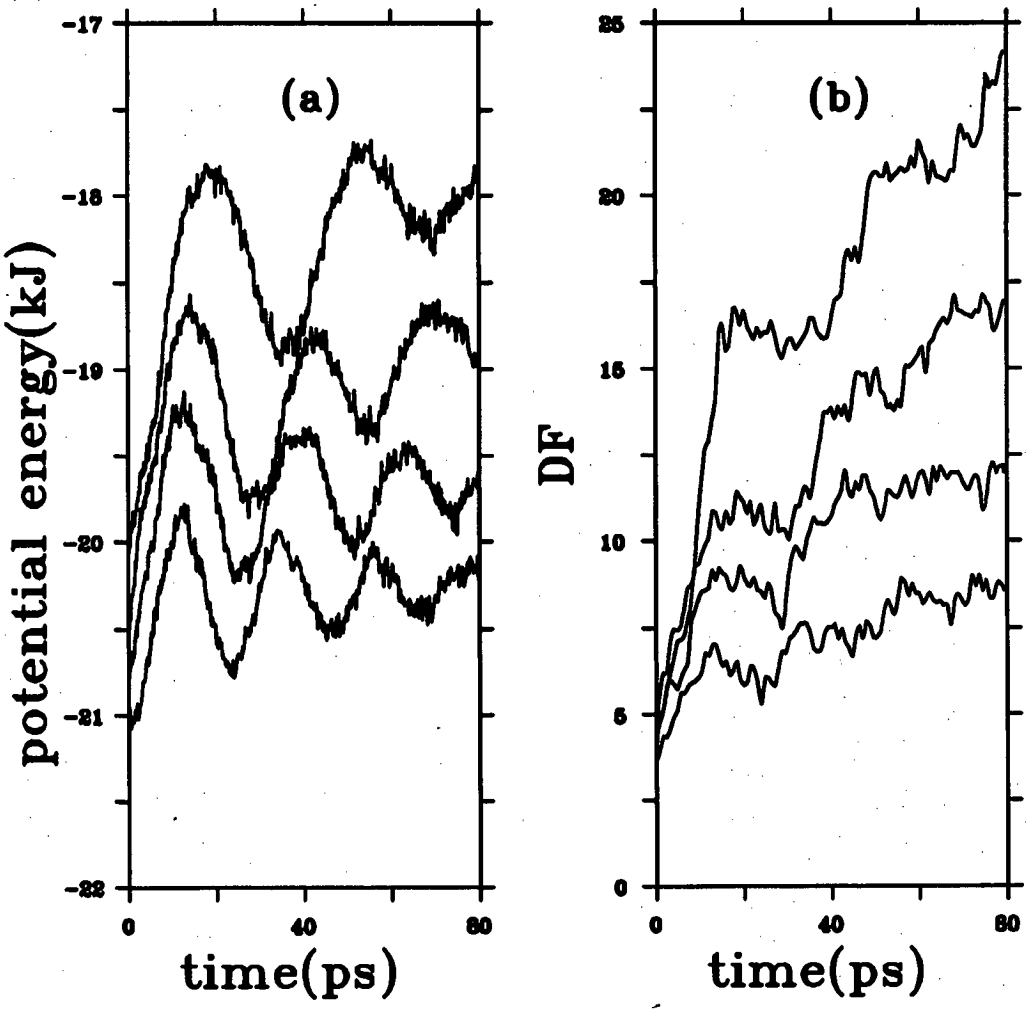

Figure 3.6: The variation of (a) the potential energy and (b) DFs. Oscillations are prominent at those temperatures. From the lowest up, the four curves in the figures correspond to temperatures of 180, 190, 200 and 210K.

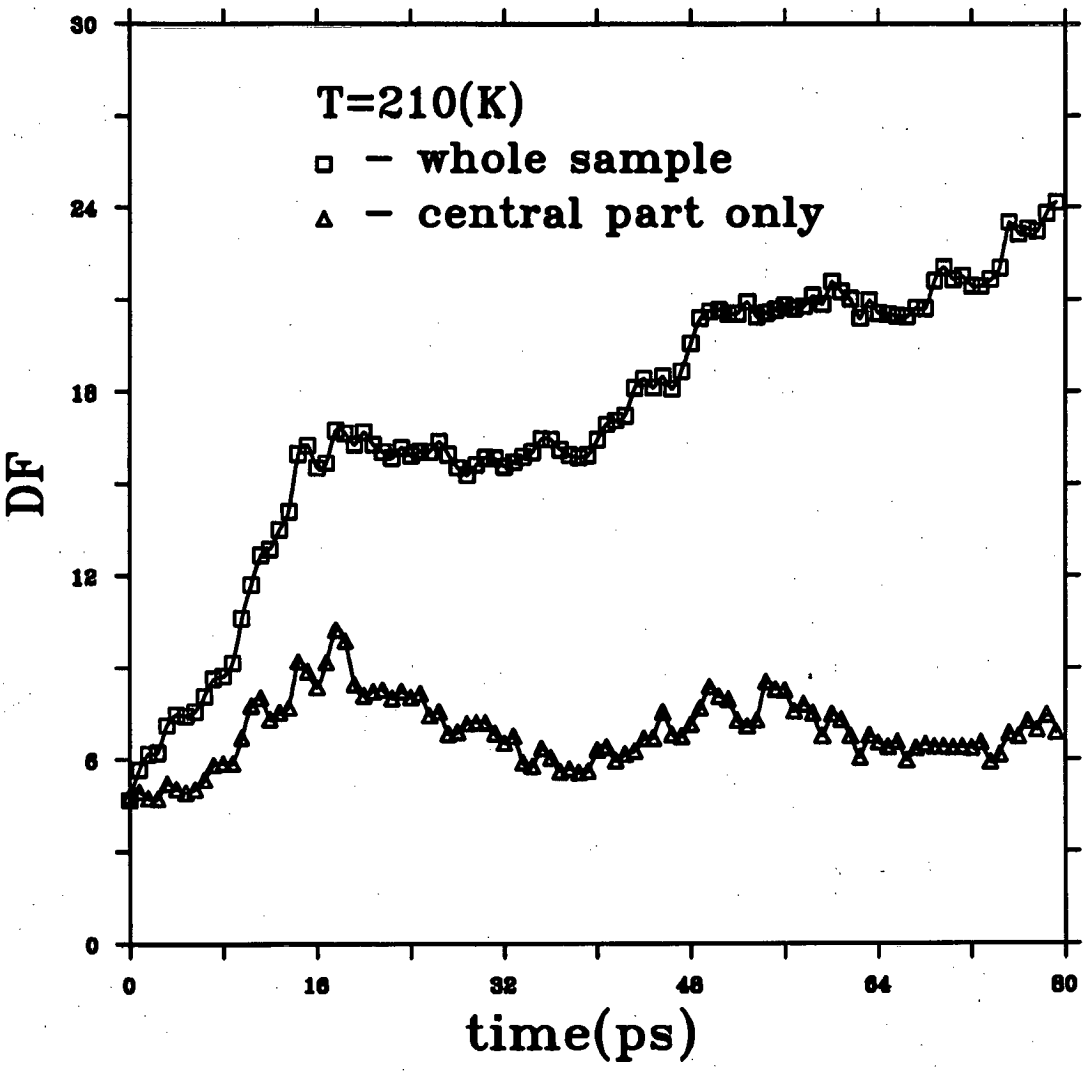

Figure 3.7: The DF of the whole sample and the DF without the outermost 7 planes. The temperature is 210K.

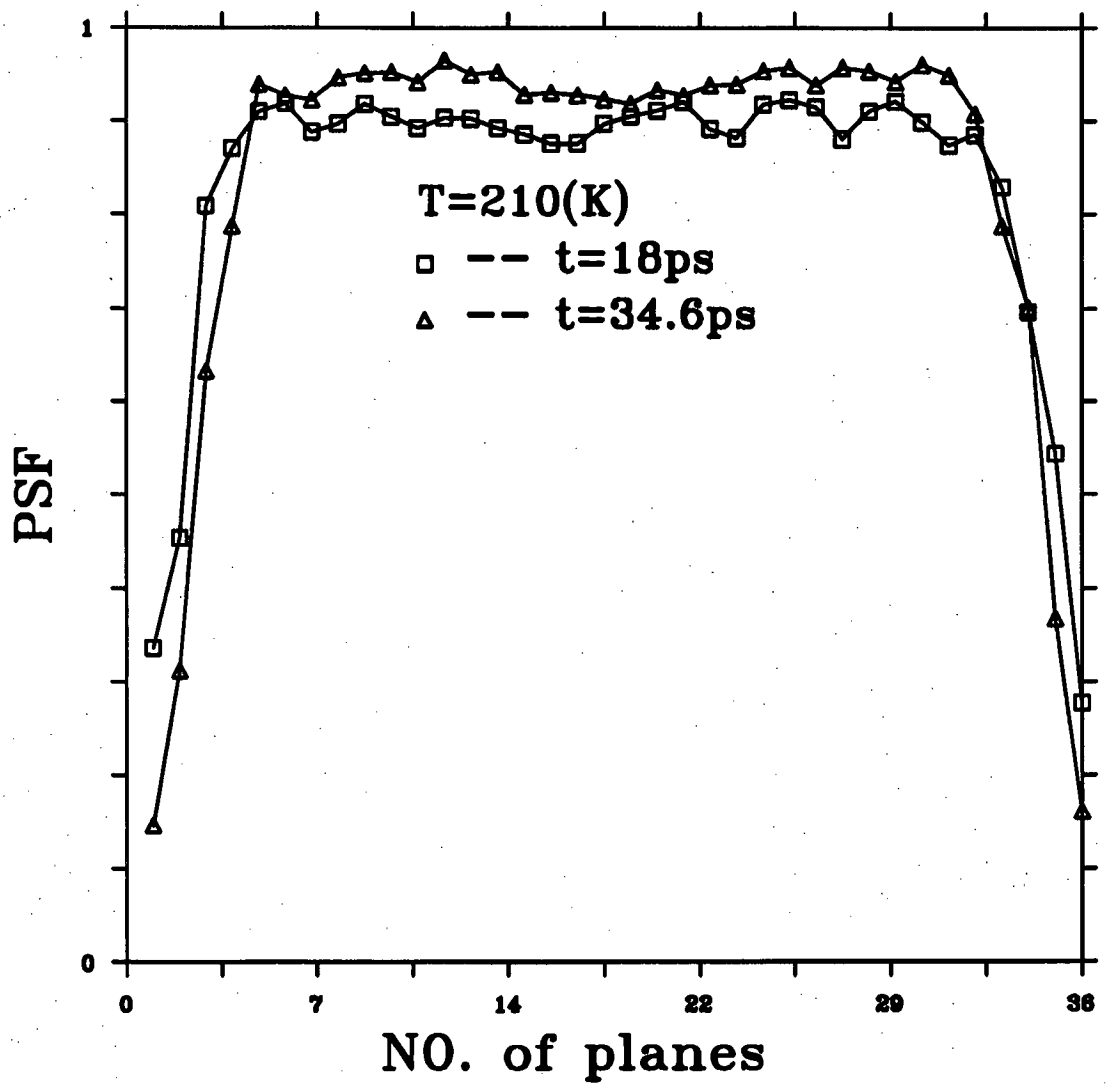

Figure 3.8: The PSF profiles at 18ps and 34.6ps of the simulation. The temperature is 210K.

clearly the relation between the potential oscillation and the change in PSFs. At 34.6ps, the planes on the surface are more disordered than they were at 18ps demonstrating the progress of the formation of the liquid films. In the central part of the sample, the values of PSF are significantly larger than they were at 18ps.

The Process of Melting for SF_6

The process of melting of SF_6 is now clearer. When the surfaces are introduced the

molecules near the surfaces begin to be translationally disordered. Liquid films are formed and the thickness of a film depends on the temperature. Meanwhile, because of the removal of the periodic boundary condition and the melting of the surface the potential energy begins to oscillate. When a certain temperature is reached, above 220K for SF_6, the oscillation will lead to the nucleation at any depth of the sample. In this situation, melting becomes faster than purely surface melting. Because of the multi-nucleation and the fact that the thickness of the liquid films is not a linear function of time, it is difficult to calculate the velocity of the propagation of the solid-liquid interface.

The oscillation in the potential energy and the DF may be explained by the lack of equilibrium of the sample. When the periodic boundary condition is suddenly removed, the molecules lose some nearest and next-nearest neighbours. This in effect increases the temperature on the surface drastically making a temperature difference between the surface and the bulk. Because of this difference in temperature, the excess heat on the surface will transport into the central part increasing the displacements of the molecules there. Meanwhile, the molecules on the surfaces are becoming more disordered and the potential energy contribution to the energy of this part of the sample is becoming larger so that the temperature of the surfaces begins to fall causing a reversed flow of heat from the central part back to the surfaces. This process will repeat until the liquid films on the surfaces become stablized and equilibrium between the films and the rest of the sample is established.

Improved Procedure

From the above discussion, the nearly periodic oscillation of the potential energy is inevitable so far as the surface melting is still progressing. To minimize this artefact, a procedure was designed to reduce the initial temperature difference between the surface and the rest of the sample so that the amplitude of the potential oscillation is small. This was achieved by first removing the periodic boundary condition in the z direction when the temperature is 180K and then keeping the temperature at that value for about 20,000 timesteps. This very long time run was necessary to ensure that the oscillation caused by the removal of the

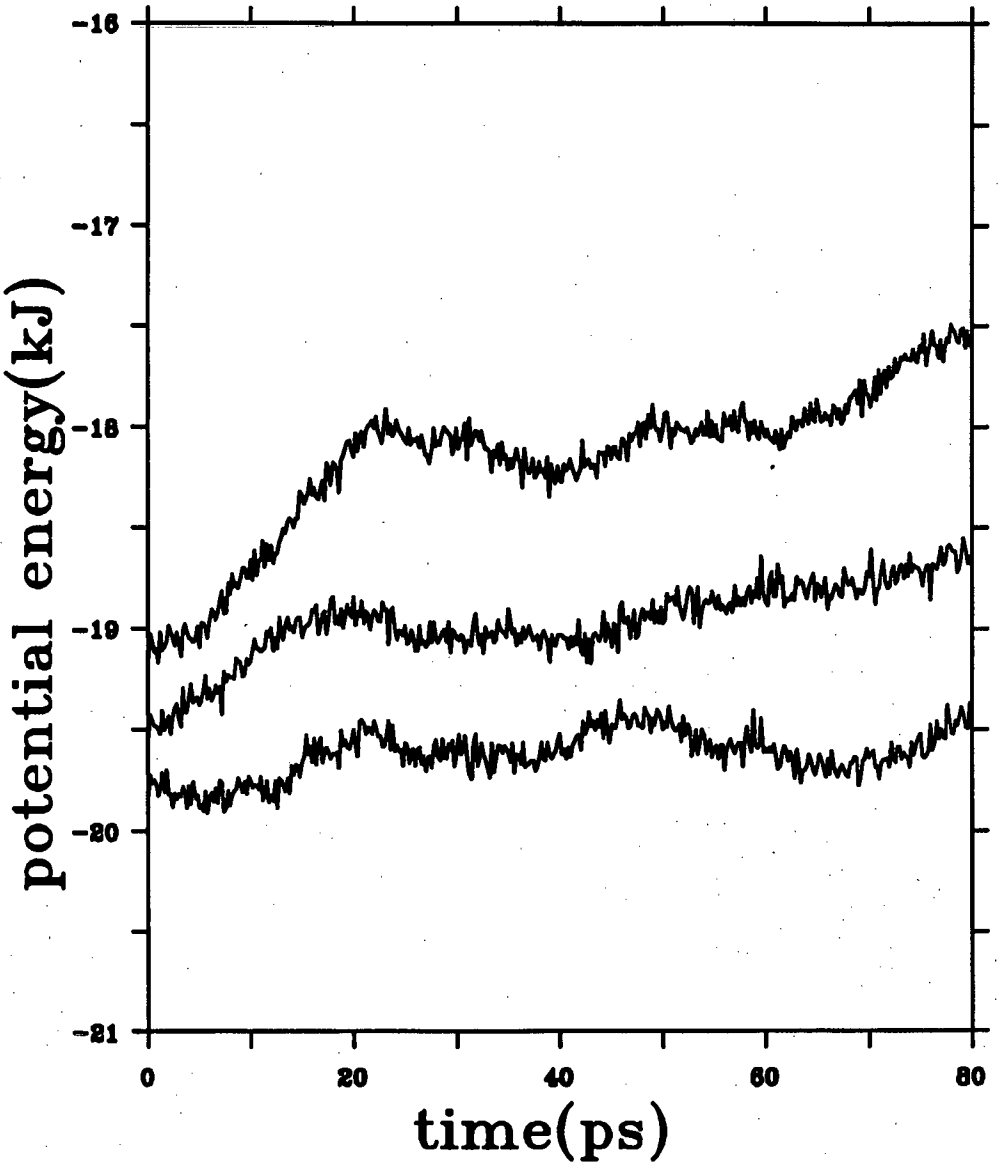

Figure 3.9: The potential energy at 190, 200 and 210K.

periodic boundary condition is small at the end of the run. After this procedure, the amplitude of the oscillation became very small. The system was then heated to different temperatures and the lattice parameter scaled to the values obtained from previous calculations on the bulk sample at the corresponding temperatures.

Following this, the process is the same as was used before. Figure 3.9 shows how much smoother the potential energies at 190 to 210K have become with this new procedure. In figure 3.10 the PSF profiles at different stages of the run at 220K are plotted. The melting obviously proceeds only from the surfaces now. The

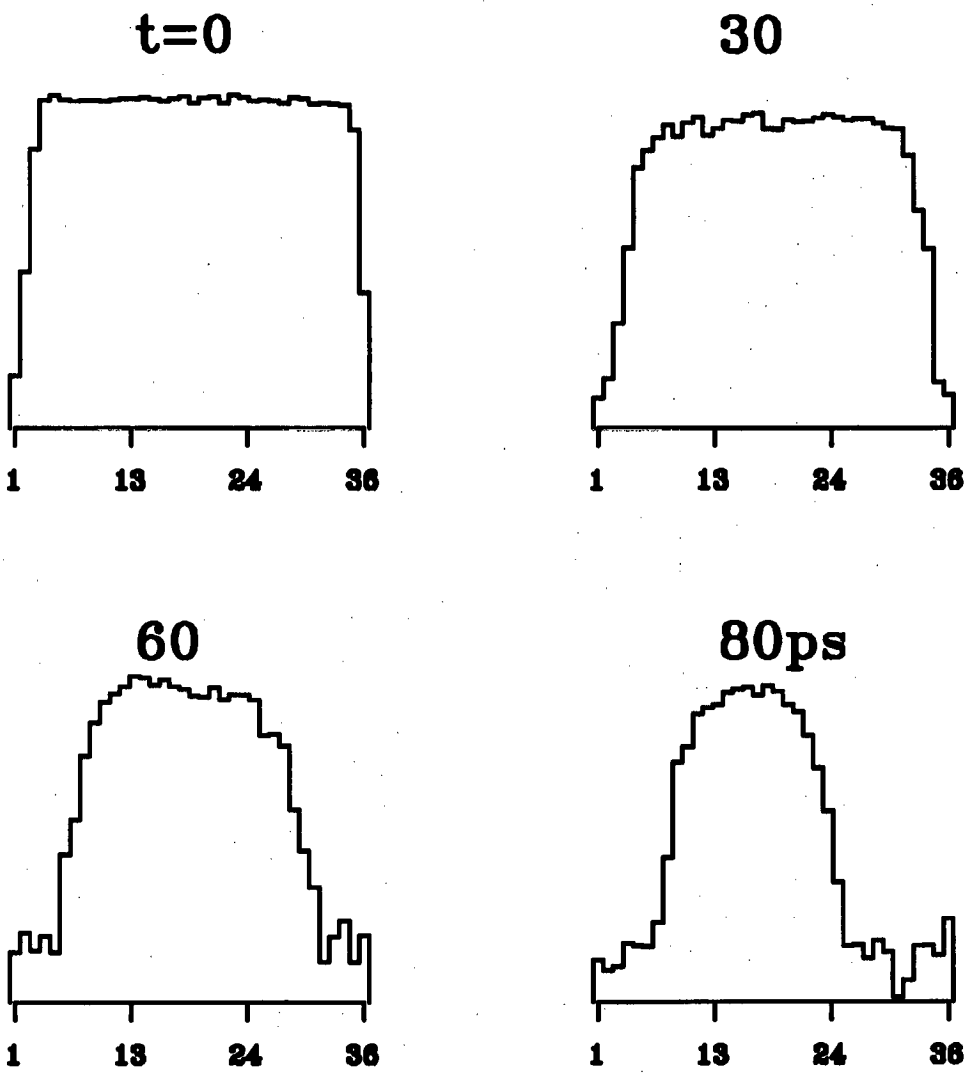

Figure 3.10: Melting at 220K. Melting starts from the surfaces.

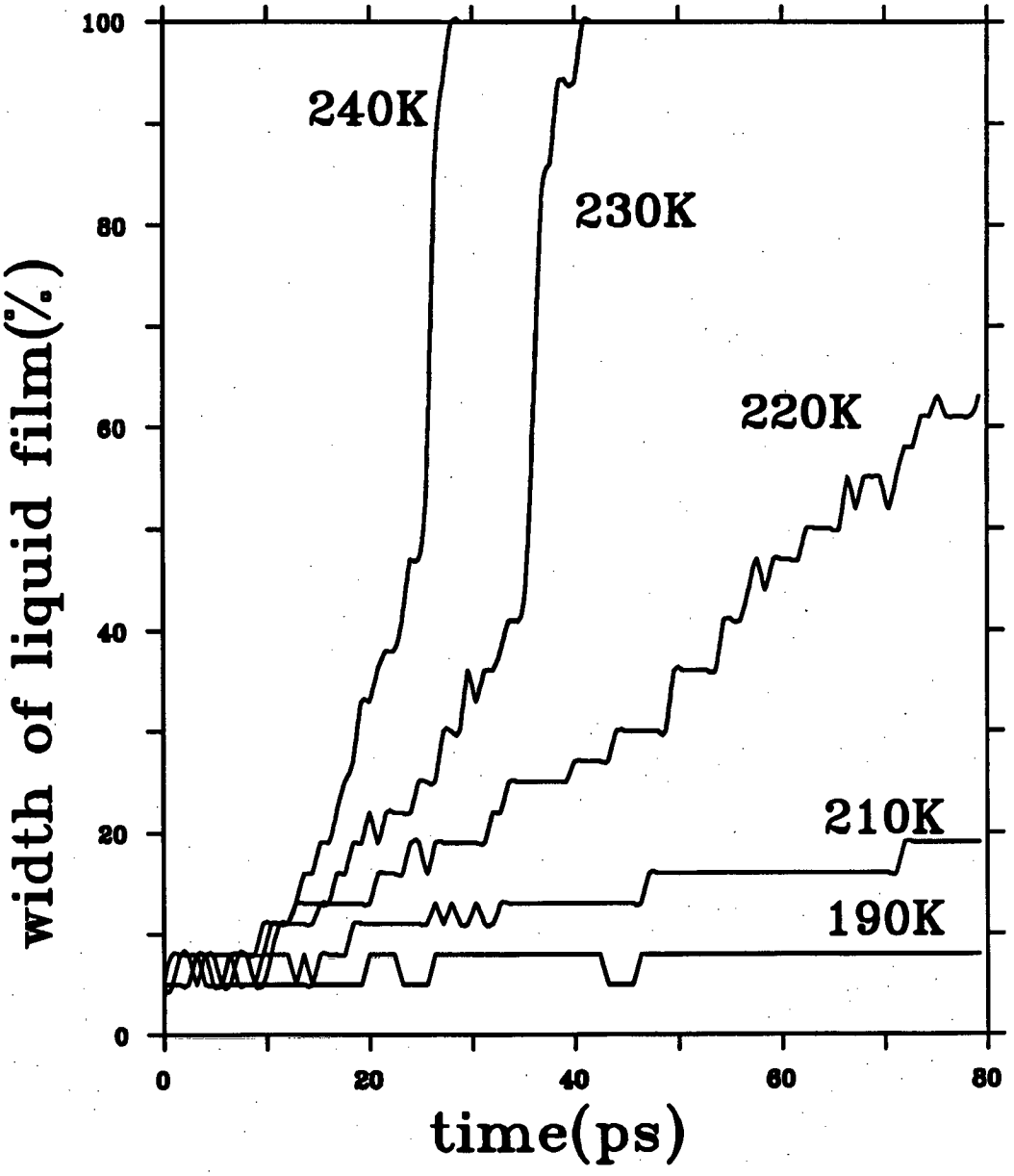

Figure 3.11: The width of liquid films as functions of time. The linear parts are used to evaluate the melting rates at different temperatures.

linear parts of the melting processes at some temperatures have become longer as shown in figure 3.11. However, the improvement is limited. The oscillation still exists especially at higher temperatures. Multi-nucleation also happens at later stages of the melting process. Other different procedures were also tried without much success so we have to be content with the results.

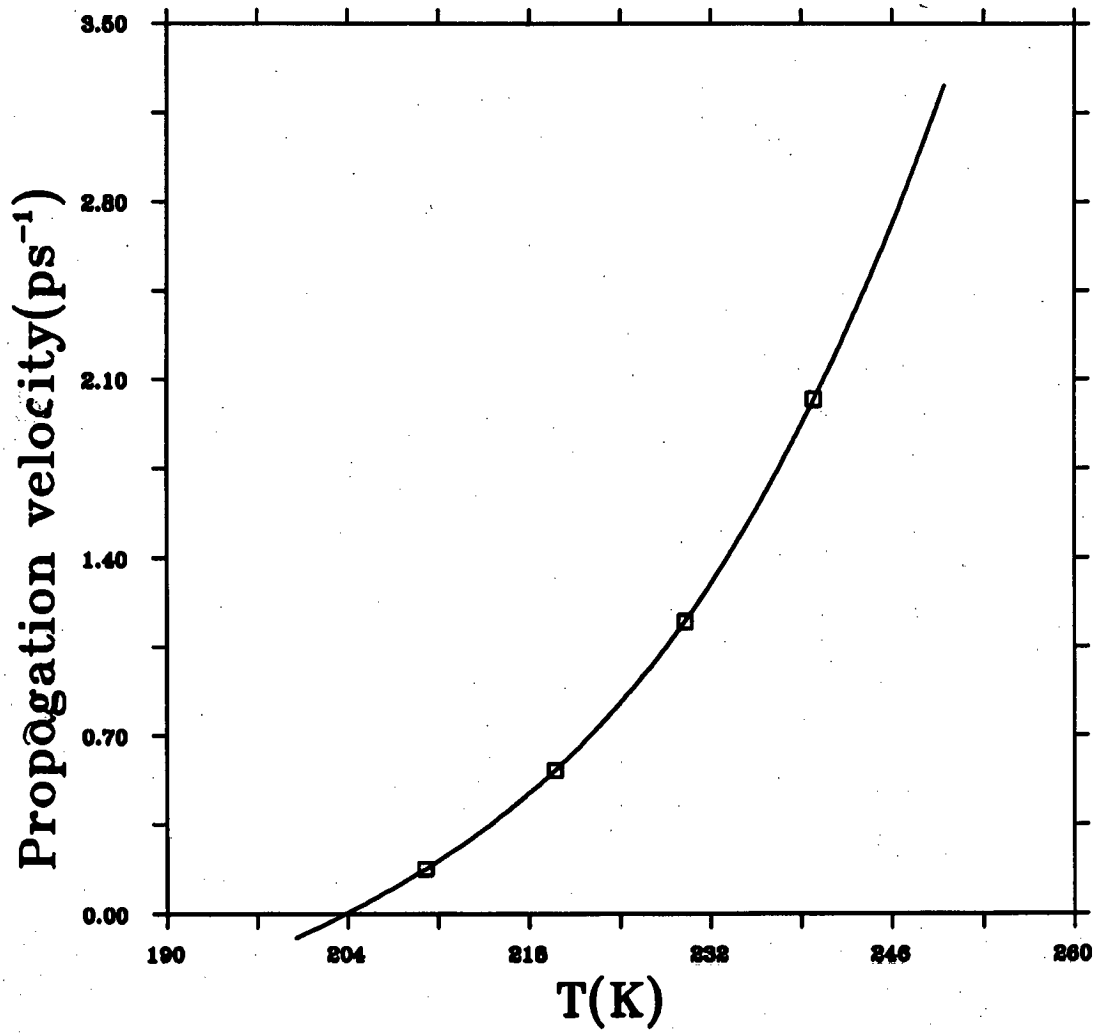

Figure 3.12: The melting rates and the melting point. The solid line is obtained by a third order polynomial fitting. The melting is at 204K.

By fitting the linear parts of the width of the liquid films, the melting rates at 210, 220, 230 and 240K are calculated. A third order polynomial is fitted to the data points. The melting point of SF_6 is then determined to be the temperature at which the rate is zero according to the polynomial function. The melting rates and the curve of the polynomial are displayed in figure 3.12 and the melting point is the abscissa of the point where the curve of the polynomial and the temperature axis meet. From the figure, this is determined to be 204K. The error of this melting point is estimated as $\pm$5K.

3.4 Discussion

The surface-induced melting method has been used to study the melting process of SF_6 and to determine the melting point of the model. It was found that the main characteristic of the surface which initiated melting of SF_6 is similar to that of silicon, benzene and aluminum, despite the quite different nature of the plastically crystalline phase. The melting point was found to be 204K. This value is about 23% lower than the temperature at which a sample with fully periodic boundary conditions 'melts' and 10% lower than the experimental value of 223K. Hence the melting point estimated by means of the surface-initiated melting is about 13% closer to the experimental value than that estimated from the bulk MD simulation. Taking into account the fact that the model has successfully predicted both the low-temperature monoclinic structure and the plastically crystalline phase this result is most acceptable.

Besides the simulation of infinite systems, clusters are also the subject of MD simulation. There is no restraint on boundaries so that the sample has free surfaces. Because of this, it is interesting to compare the cluster and the semi-infinite system. The cluster simulation of SF_6 has already been carried out by Fuchs, Pawley and Boyer[54, 55]. The sizes of the clusters varied from 128 to 512 molecules. For a cluster of 512 molecules, the outermost three layers of molecules are obviously different from the rest of the sample in terms of diffusive movements. This phenomenon is similar to the forming of liquid-like films on the surfaces of the semi-infinite samples. It has also been noticed that, for clusters of different sizes melting happens at very different temperatures. For a cluster of 128 molecules, melting was observed at as low as 125K but for a cluster of 512 molecules the inner regions seem to remain in the plastic phase even at 200K, in agreement with the present simulation.

One difficulty in the MD simulation of melting of a cluster comes from the finite size of the system. It is reasonable to assume that the disorder oscillation happening in the semi-infinite system also happens in the MD simulation of clusters. Moreover, the larger surface-to-body ratio of a cluster may make this artefact even more serious. This might have contributed to the the size-dependence of the

melting point observed in some cluster MD simulations.

Chapter 4

Fluctuations and Elastic Constants

4.1 Introduction

It is well known that in a system of N atoms (or molecules), the relative fluctuation of a thermodynamic variable A from its ensemble average value $\bar{A}$ is of the order of $1/N$ for most of the statistical ensembles, i.e. $< (A-\bar{A})^2 > \propto 1/N$. For a macroscopic system, N is of the order of 10^{23} so the fluctuations are very small and this phenomenon is hardly a problem and can often be ignored completely. For a system which can be studied through the MD method, however, the number of molecules is usually very limited. It ranges from several hundred to several thousand. In the MD simulations, therefore, much greater fluctuations of the thermodynamic quantities are expected. These fluctuations can be very significant and will certainly bring into the measurements uncertainties that one always wishes to minimize. In the extreme situation when N is too small one may find it meaningless to define any thermodynamic quantities.

While fluctuations of some properties seem to be unavoidable troubles, they are sometimes useful in MD simulations because they are related to some other thermodynamic properties so that these properties, which may not be explicitly defined by the molecular trajectories, can be calculated. For instance, the volume compressibility, which is obviously unavailable from any combination of the molecular coordinates, velocities or any higher order derivatives of them, can be calcu-

lated from the fluctuations of the volume of the system which is a well defined variable in any (HPN) MD simulations (see equation 4.1). The general discussion of the relations between thermodynamic properties and the fluctuations can be found in many text books such as reference[14]. In this chapter, we will make use of this kind of relation to calculate the bulk modulus, the heat capacity, the expansivity and particularly the elastic constants of SF_6 in both the low-temperature monoclinic phase and the bcc plastic crystal phase. The attention will be focused especially on the behaviour of those properties near the solid-solid phase transition and the melting point. The thermodynamic properties that will be calculated are those measurable in experiment and are the macroscopic manifestation of the microscopic nature of the matter (or the model of the matter to be exact). The knowledge about these properties is helpful to link the computer simulation of a model and the real substance. To our knowledge, this work is the first attempt to use the fluctuations to calculate thermodynamic properties of a molecular system over a large range of temperature and involving a phase transition.

The calculations which will be described in this chapter were carried out on the ECS. On this MIMD machine the sizes of shapes of the MD-cells are easy to manipulate. The high performance of the machine is another important reason for using it as the calculations are very time-consuming.

4.2 Thermodynamic Properties

According to the theory of statistical mechanics, for different ensembles the fluctuation of a thermodynamic, or non-thermodynamic variable such as the kinetic energy, is related to other properties in different ways. Ray, Haile and Graben have discussed the relations between the fluctuations and the physical properties in the (HPN) ensemble[80, 79] (isoenthalpic-isobaric ensemble) which attracted very little attention before it was applied in the MD simulations. Based on their work we can calculate the adiabatic volume compressibility χ_s, isobaric heat capacity C_p and the volume expansivity α through the following formulae.

$$\chi_s = 1/B_s = \beta \frac{< (\delta V)^2 >}{< V >} \tag{4.1}$$

$$C_p = \frac{3kN}{1 - \frac{\beta^2}{3N} < (\delta K)^2 >} \tag{4.2}$$

$$\alpha = \frac{\beta^2 C_p}{3N} \times \frac{< \delta KV >}{< V >}. \tag{4.3}$$

where K is the total kinetic energy, V is the volume of the MD cell, N is the number of molecules in the sample, B_s is the adiabatic bulk modulus, k is Boltzmann's constant and $\beta = 1/kT$. In these formulae, it has been assumed that a molecule has six degrees of freedom so that they can be directly used for SF_6. The mean value of the fluctuations are defined as
$< \delta A^2 >=< (A-\bar{A})^2 >$ and $< \delta AB >=< (A-\bar{A})(B-\bar{B}) >$.
For the sake of convenience, later in this chapter, the unit of C_p is taken to be Nk. These formulae are derived from general ensemble theory and are valid in any MD simulations that generate (HPN) ensembles.

4.2.1 The Implementation of the Method

The equations relating the fluctuations of the basic thermodynamic variables and other properties are simple and clear. The remaining problem before a calculation could really begin is to determine how long a simulation should be to get reasonably accurate results from those formulae. The calculation is viable only when the time needed is within the reach of the computers we are using. So far there has

not yet been a general theory concerning this issue. The only work we know is that of Haile and Graben[83]. In that work, a liquid of 256 atoms interacting with Lennard-Jones type of potential was simulated and χ_s and C_p were calculated at a fixed temperature. In their work, an MD method which only allows the volume to be a dynamic variable but not the shape was used. This is of course justified because liquid has not the resistance to the shear stress. The accuracy of the compressibility seems to be high when compared with that obtained through an empirical equation of state. The value of C_p, however, has a larger discrepancy and the explanation of this is not very convincing because of the lack of the convergence test over adequate duration of time. In the present work on SF_6 we wish to know if the method works for the more general MD method we are using and if the method is applicable for solids. SF_6 has two very different solid phases and this gives us a very good chance to test the method.

As the first step of the calculation, a test run was first carried out for a system of 1848 molecules and the value of the piston mass[9, 10] was set at a tenth of the total mass of the MD-cell. This choice was suggested by Craven[84] in his study of benzene. The purpose of chosing the piston mass in this way is to make the vibrational period of the volume roughly equal to the time it takes the acoustic wave to travel through the sample. For the system under discussion, the value of the piston mass is 26981 a.m.u which is about 185 times of the mass of an SF_6 molecule. The volume vibration period τ, which can be calculated from equation 1.11, is 4.4ps, about four times of the typical period of the molecular oscillation.

The main problem of using a large piston mass in the simulation seems to be that it takes too long for the system to be equilibrated. In the MD run mentioned above, by monitoring the volume fluctuation, it was found that the system did not equilibrate well even at the end of the 70,000 timesteps run. Figure 4.1 shows the variation of the volume versus time. The decay of the amplitude of the volume fluctuation follows roughly a slow exponential rule and it should stablize at a certain value when the system is equilibrated. This slow process may have suggested that when a large piston mass is used the coupling between the volume fluctuation and the molecular motion is very weak so that the unphysical large-

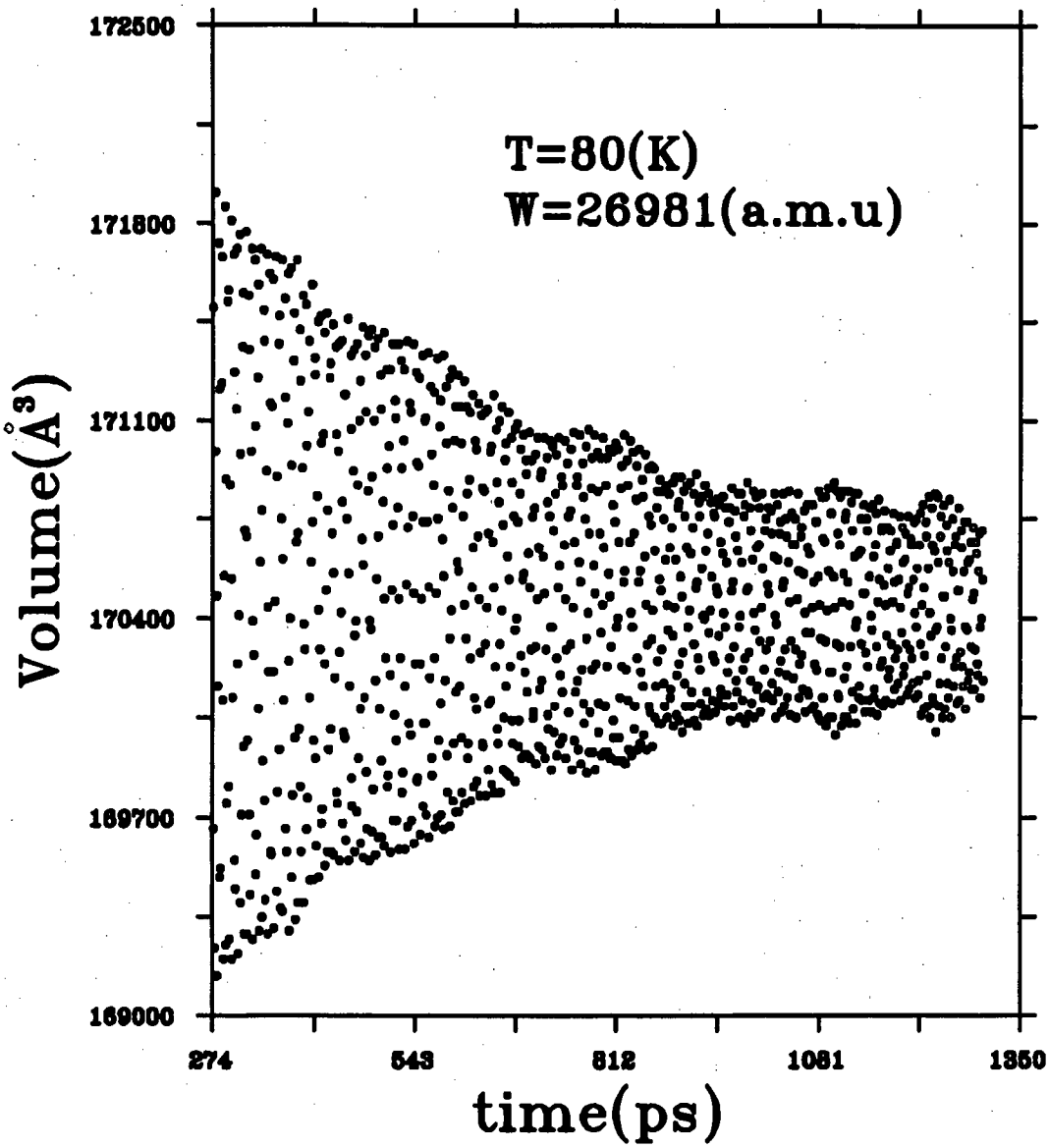

Figure 4.1: The volume fluctuation of the system with a large piston mass.

amplitude oscillation of the volume is difficult to dissipate through the damping mechanisms in the molecular system. It is obvious that even though this choice of the piston mass makes sense physically it is not really suitable for the current calculation which needs long runs and many data points at different temperatures.

Because of the slow equilibration process and because the piston mass does not affect the static properties such as the crystal structure parameters of the simulated system, it seems to be more practical to choose a smaller value for the piston

mass to shorten the equilibration stage. So far we have not found any significant discrepancy in the equilibrium physical properties such as the lattice parameters, the r.m.s of the molecular movements or the velocity autocorrelation functions because of the change of the piston mass. The only trouble we have with a very small piston mass is that it may cause a program crash when the structure changes happen or at the beginning of the runs when initial stress makes the cell matrix change unphysically. As indicated in chapter 1, this instability happens only when the piston mass is very small, about 1/100th of the mass of an SF_6 molecule for a system of more than 1,000 molecules. However, we do not want to give the reader the impression that the smaller the piston mass the quicker the equilibration. It is worth mentioning that the coupling between the molecular motion and the volume fluctuation of the MD-cell may also play a very important role in the process of getting into the equilibrium state.

Following the above, a smaller piston mass was used. It was made equal to the mass of an SF_6 molecule. Several physical properties were calculated in both the monoclinic phase and plastic phase. The calculation was combined with the calculation of the elastic constants which is discussed in the following section. Two samples of different sizes were constructed for the two phases of the solid SF_6. The one with 1848 molecules, which has $4\times7\times11$ monoclinic unit-cells, is for the low-temperature phase and the one with 1024 molecules, which has $8\times8\times8$ bcc unit-cells, is for the plastic phase. As mentioned in chapter, the ECS has more 400 transputers. On the largest domain, which has 132 transputers, one timestep of simulation takes about 0.5s of the ECS time for the system of 1024 molecules and 1.0s for the system of 1848 molecules. A typical run of about 40,000 timesteps takes about 10 hours of the ECS time.

When the piston mass is 146a.m.u, which is the same as the mass of an SF_6 molecule, the corresponding volume vibration period τ_0 is about 0.33ps according to equation 1.11. The timestep is set to be 0.015ps so there are still more than 20 timesteps in one period of the volume vibration.

The convergence behaviours of those properties are tested first at the temperature of about 134K in the plastic-crystalline phase. The test run lasted for 45,000 timesteps and the MD-cell matrix h and other basic properties such as volume and temperature were stored every three timesteps. So in fact only 15,000 data were stored and used for the calculation. The adoption of this strategy was designed to make full use of the results of the simulations.

Table 4.1 shows the properties calculated at different stages of the run. The values were obtained at the timesteps indicated in the table. Generally speaking, the convergence is quite good after about 21,000 timesteps, but under 9,000 timesteps the results show very large deviation in the value of the properties and are thus considered very inaccurate. The errors for the final results were estimated from the values at the last several different stages of the run and were determined to be less than 5%. Better estimates may be achieved by carrying out many independent runs under the same conditions. Apart from this estimation of the errors, the value of B_s can be compared with that calculated from the period of the volume fluctuation (see chapter 1). The other two properties, the heat capacity and the expansivity, can be compared with the values derived from the data of the energy and volume of the system at different temperatures. This comparison is not very useful in determining the error of the calculation but it has been been used to check the general correctness of the whole computation scheme.

A similar test was also carried out in the monoclinic phase at the temperature of about 80K. The results are listed in table 4.2. The convergence behaviours of the properties are very similar to that in the bcc phase, but the errors estimated from the data of the last several stages are larger. This may have been related to the fact that in the monoclinic phase the inter-molecular interactions are more harmonic so that any longtime fluctuation last longer than in a phase with less harmonic interactions.

From this test it can be asserted that as the positive point the method can be used in the present MD simulation and produces reasonably good results, and as the negative point the acceptable results can only be achieved through very long simulations even for a well equilibrated system. In Haile and Graben's work[83] the

timesteps	B_s(10kbar)	$C_p(Nk)$	$\alpha(10^{-4}\mathrm{K}^{-1})$	C_p/C_v
3,000	4.174	7.417	9.083	1.466
9,000	5.033	6.012	6.012	1.303
15,000	4.732	6.259	6.396	1.310
21,000	4.644	6.519	6.965	1.346
27,000	4.617	6.558	7.095	1.355
33,000	4.553	6.607	7.192	1.357
39,000	4.582	6.498	6.938	1.340
45,000	4.566	6.534	7.066	1.349

Table 4.1: Convergence test for the bcc phase. The heat capacity has the unit of Nk, N =1024.

timesteps	B_s(10kbar)	$C_p(Nk)$	$\alpha(10^{-4}\mathrm{K}^{-1})$	C_p/C_v
3,000	5.560	7.552	8.136	1.258
9,000	5.621	7.621	8.076	1.255
15,000	5.945	7.446	7.933	1.266
21,000	5.921	7.411	7.728	1.253
27,000	6.178	7.172	7.514	1.258
33,000	6.216	7.100	7.346	1.250
39,000	6.246	7.241	7.572	1.262
45,000	6.254	7.154	7.182	1.242

Table 4.2: Convergence test for the monoclinic phase, N =1848.

simulation lasted for only up to 4,000 timesteps for the system of 256 molecules. Judging from the simulations we have carried out, their problem with the value of C_p might simply be that the run was not long enough. Even though the liquid system may be very different from a molecular solid system the convergence behaviour should not be significantly poorer because we have already seen that not much difference has been found between the crystalline phase and the plastic phase in this aspect.

4.2.2 Results and Discussions

Since the main purpose of the calculation was to investigate the behaviour of the model system near the phase transition points it is not necessary to gain very high accuracy for each specific measurement of those properties. From the convergence test, it was believed that 30,000 timesteps would be adequate to gain enough accuracy for the purpose of this study and it is hoped that these results can still be compared to the future experiments or other simulations such as MC calculations on the substance.

The calculation was carried out over a wide temperature range covering two phase transitions. Apart from C_p, χ_s and α the isometric C_v heat capacity was also calculated from its relation with those three through

$$C_v = C_p(1 + \frac{TV\alpha^2}{C_p\chi_s})^{-1} \tag{4.4}$$

and the results are listed in table 4.3.

In the monoclinic phase, the value of the isometric heat capacity C_v is very close to $6(Nk)$ which is the value when the classical energy partition law, which leads to the Dulong-Petit law, is applicable. According to this law, the specific heat of a solid is $N_\mu R$ where N_μ is the number of degrees of freedom of the constituent elements. The low-temperature phase of SF_6 is crystalline and the molecules only experience small translational and librational vibrations so the interactions are harmonic and the potential energy parts of the Hamiltonian can be represented by quadratic forms so that the energy partition law is valid in this case. However,

T(K)	B_s(10kbar)	$C_p(Nk)$	$\alpha(10^{-4}\mathrm{K}^{-1})$	C_v
		monoclinic		
48.3	6.93	6.66	6.44	5.86
79.1	6.25	7.15	7.18	5.75
113.4	5.50	8.15	9.08	5.82
137.5	4.59	11.05	14.6	5.93
		bcc		
133.9	4.57	6.53	7.07	4.84
173.8	3.84	6.64	7.79	4.52
194.1	3.25	7.19	9.46	4.44
206.4	2.84	7.96	11.5	4.48
220.0	2.54	8.96	14.4	4.38
251.5	1.56	17.0	38.53	4.31

Table 4.3: Bulk modulus, heat capacities, and volume expansivity of SF_6 in the monoclinic phase and bcc phase. The heat capacity has the unit of Nk.

even at 137.5K, a temperature at which a small number of reorientation events can be detected, the energy partition law still seems to hold. The change in C_v with temperature is within the calculation error. So in order to detect the relation between the deviation from the law and the temperature we need more accurate measurements or use other possibly more sensitive properties.

One of the properties which is more sensitive to the the anharmonicity in the system is the volume expansivity. The value of this quantity increases with temperature more rapidly even when the temperature is not very near the solid-solid phase transition point. The cause of this increase is due to the well-known asymmetry of the inter-molecular potential function.

In the plastic phase, the anharmonicity becomes much more prominent. As described in chapter 1, in this phase the molecules have large amplitude of librational motion and reorient frequently. In this phase, the energy partition law is not valid since the higher order terms in the expression of the potential energy expanded in the vicinity of the equilibrium positions of the molecules become significant

compared to the second order term. This is why the value of C_v calculated in the bcc phase is about 25% smaller than that predicted by the energy partition law.

In general the value of C_v of SF_6 decreases slightly in the bcc phase as the temperature increases. This is consistent with the temperature-dependence of the reorientation rate. When the temperature increases the molecules become more like free rotators in space and the system become more anharmonic.

Despite the large increase in the anharmonicity in the system as revealed in chapter 1 through the single molecule potential(SMP) calculation and the reorientation study, C_v changes slowly. This phenomenon can be understood if one take notice that our simulations have been performed under constant pressure except when the surface-initiated melting was studied. Under constant pressure, the volume is free to expand or contract as the temperature varies. The change in the volume will lead to the change of the molecular spacing and thus the interactions between molecules. In terms of SMPs, the shapes of potential wells will be greatly modified because of the volume change. If the simulation is under constant volume the situation will be much different. The molecules will be forced to keep very much the same spacing by the increasing pressure owing to the increase in the temperature so the potential can remain the same as it was when the temperature is lower. When this is the case, the anharmonicity will not change so prominently as when the constant pressure condition is imposed.

Figure 4.2 shows that the bulk modulus does not change drastically near the solid-solid phase transition, the data points almost fall on a straight line. While the bulk modulus can only give information about the system's response to hydrostatic pressure, the more subtle changes in the elastic properties when the phase transition happens is the topic of the next section. The adiabatic heat capacity C_p diverges as the temperature nears the phase transition points. The thermal expansivity α, which is not plotted, has a similar temperature dependence to that of C_p. In fact these two are closely related. When α rises, more heat has to be absorbed to make up the work done by the system as the temperature rises because of the increase of the volume.

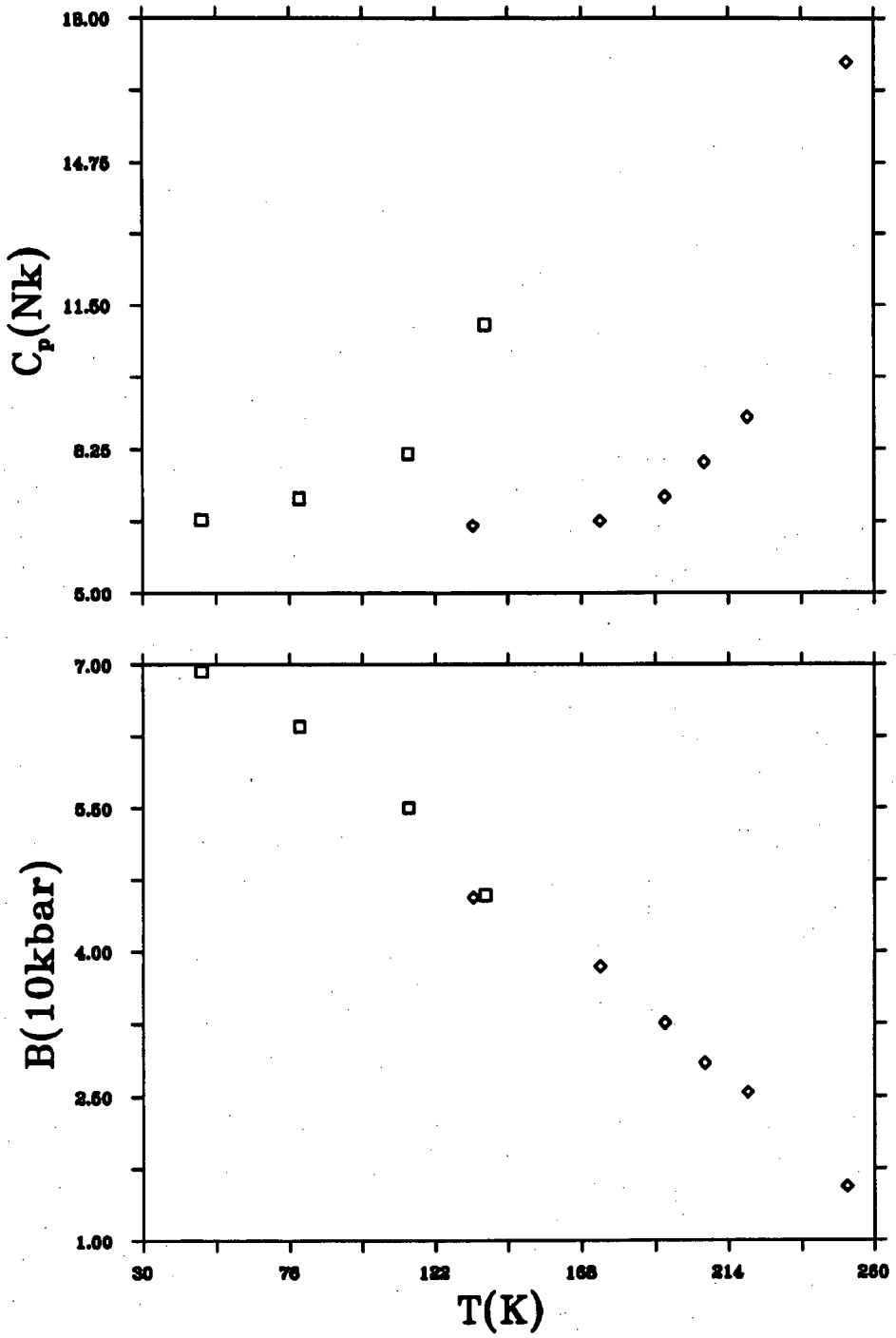

Figure 4.2: The heat capacity and the bulk modulus as functions of temperature. The unit for B_s is 10kbar and Nk for C_p. The different symbols refer to the different phases.

4.3 Elastic Constants

When a solid is under stress, strain will develop accordingly. The stress-strain relations of a material reflect the interactions between the constituent elements (ions, atoms or molecules) in it. For an MD simulation of the substance, the interactions are represented by the model potential function(s). If the stress-strain relation has been established by experiment, the investigation of this relation in the MD simulation can be used to examine how well the potential functions reflect the real interactions in the substance. Another application of the study of elastic properties was initiated by Born and Huang[24] who analyzed the relation between the mechanical stability and the elastic constants. In this section, we will describe the method of calculating the elastic constants using the fluctuations in MD simulations and present the results for solid SF_6.

Apart from the present work on SF_6, there have been some other reports on the calculation of elastic constants using MD method. For example, Sprik and co-workers applied this method to a system of argon atoms interacting with a Lenard-Jones potential. The main problem that they found was the slow convergence of the calculation[88]. In some other attempts the results are not satisfactory[86]. From the data given in[89] by Ray, the error of the calculation was unacceptably higher than 40%. We are interested in, among other things, how good the method is for SF_6.

4.3.1 The Method

If the distortion of a solid is small compared to the dimensions of the solid, the stress is a linear function of the strain and the generalized Hooke's Law is valid:

$$\epsilon = \mathbf{S}\sigma \quad or \quad \sigma = \mathbf{C}\epsilon \tag{4.5}$$

where σ is the stress tensor, which is a measure of both the pressure and the shear stress in the system, and ϵ the strain tensor, which is used to describe the extent of the distortion. The coefficients are compliances $\mathbf{S}$ and elastic constants $\mathbf{C}$. These

two are tensors of rank four and have 81 components each. Usually these tensors can be written explicitly as $S_{ij,kl}$ and $C_{ij,kl}$.

In the present (HPN) MD simulation, the elements of the h matrix vary dynamically so that both the volume and the shape can evolve with time. Any homogeneous deformation can be described by the h matrix, and the strain of the MD sample could be described by this matrix too. Parrinello and Rahman[81, 82] have found this to be

$$\epsilon = \frac{1}{2}({h^t}_0^{-1}\mathbf{G}h_0^{-1} - \mathbf{1}) \tag{4.6}$$

where $\mathbf{G}=h^t h$ and $h_0 =< h >$ is the h matrix in the reference state. As implied in its definition, h_0 is simply the mean value in the equilibrium state. In our simulation the h matrix is always kept symmetric so that h^t could be replaced by h.

In the (HPN) ensemble MD we are using, the only external stress that can be applied to the system is the hydrostatic pressure P, though this can be generalized to include the shear stress as well[81]. The generalized MD method generates (HtN) ensemble, where t stands for the external stress, which is an invariant quantity of the system in the (HtN) MD simulation. If this more generalized MD method is used we can find immediately a direct method to calculate the elastic constants by applying external stress to the sample and measuring the corresponding equilibrium strain which has been related to h through equation 4.6. Meanwhile, Parrinello and Rahman also found that the elastic constants can be calculated from the fluctuation of the strain tensor in the (HtN) ensemble and this is what we are most interested in here. The formula they gave in [82] is

$$< \delta\epsilon_{ij}\delta\epsilon_{kl} >= \frac{kT}{V_0}S_{ij,kl} \tag{4.7}$$

where V_0 is the equilibrium volume of the system, k is the Boltzmann's constant, T is the temperature and $\delta\epsilon_{ij} = \epsilon_{ij} - < \epsilon_{ij} >$.

When the system is under zero hydrostatic pressure and zero stress, the (HtN) ensemble MD and (HPN) ensemble MD are equivalent. This equivalence enables us to make use of the above formula to carry out the the calculation of the elastic constants without recoursing to the more generalized MD method.

4.3.2 Details of the Calculation

The basic procedure of the calculation is to apply equation 4.7 to obtain the 81 elements of the tensor of compliances. Because of the symmetry of the cartesian indices the compliances could then be reduced to a 6×6 matrix. The indices of the matrix elements are in accord with Vogt's convention[24], the indices 11, 22, 33 , 23, 13, and 12 in the tensor form are condensed to 1 to 6 in the 6×6 matrix form. If one or two indices of an element in the matrix form are greater than three, factors 2 or 4 respectively are introduced. For example, S_{14}=$2S_{11,23}$ and S_{54}=$4S_{31,23}$.

Since it is the elastic constants, not the compliances, that are more frequently used the matrix of compliances is inverted to obtain the elastic constants, also in the 6×6 matrix form. In the rest of this section, we always present the results in the Vogt condensed form.

In this calculation of the elastic constants, the MD samples and other system specifications are exactly the same as the ones in the calculation of the bulk modulus and other properties in section 4.2. The previous calculation of the bulk modulus can be used to check the present calculation because the bulk modulus can also be calculated from the compliances through the equation

$$B_s = (\sum_{i,j\leq 3} S_{ij})^{-1}. \tag{4.8}$$

The number of nonvanishing elements of the elastic constants is further limited by the symmetry of the crystal. In the plastic phase, the structure is bcc so there are 9 non-vanishing elements. Among them, C_{11}=C_{22}=C_{33}, C_{12}=C_{13}=C_{23} and C_{44}=C_{55}=C_{66} leaving only three independent. In the monoclinic phase there should be 13 nonvanishing elements and they are all independent. These are the 6 diagonal elements and C_{12}, C_{23}, C_{13}, C_{15}, C_{25}, C_{35} and C_{56}. The convergence of the elastic constants can be monitored by the values of those symmetry related elements of the elastic constants tensor. Another way of assessing the accuracy is to observe those elements that are required to be zero by symmetry requirements. This method is more useful in the monoclinic phase since all the non-zero

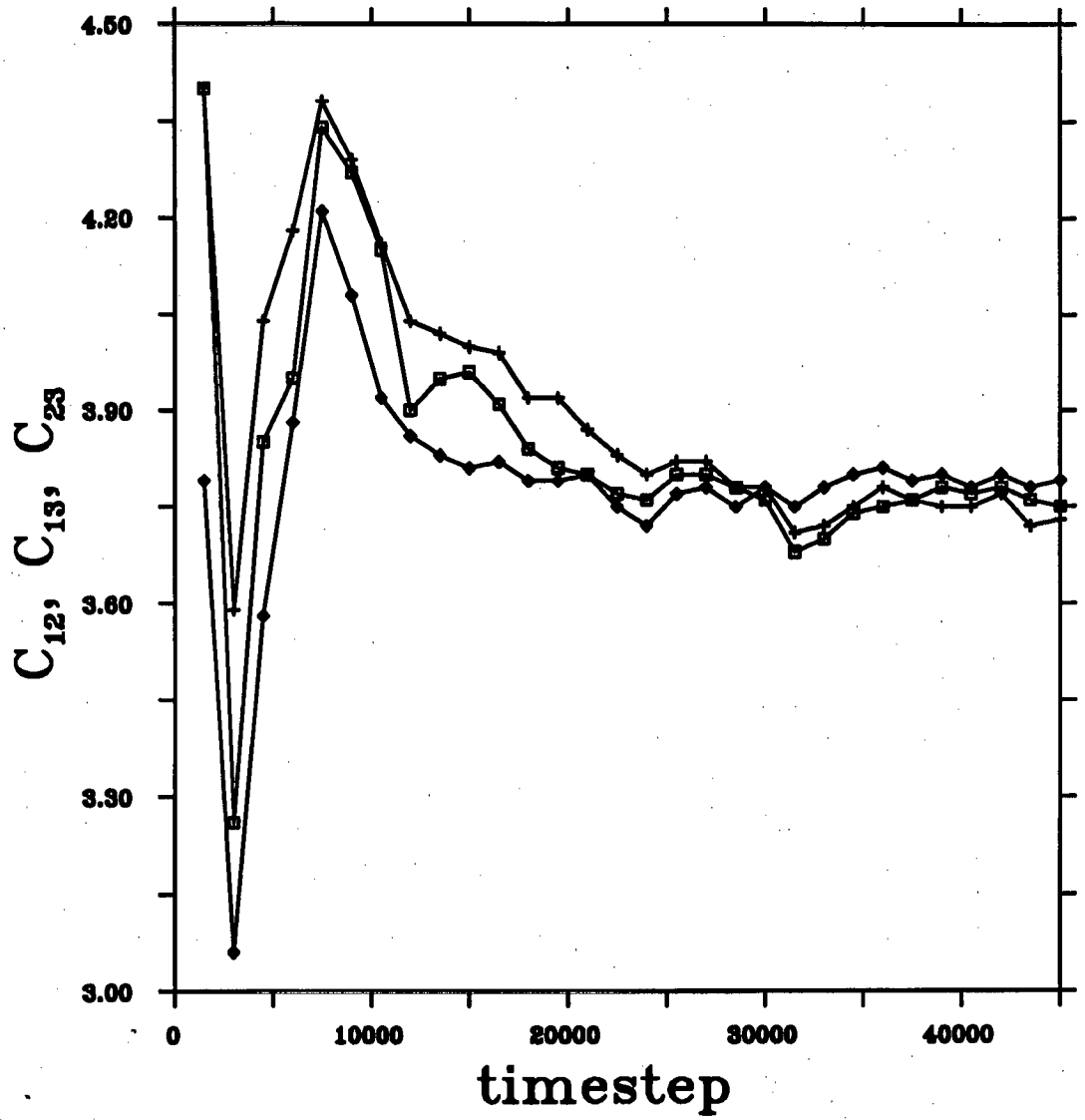

Figure 4.3: The three non-vanishing off-diagonal elastic constants as a function of the timesteps. The unit is 10kbar. An even longer run was carried out with little improvement in the convergence.

elements are independent and there are no comparisons to supply any information concerning the errors of the calculation.

In figure 4.3 three elastic constants C_{12}, C_{13} and C_{23} in the bcc phase are plotted as functions of the time. This is to show the convergence of the calculation. The three constants should become identical with small modification of fluctuations if the calculation is a success. From the figure one can see that this does happen

6.053	3.732	3.754	0.021	0.024	0.005
	6.185	3.793	−0.049	−0.083	0.042
		6.228	−0.034	−0.077	0.098
			1.120	0.001	−0.005
				1.067	−0.057
					1.074

Table 4.4: The upper right triangle part of the elastic constants matrix at 134K. The unit is 10kbar. The structure is bcc.

satisfactorily. The difference between those constants is no more than 2% at the end of the run which lasted for a total of 45,000 timesteps. This result is good if we notice that in an attempt made by Ray[89] using the same method the corresponding error is at least 40% even after a 70,000 timesteps run! In his work a timestep was $0.005\sigma(m/\epsilon)^{1/2}$ where σ and ϵ are the L-J parameters and m is the mass of an atom. For a system of argon atoms, the timestep is about 0.01ps so there is no great difference in the total simulation time in the two simulations.

The convergence of the other two groups of constants was also quite good. Table 4.4 and table 4.5 show the calculated elastic constants matrix for the bcc and monoclinic structures. These are obtained from MD runs of 45,000 timesteps. From the elements in the matrices one can roughly assess the accuracy of the calculation. The largest elements that should be zero by the symmetry requirements are smaller than 0.1 and the difference between the symmetrically identical elements (only for the bcc structure) is less than 10% of the value of the elements. If the mean value of a group of identical elements is calculated, the standard errors for the C_{11}, C_{12} and C_{44} groups are found to be 0.06, 0.02 and 0.02, or roughly 1.0, 0.5 and 2.0% of the mean values respectively.

Some independent runs were made to obtain more information about the accuracy and the parameter-dependence of the calculation. A longer run of 90,000 timesteps was carried out in the plastic phase and in another run a larger piston mass of 1460a.m.u was used. In the first case, it was found that the accuracy of the calculation was improved just slightly after 45,000 timesteps. The elastic constants

11.04	2.713	4.318	−0.007	0.254	0.064
	13.42	3.390	−0.070	−1.033	0.079
		11.82	0.091	0.454	−0.004
			4.026	0.029	−0.864
				1.840	−0.026
					3.504

Table 4.5: The upper right triangle part of the elastic constants matrix in the monoclinic phase at about 80K. The unit is 10kbar.

	C_{11}	C_{22}	C_{33}	C_{12}	C_{23}	C_{13}	C_{44}	C_{55}	C_{66}
run A	6.05	6.19	6.23	3.73	3.75	3.79	1.12	1.07	1.07
run B	5.99	6.10	6.04	3.67	3.61	3.70	1.11	1.04	1.05

Table 4.6: The comparison of the elastic constants calculated over 45,000 timesteps (run A) and 90,000 timesteps (run B) for the bcc structure.

are listed in table 4.6 together with the results from the previous 45,000 timesteps run.

4.3.3 Results and Discussions

In table 4.7 and table 4.8 the elastic constants at different temperatures are given for both the monoclinic and bcc phase. These are the means over 30,000 timesteps except those at 80K and 134K. Apart from the above general discussion about the accuracy of the calculation, the standard deviations are calculated from the symmetrically identical constants.

Temperature Dependence

In the plastic phase, the relations between the elastic constants and the temperature are almost linear. C_{11} is always larger than C_{12} and C_{44} is always larger than zero. Among the three constants, only C_{44} seems to fall a little faster when the

T(K)	C_{11}	C_{22}	C_{33}	C_{44}	C_{55}	C_{66}	
48.3	11.97	15.61	12.89	4.158	2.073	3.489	
79.1	11.03	13.42	11.82	4.026	1.840	3.504	
113.4	9.716	11.37	9.915	2.896	1.545	2.734	
137.5	7.710	9.380	7.616	2.327	1.133	2.266	
	C_{12}	C_{13}	C_{23}	C_{15}	C_{25}	C_{35}	C_{46}
48.3	2.727	4.615	3.483	0.663	−1.385	0.566	−0.739
79.1	2.713	4.318	3.390	0.254	−1.033	0.454	−0.864
113.4	2.550	3.747	2.967	0.061	−0.943	0.464	−0.515
137.5	2.635	3.095	2.765	−0.203	−0.786	0.309	−0.370

Table 4.7: The elastic constants in monoclinic phase. The unit is 10kbar.

T(K)	C_{11}	C_{12}	C_{44}
133.9	6.16(6)	3.76(2)	1.09(2)
173.8	5.14(7)	3.19(4)	1.12(1)
194.1	4.31(2)	2.72(3)	1.12(3)
206.4	3.75(2)	2.37(3)	1.07(2)
220.0	3.27(4)	2.18(3)	1.04(2)
251.5	1.91(1)	1.38(0)	0.81(2)

Table 4.8: The three independent elastic constants in the plastic phase. The standard deviations calculated from the symmetrically identical elements are in the brackets.

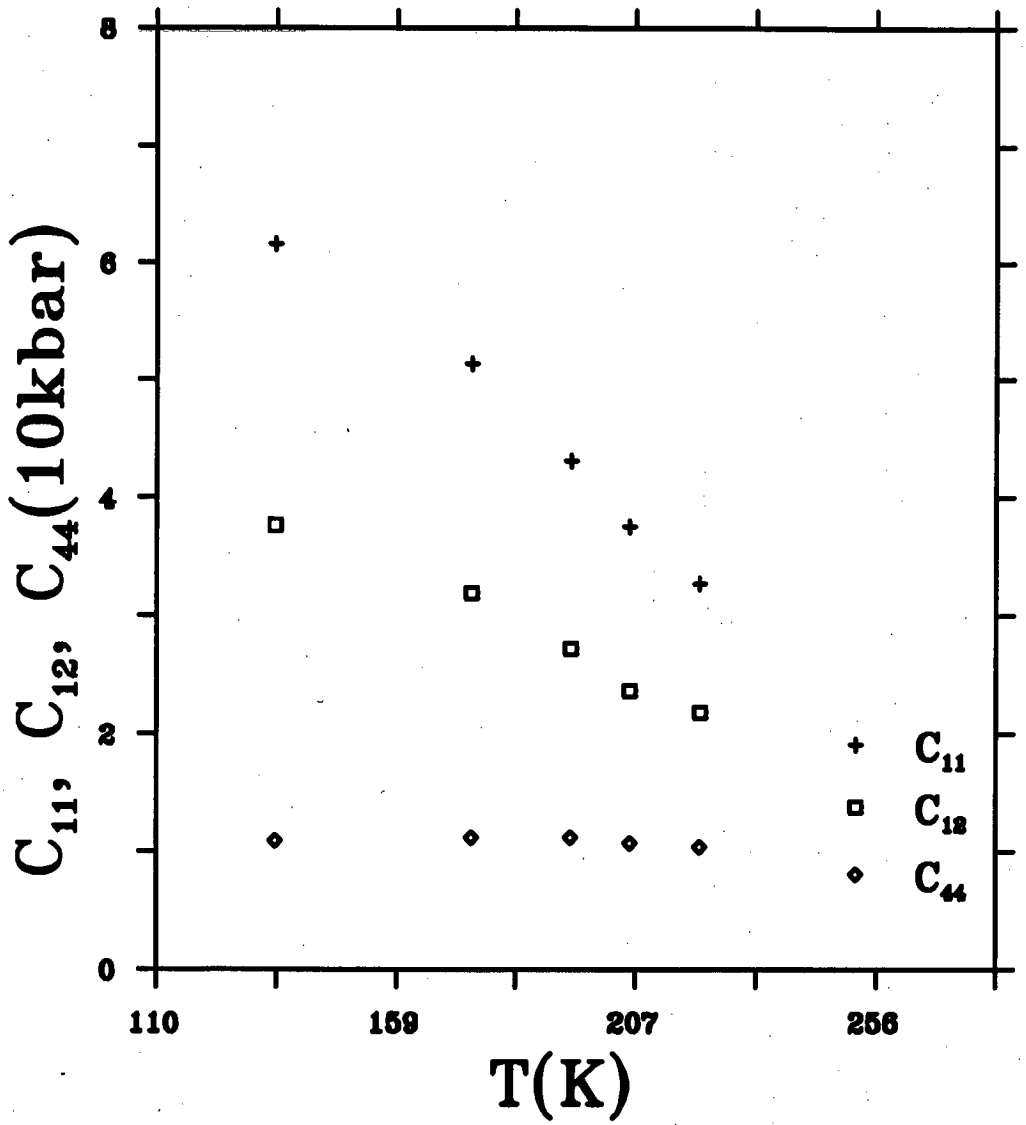

Figure 4.4: The temperature dependence of the three independent elastic constants in the plastic phase. The unit is 10kbar.

temperature is near the MD bulk sample's melting point for SF_6, which is about 270K (see chapter 3).

According to Born's criterion concerning the mechanical stability of solids[24], the stability conditions for a solid are that all the principal minors of the elastic constants matrices are greater than zero. For a solid of cubic symmetry the condition is reduced to $C_{11} > C_{12}$ and $C_{44} > 0$. From table 4.8, one can see that these conditions are met at all the temperatures. The only possible signs of

the tendency to have mechanical instability detected from the elastic constants calculation near the melting point might be the slightly quicker decrease of C_{44}.

There are thirteen non-vanishing elastic constants for a monoclinic structure. Except C_{25} and C_{46} all the other constants decrease as the temperature increases. Among the six diagonal elements, one can see in figure 4.5 that C_{11} and C_{33} are close in value and are always smaller than C_{22}, and C_{55} is always smaller than C_{44} and C_{66}. This suggests that it is always easier for the crystal to have a shear distortion which is perpendicular to the mirror plane of the monoclinic structure. This distortion can be described by the strain component e_2 in equation 2.8. The fact that this component e_2 is the primary order parameter in the solid-solid phase transition may be related to the 'relative instability' of the structue revealed by C_{55}.

Again in the monoclinic phase, Born's criterion is met and the solid is stable. Therefore any possible instability in the structure seems to happen in a very short range of temperature, at melting or at some other structural transition, and the structure changes happen very quickly when the instability occurs. The time scale which is needed for the calculation of elastic constants might be just too long that the observation of the development of the instability is not possible.

Acoustic Velocities

When the elastic constants are known, the dispersion relation for elastic waves can then be calculated and the wave velocities along any directions could be obtained[85]. For example, in the plastic phase the structure is bcc. The velocities of the longitudinal and transverse waves along a cubic edge are $V_l = (C_{11}/\rho)^{\frac{1}{2}}$ and $V_t = (C_{44}/\rho)^{\frac{1}{2}}$ where ρ is the density of the substance. These velocities can be measured by, for example, Brillouin scattering method[23]. Since C_{44} has very weak temperature dependence until it is very near the melting point of the bulk MD sample(about 270K), it is expected the transverse acoustic velocity remains very much the same value throughout the plastic phase.

If the elastic constants of the monoclinic phase are to be used, one should notice that because of the symmetry requirement of the h matrix, only the cartesian axis

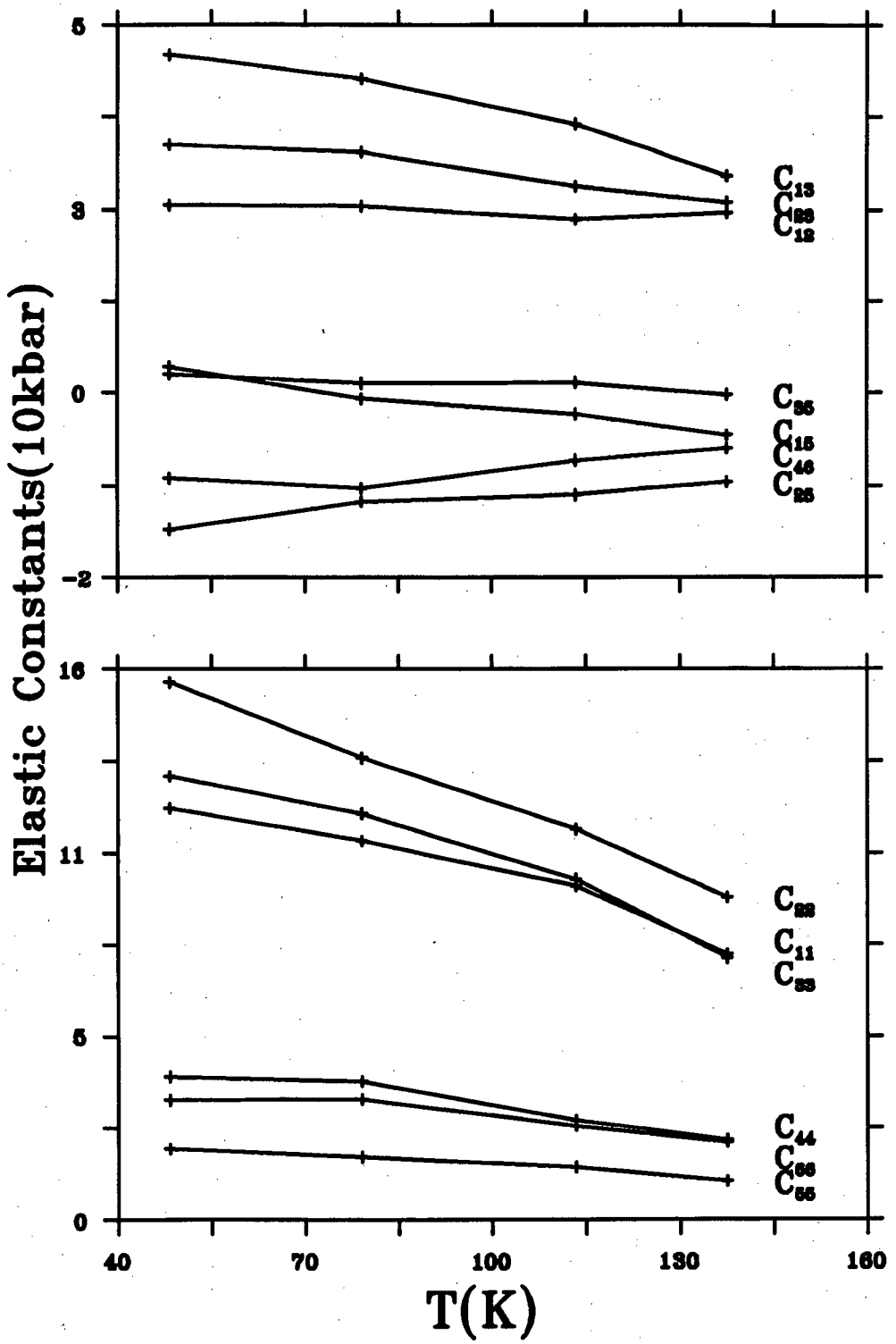

Figure 4.5: The temperature dependence of the elastic constants in the monoclinic phase.

y coincides with the equilibrium monoclinic unit-cell vector **b**. Thus there is an angle between the unit-cell vector **a** (or **c**) and the cartesian axis x (or z). The angles can be easily worked out from the construct of the MD sample and the lattice parameters given in chapter 2.

4.3.4 Further Discussions

Linear Compressibility

Like the bulk modulus, the linear compressibility along any direction **l**, χ_l, can also be evaluated from the compliances. For the monoclinic structure, the relevant equation is

$$\begin{aligned}\chi_l &= (S_{11}+S_{12}+S_{13})l_1^2+(S_{12}+S_{22}+S_{23})l_2^2+ \\ &\quad (S_{13}+S_{23}+S_{33})l_3^2+(S_{15}+S_{25}+S_{35})l_3l_1 \qquad (4.9)\end{aligned}$$

where l_i is the ith direction cosine[90]. For the bcc structure, the linear compressibility is isotropic and is 1/3 of the bulk compressibility in value.

Specific Heat at Low Temperature

We have calculated the heat capacity at as low as 50K. But this is only the classical theory which fails at temperatures near zero(K). At very low temperatures, the quantum effect becomes more prominent and the discrete aspect of the energy of the system must be taken into account. An approximate theory of the specific heat at very low temperature is Debye's elastic wave method. In this method, the vibrations of a solid are assumed to be elastic waves and the specific heat can be calculated from the velocities of the transverse and longitudinal elastic waves. When the solid is not isotropic this raises the question of calculating the integral

$$\frac{1}{4\pi}\int(\frac{1}{V_1}+\frac{1}{V_2}+\frac{1}{V_3})d\Omega$$

where V_1, V_2 and V_3 are the three wave velocities of the waves traveling along the direction lying in the solid angle $d\Omega$[24]. So from the calculation of the elastic constants, we can calculate the Debye parameters for the model. An estimate of

the low-temperature bound for the use of classical theory will then be the Debye temperature[24].

The Effect of Piston Mass

As has been mentioned previously, the change of the piston mass alters the rate of equilibration. But what is its effect on the calculation of the elastic constants if equilibrium has already been achieved? In theory, the MD method generates an ensemble which is independent of this parameter, so the calculation should not be affected if the calculation is over a period of time which is long enough for the trajectory to explore enough phase space. But as the piston mass is increased, the rates of fluctuations of volume etc. become slower. So far as these quantities are concerned, for a limited period of time, the phase space volume covered by the trajectory is smaller. One may thus postulate that for a larger piston mass, it takes longer for the calculation to have the same accuracy as it is for one with smaller piston mass. As the volume fluctuation period is proportional to the square root of the piston mass, this period of time T_n, which is needed for a calculation with certain accuracy, may also have the same relation i.e. $T_n \propto M_p^{1/2}$. This approximate relation may explain the poorer convergence in [88] when the piston mass was increased by ten times.

Other Fluctuation Methods

Because of the slow convergence of the method used here, Ray and his co-workers have proposed other ways of calculating the elastic constants[86, 87]. They found that the adiabatic elastic constants can also be calculated in the (EhN) MD simulation and the isothermal elastic constants can be calculated using (ThN) MD ensemble. The MD-cell matrix h in these two MD methods are invariant so they are in fact generalized constant volume methods. The isothermal elastic constants could be transformed to adiabatic elastic constants through well-established thermodynamic relations. Those were reportedly quicker but the improvement is not dramatic. The time needed is still of the same order of magnitude as in the method used in the present work. However we think it is worth calculating the elastic constants for SF_6 using this method and comparing the results with what we have obtained in this chapter as this may shed some light on the cause of the

difference between the covergence behaviour observed by us and that by some other workers[89].

Bibliography

[1] Heermann, D.W.: *Computer Simulation Methods*, 2nd ed., (Springer-Verlag, Berlin Heidelberg 1990)

[2] *Monte Carlo Methods in Statistical Physics*, edited by Binder, K., (Springer-Verlag, Berlin, 1979)

[3] Rahman, A., Phys. Rev. **136**, A405(1964)

[4] Alder, B. J. and Wainwright, T. E., J. Chem. Phys. **33**, 1439(1960)

[5] Pryde, J. A., *The Liquid State*, (Hutchinson University Library, London, 1966)

[6] Allen, M. P. and Tildesley, D. J., *Computer Simulations of Liquids*, (Claredon , Oxford, 1987)

[7] Hoover, Wm. G., *Molecular Dynamics*, (Springer-Verlag, Berlin, 1986)

[8] *Molecular Dynamics Simulations of Statistical Mechanical System: Proceedings of the International School of Physics 'Enrico Fermi' Course XCVII*, edited by G. Ciccotti and W. G. Hoover, (North-Holland, 1986)

[9] Andersen, H.C., J. Chem. Phys. **72**,2384(1980).

[10] Parrinello, M. and Rahman, A., Phy. Rev. Lett. **45**, 1196(1980).

[11] Nosé, S. and Klein, M. L., Mol. Phys. **50**, 1055(1983)

[12] Nosé, S., J. Phys. Condens. Matter, **2**, SA115(1990)

[13] Cagin, T. and Pettitt, M., Mol. Phys. **72**, 169(1991)

[14] Hill, T. L., *Statistical Mechanics*, (McGraw-Hill, New York, 1956)

[15] Wright, J. D., *Molecular Crystals*, (Cambridge University Press, Cambridge, 1987)

[16] Gilbert, M. and Drifford, M., Adv. Raman Spectrosc. **1**, 204(1972)

[17] G.Dolling, Powell, B. M. and Sears, V. F., Molec. Phys., **37**,1859(1979).

[18] Eucken, A. and Schroder, E., Z. Phys. Chem. B**41**, 3071938

[19] Taylor, J. C. and Waugh, A. B., J. Solid State Chem. **18**, 241(1976)

[20] Michel, J., Drifford, M., and Rigny, P., J. Chim. Phys., **67**, 31(1970)

[21] Blinc, R. and Lahajnar, Phys. Rev. Lett. **19**, 685(1967)

[22] Timmermans, J., J. Phys. Chem. Solids, **18**, 1(1961)

[23] *The Plastically Crystalline State*, Edited by J. N. Sherwood (John Wiley & Sons 1979)

[24] Born, M. and Huang, K., Dynamical Theory of Crystal Lattices, (Clarendon, Oxford, 1954)

[25] Garg, S. K., J. Chem. Phys. **66**, 2517(1977)

[26] Raynerd, G., Tatlock, G.J. and Venables, J.A., Act. Crys., B**38**, 1896(1982).

[27] Powell, B.M. , Dove, M. T., Pawley, G.S. and Bartell, L.S., Molec. Phys.,**62**,1127(1987)

[28] Dove, M.T., Powell, B.M., Pawley, G.S. and Bartell, L.S., Molec. Phys., **65**,353(1988)

[29] Taylor, J. C.; Wilson, P. W. Acta. Crystallogr. **B29**, 7(1973).

[30] Levy, J. M., Taylor, J. C. and Wilson, P. W. Acta. Crystallogr. **B31**, 398(1975).

[31] Pawley, G. S., Molec. Phys., **43**,1321(1981)

[32] Pawley, G.S. and Thomas, G.W., Phy. Rev. Lett. **48**, 410(1982).

[33] Hockney, R.W. and Jesshope, C.R.: *Parallel Computers* (Adam Hilger, Bristol 1981)

[34] Dove, M.T.and Pawley, G.S., J. Phys. C, **16**, 5969(1983).

[35] Pawley, G.S. and Thomas, G.W., J. Comput. Phys.,**47**, 165(1982)

[36] Refson, K. and Pawley, G. S., Molec. Phys., **61**, 669(1987)

[37] Bowler, K. C., Kenway, R. D., Pawley, G. S. and Roweth, D. , *An Introduction to OCCAM-2 Programming*, (Chartwell-Bratt, 1987)

[38] Craven, C. J., and Pawley, G. S., Comput. Phys. Comm.,**62**, 169(1991)

[39] Beeman, D., J. Comput. Phys., **20**, 130(1976)

[40] Refson, K. and Pawley, G. S., Comput. Phys. Comm.,**62**, 279(1991)

[41] Verlet, L. Phys. Rev. **159**, 98(1967)

[42] Hockney, R. W. and Eastwood, J. W., *Computer Simulation Using Particles*, (McGraw-Hill, New York, 1981)

[43] Gear, C. W., *Numerical Initial Value Problems in Ordinary Differential Equations*(Prentice-Hall, New York, 1971)

[44] Berendsen, H. J. C. and Van Gunsteren, W. F., *Enrico Fermi School on "Molecular-Dynamics Simulation of Statistical-Mechanical Systems"* Varenna, 1985, eds. Ciccotti G. P. F. and Hoover, W. G., (Horth-Holland, Amsterdam, 1986)pp. 43-65

[45] Venneri, G. D. and Hoover, W. G., J. Comput. Phys., **73**, 468(1987)

[46] Amini, M. and Fincham, D., Comput. Phys. Comm.,**56**, 313(1990)

[47] Synge, J. L. and Griffith, B. A., *Principles of Mechanics* (3rd ed. McGraw-Hill, Tokyo, 1970)

[48] Williams, D.E., Acta Cryst. A28, 629(1972)

[49] Della Valle R. G. and Pawley, G. S., Acta Cryst. **A40**, 297(1984)

[50] Press, W, *Single-Particle Rotations in Molecular Crystals, Springer Tracts in Modern Physics*, vol. 92 (Springer, Berlin, 1981)

[51] Lu Hua and Pawley, G.S., *Molecular Simulation*, **7**, 89(1991)

[52] Hua, L. and Pawley, G.S., Z. Kristallogr., (1991), in press.

[53] DuVal, P., *Homographies, Quaternions and Rotations* (Oxford Mathematical Monograph, 1964)

[54] Fuchs, A. H. and Pawley, G.S., J. Phys. France **49**, 41(1988)

[55] Boyer, L.L. and Pawley, G.S., J. Compt. Phys. **78**, No. 2, 405(1988)

[56] Pawley, G.S. and Dove, M.T., Molec. Phys.,**55**,1147(1985)

[57] Glasstone, S., Laidler, K. J. and Eyring, H., *The Theory of Rate Processes*, (McGraw-Hill, New York, 1941)

[58] Boden, N, Davis, P. P., Stam, C. H. and Wesselink, G. A., Molec. Phys.,**25**, 87(1973)

[59] Waugh, J. S. and Fedin, E. I., Soviet Phys. Solid State, **4**, 1633(1963)

[60] Brot, C., Chem. Phys. Lett. **3**, 319(1969)

[61] Dickerson, R. E., *Molecular Thermodynamics*, (W.A. Benjamin, California, pp 222.)

[62] Swalin, R. A., *Thermodynamics of Solids*, (2ed edition, John Wiley & Sons, New York, 1972)

[63] Temperley, H. N. V., *Changes of State*, (Cleaver-Hume Press, London, 1956)

[64] Ubbelohde, A. R., *The Molten State of Matter*, (John Wiley & Sons, Bristol, 1978)

[65] Broughton, J. Q. and Gilmer, G. H., Phys. Rev. Lett. **56**, 2692(1986).

[66] Hoover, W. G. and Ross, M., Contemp. Phys., **12**, 339(1971)

[67] Phillpot, S. R., Lutsko, J. F., Wolf, D., and Yip, S., Phys. Rev. B 40 2831(1989).

[68] Motorin, V. I. and Musher, S. L., J. Chem. Phys. **81**, 465(1984)

[69] Freken, J. W. M., Maree, P. M. J. and van der Veen, J. F., Phys. Rev. **B34**, 7506(1986).

[70] Nguyen, T., Ho, P. S., Kwok, T., Nitta, C. and Yip, S., Phys. Rev. Lett. **57**, 1919(1986).

[71] Temperley, H. N. V. and Trevena, D. H., *Liquids and Their Properties*, (Ellis Horwood Ltd, Chichester, 1978)

[72] Lipowsky, R. and Speth, W., Phys. Rev. **B28**, 3983(1983).

[73] Stoltze, P., Norskov, J. K. and Landman, U., Phys. Rev. Lett. **61**, 440(1988).

[74] Kluge, M. D. and Ray, J. R., Phys. Rev. **B39**,1738(1989)

[75] Siegal, S., Northrup, D. A. Inorg. Chem. **5** 2187(1966).

[76] Bartell, L. S. and Powell, B. M. Molec. Phys. (in press).

[77] Lawrence S. Bartell and Shimin Xu, J. Phys. Chem. (in press).

[78] Wu, E. Y. and Friauf, R. J., Comput. Phys. Commun. **59** 259(1990)

[79] Haile, J. M. and Graben, H. W., Molec. Phys. **40** 1433(1980)

[80] Ray, J. R., Graben, H. W and Haile, J. M., Nuovo Cim. **64B** 191(1981).

[81] Parrinello, M. and Rahman, A., J. Appl. Phys. **52**, 7182(1981).

[82] Parrinello, M. and Rahman, A., J. Chem. Phys. **76**, 2662(1982).

[83] Haile, J. M. and Graben, H. W., J. Chem. Phys. **73**, 2412(1980).

[84] Craven, C. J., Ph.D thesis, University of Edinburgh.

[85] Landau, L. D. and Lifshitz, E. M., *Theory of Elasticity* (Pergman, Oxford, 1986)

[86] Ray, J. R., Moody, M. C. and Rahman, A., J. Chem. Phys. **32**, 733(1985).

[87] Ray, J. R., Moody, M. C. and Rahman, A., J. Chem. Phys. **33**, 895(1986).

[88] Sprik, M., Impey, R. W. and Klein, M. L., Phys. Rev. **B29**, 4368(1984).

[89] Ray, J. R., Comput. Phys. Rep. **8**, 109(1988)

[90] Nye, J. R., *Physical Properties of Crystals*, (Oxford, London, 1957)

[91] Downs, J., Gubbins, K. E., Murad, S. and Gray, C. G., Molec. Phys. **37**, 129(1979)